Yield Stress Augmentation of Fine-Particle Slurries by Coarse Particles

by

Abiodun E. Olayode

A thesis submitted in partial fulfillment of the requirements for the degree of

Master of Science

in

Chemical Engineering

Department of Chemical and Materials Engineering

University of Alberta

Abstract

The transport of thickened tailings through pipelines in the mineral processing industry is challenging partly because knowledge of the yield stress of these complex non-Newtonian mixtures is required for design and optimal operation. Unfortunately, the yield stress of these mixtures cannot be accurately predicted partially because of the complexities introduced by the presence of coarse particles. It is known that the presence of coarse particles increases the yield stress of an initial flocculated fine-particle suspension. Also, the rheological characterization of these fine-coarse particle suspensions, which are often referred to as bimodal suspensions, is tedious and very difficult due to the fast settling nature of the coarse particles.

In this study, an experimental program was completed to obtain improved vane yield stress data for a wide range of bimodal suspension types and concentrations. Kaolin slurries and industrial mature fine tailings were prepared at different concentrations and tested with three types of sand of different shapes and sizes. The performance of three semi-empirical yield stress correlations were tested and compared on these yield stress measurements. The contribution of coarse particle properties, such as shape and size, to yield stress augmentation was also investigated.

Results show that in addition to concentration, the effect of coarse particle shape and size is significant and contribute to the yield stress increase. Specifically, higher yield stress values were observed with the angular sand when compared with rounded sand of similar size. When yield stress is expressed as a function of coarse particle concentration ratio (in situ/ maximum packing, i.e. $C_s/C_{max,s}$), the higher increase in yield stress due to coarse particle shape is normalized for sands with sizes larger than $d_{50} \approx 100\mu m$.

In terms of semi-empirical correlation performance, the Deltares correlation gave the best prediction, followed by the Thomas and the Lim et al. correlations. The use of a concentration ratio, $C_s/C_{max,s}$, captures the effect of shape and improved the predictive capabilities of the Deltares and Thomas correlations.

In conclusion, it appears that coarse particle contribution to yield stress increase is through an indirect physical interaction with aggregates in the fine-particle suspension, suggesting coarse particles are “rheologically inert” i.e. they simply occupy space. To improve upon the current understanding of the effect of coarse particle properties on yield stress, further investigations of smaller coarse particles ($d_{50} \leq 100\mu m$) are required as well as tests involving polymodal suspensions.

Acknowledgment

First and foremost, I would like to thank Almighty God for the grace of completion.

I wish to express my profound gratitude to my supervisor Dr Sean Sanders. First, for giving the opportunity to realize my dreams, and secondly, for his unwavering belief in me, his continuous support and excellent supervision throughout my program, despite his very busy schedule. I am always proud and honored to have you as my supervisor. Thank you very much, Sir!

Special appreciation to Dr David Breakey and Nitish Ranjan Sarker for their immense contribution and assistance during this period. You are truly wonderful and excellent people.

I would like to thank Terry Runyon for her continuous administrative support, and to my wonderful colleagues in the Pipeline Transport Process Research Group at the University of Alberta; Akash Saxena, Oluwaseun Adedeji, Simon Sun, Aaron Cheung, Lisheng Zhang, Maedeh Marefatallah, Hamed Sepehr, Ghassan Khan, and Aref Kangarshahi.

A sincere appreciation goes to the NSERC Industrial Research Chair in Pipeline Transport Processes for necessary financial support. I am grateful to the Saskatchewan Research Council's Pipe Flow Technology Centre for shared resources and contributions towards this project. And to Barry Bara at Syncrude Research Centre, Edmonton for provided the industrial tailings used in this project.

I want to specially thank my family and friends for their support, patience, encouragement and understanding during this period.

I am saying thank you, and I appreciate every one of you.

Table of Contents

List of Figures

List of Tables

List of Symbols

Symbols	Description	Units
A	Fitting parameter, Equation (2.7)	-
A'	Fitting parameter, Equation (2.8)	-
a	Fitting parameter, Equation (2.10)	-
a'	Fitting parameter, Equation (2.15)	-
b	Constant (0.002), Equation (2.10)	-
b'	Constant, Equation (3.9)	-
c	Fitting constant, Equation (2.10)	-
C	Solids volume concentration	-
d	Diameter	m
d_p	Fine particle diameter	m
d_{50}	Mass median particle	m
D_v	Vane diameter	m
D_c	Diameter	m
g	Gravitational acceleration constant	m/s^2
h_f	Final height of suspension	m
h_o	Initial height of suspension	m
H_v	Height of vane	m
K_v	Vane constant	-
L	Length of concentric cylinder rotor	m
M_f	Mass of fine particles	g
m	Fitting parameter, Equation (3.8)	-
n	Number of batch settling test	-
n'	Fitting parameter, Equation (3.9)	-
N	Mixer speed	RPM
P_{base}	Base pressure	Pa/m
r	Distance from center of cup to a point in the annulus of concentric cylinder	m

Symbols	Description	Units
R	Radius	m
Re_{crit}	Critical Reynolds number	-
S	Coarse solids fraction	-
T	Torque	$N.m$
V_c	Deposition velocity	m/s
V_t	Laminar-to-turbulent transition velocity	m/s
$\forall_l$	Volume of liquid (water)	mL
$\forall_f$	Volume of fluid	mL
$\forall_s$	Volume of solid	mL
W_f	Water content-to-clay ratio	-
Z_{above}	Height above vane	m
Z_{below}	Height below vane	m

Greek Symbols	Description	Units
α	Fitting parameter, Equation (2.8)	-
β	Fitting constant, Equation (2.8)	-
η_r	Relative viscosity Equation (2.8)	-
$\dot{\gamma}$	Shear rate	s^{-1}
λ	Linear concentration Equation (2.8)	-
μ_L	Viscosity of liquid (water)	$Pa.s$
μ_m	Mixture viscosity	$Pa.s$
μ_p	Plastic viscosity	$Pa.s$
ω	Angular velocity	s^{-1}
ρ	Density	kg/m^3
τ	Yield stress	Pa
$\tau_{y,f}$	Vane yield stress of fine suspension	Pa

Greek Symbols	Description	Units
$\tau_{r\theta}$	Local shear stress at a distance r	Pa
$\tau_{y,m}$	Vane yield stress of bimodal suspensions	Pa
$\tau_{y,v}$	Vane yield stress	Pa
$\tau_{y,N}$	Normalized vane yield stress	-
τ_r	Vane yield stress ratio	-
τ_w	Wall shear stress	Pa

Subscripts	Description	Units
avg	Average	-
b	Bulk	-
B	Bingham	-
cp,f	Close packing fraction of fine	-
$crit$	Critical	-
f	Fine particle	-
g,f	Gel point of fine	-
g,m	Mixture gel point	-
m	Mixture	-
min	Minimum	-
max	Maximum	-
o	Initial	-
p	Fine particle	-
s	Coarse	-
t	Transition	-
v	Vane	-

Chapter 1 INTRODUCTION

1.1 Background

The production of large volumes of tailings is common in the mineral processing and mining industries [1, 2]. For example, in the open-pit mining method of bitumen extraction from oil sands deposits, a large volume of tailings is produced and hydraulically transported to a tailings pond where it is deposited [3, 4]. This slurry is mostly composed of sand, clay, silt, unrecovered hydrocarbon, and water. In the dedicated disposal area (DDA), the fast-settling sand fraction (particles > 44 µm) settles, forming beaches [5]. The fluid fine tailings (FFT), which comprise approximately 45% by volume of the total tailings, is made up of fine particles (< 44 µm) and water [2]. Due to the colloidal nature of its constituent fine particles, the FFT is not stable and slowly consolidates over many years to become mature fine tailings (MFT). The MFT is stable and has a higher solids concentration (typically 35% by weight) than the FFT [2, 5]. This stable MFT traps a vast amount of process water that could otherwise be recovered; and because of this, the pond containing the MFT cover a substantial portion of land. According to the Alberta Energy Regulator (AER) in 2011, over 130 km^2 of land was covered by tailings pond [2, 6]. A growing inventory of MFT has become a significant environmental concern that requires prompt attention because of the threat it poses to the immediate ecosystem and to surrounding communities. Some of these environmental concerns include: potential storage failure, slow rate of land reclamation, poor geotechnical strength of recovered areas, high water demand for operations, and increased energy to reheat process water [2].

In an effort to resolve the challenges of oil sands tailings placement, the Government of Alberta has introduced and frequently updated a Tailings Management Framework (TMF) as an intervention tool to properly manage tailings disposal space [7], and to reduce the impact of FFT placement on the environment. These interventions have compelled operators to develop new technologies to enhance the dewatering of MFT, to promote the quick release and recycle of warm process water, reduce tailings inventory, and to accelerate improved land recovery [2]. Over the past 10 years, several tailings dewatering and drying technologies have been developed to resolve tailings placement challenges [5]. Some of these technologies include tailings reduction operations

(TRO), composite tailings (CT), and thin-lift dewatering [5]. Many of these technologies have adopted commercial water treatment methods to de-stabilize fine particles in the MFT to accelerate dewatering and drying processes. These methods involve mixing of MFT with polymer flocculant to promote fine particle aggregation [8, 9]. This treatment produces very concentrated suspensions of fine particles and these mixtures are further processed to remove the liberated process water through enhanced drying techniques [9]. To accelerate the release and recovery of liberated process water, suspensions are transported through the pipeline and discharged into engineered dedicated disposal areas (DDA) where slope bank allows the quick drainage and recycling of the liberated process water [8, 9].

One of the tailings treatment method (composite or consolidated tailings) adopts the dewatering and drying techniques discussed above, and in addition to the MFT-coagulant/flocculant mixtures, coarse particles are added to enhance tailings dewatering, drying, and land reclamation processes [9, 10]. This enhances the dewatering of the mixtures by capturing and locking the coagulated fines within the interstices of the coarse particles, which improves the trafficability of reclaimed land. Figure 1.1 presents a schematic of a generic tailings treatment process. The previously described dewatering technologies remain limited due to the inefficient pipeline transport and storage of these treated tailings [11]. The effectiveness of the pipeline transport and storage systems strongly depends on the rheology of the treated suspension.

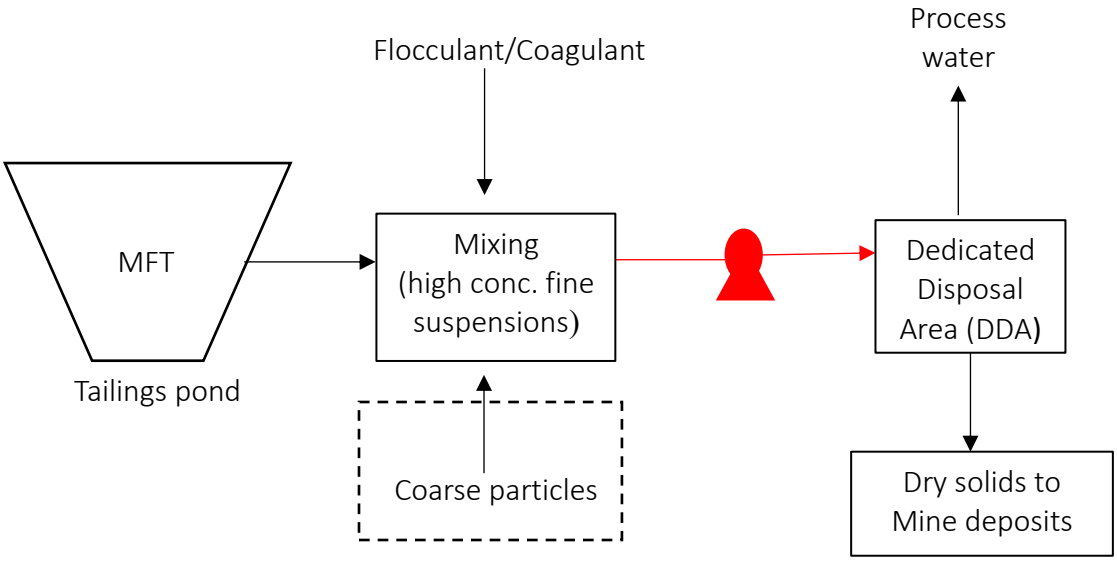

Figure 1-1: General overview of oil sands tailings treatment.

The rheology of a fine particle suspension (such as MFT) is known to be non-Newtonian and is often described with yield stress models such as the Bingham, Casson or Herschel-Bulkley models [12]. The determination of the rheology of these suspensions (of the carrier liquid and $< 44\mu m$ particles) presents many complications due to variability in the physical and chemical conditions of suspensions resulting from changes in operations. In addition to the complexity of the rheology of fines-only suspensions, the presence of coarse solids can change the mixture's flow resistance [12,13,14]. This is shown in Figure 1-2, where the relative Bingham yield stress, which is the ratio of the Bingham yield stress of the fine-coarse suspensions, i.e. a bimodal suspension, to the Bingham yield stress of fine particle suspension, increases as a function of sand concentration. These bimodal suspensions containing both fine and coarse solids often show a non-Newtonian, yield stress behavior, a characteristic imparted by the flocculating fines fraction [12].

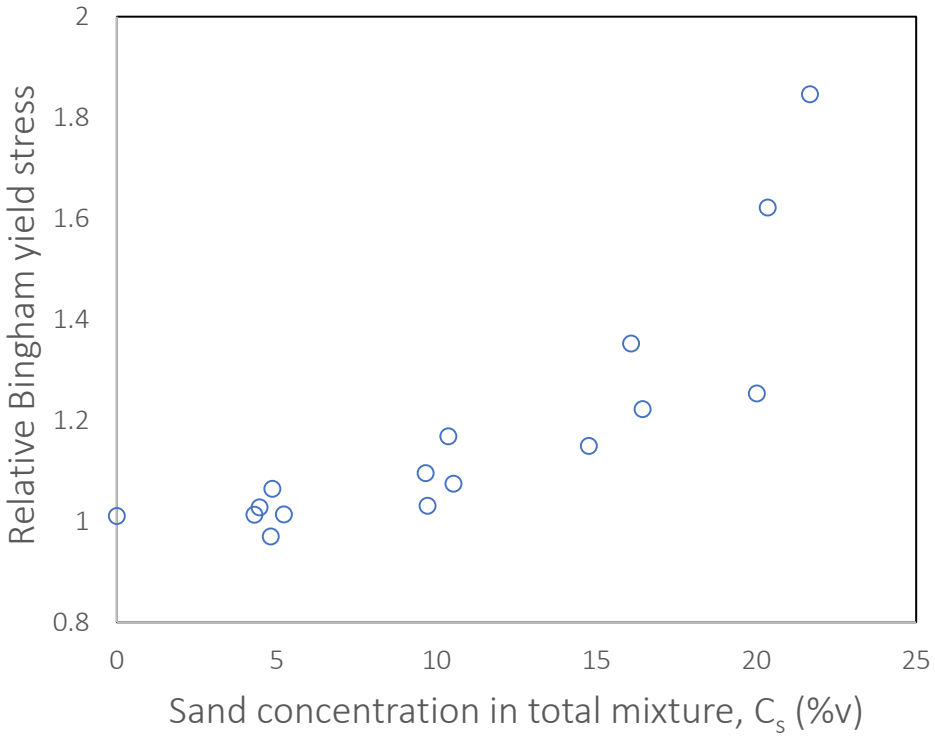

Figure 1-2: A typical graph showing the augmented yield stress of kaolin suspension with Granusil sand of $d_{50} = 190\mu m$ (Adapted from Rahman[14]).

Pipeline transport and placement of these concentrated suspensions are affected by their rheology, and especially by the yield stress parameter [12]. Figure 1-3 illustrates the relationship between a typical tailings deposit thickness and yield stress [15]. When these treated tailings are deposited in shallow slope banks of the DDA, they form deposit slopes. This deposit slope is an important parameter for storage facility design and management because it determines storage capacity, slope stability, erosion susceptibility and overall drainage system efficiency [16]. The prediction of the thickness of deposited tailings depends on the suspension rheology, and particularly the yield stress [16]. Yield stress is a key input in many semi-empirical correlations (e.g., [17]) for predicting deposit thickness.

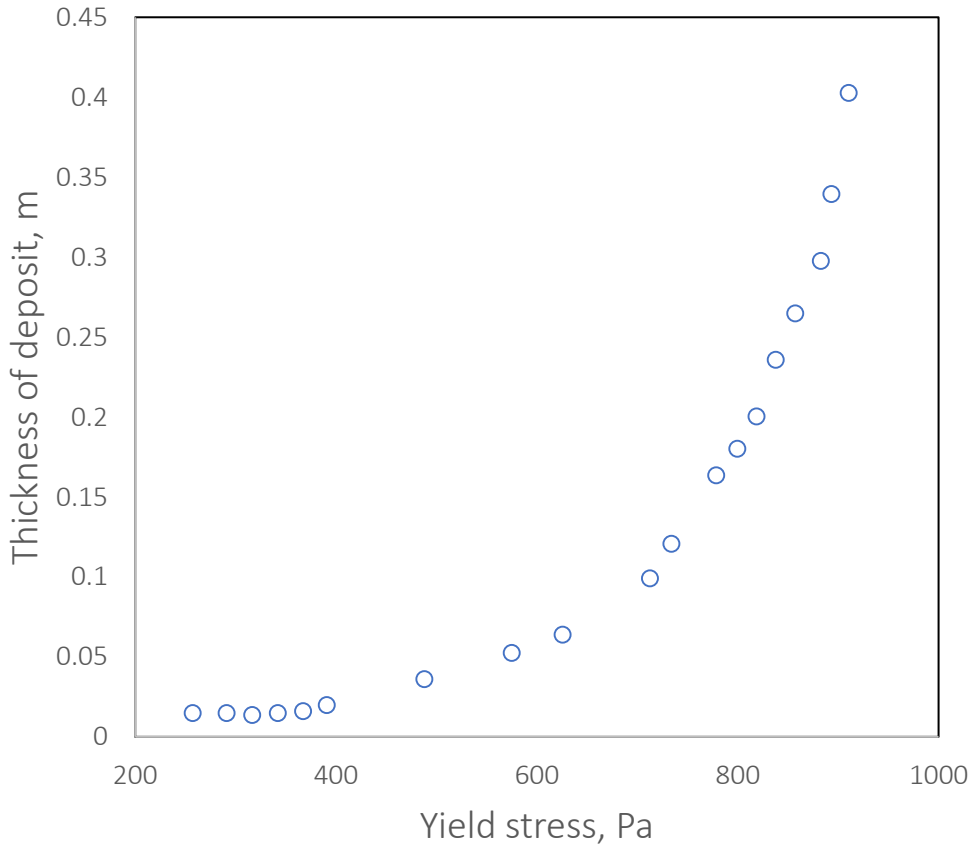

Figure 1-3: Deposit thickness as a function of yield stress for debris flow (Adapted from Reaîtrme et al. [10]).

The yield stress of a bimodal suspension also plays a vital role in the design and operation of the transport pipeline because it is needed to determine flow stability boundaries. According to Poloski et al. [18], stable flow occurs when coarse particles are either fully or partially suspended, and an unstable one occurs when the mechanisms to suspend particles are either insufficient or unavailable such that coarse particles form a sliding or stationary bed. These flow regions are also defined by the operating velocity regime and classified as follows [18]: stable- turbulent (S-T), unstable-turbulent (U-T), stable-laminar (S-L), and unstable-laminar (U-L). Following this classification, a stable flow condition can be attained in both laminar and turbulent flow regimes. The role and importance of yield stress in the pipeline transport of coarse particles in a non-Newtonian suspension is illustrated with the simplified Poloski et al. [18] "stability map" shown in Figure 1-4, where flow velocity has been plotted against slurry rheology. The figure presents the four different flow regimes described above for a pipeline conveying coarse particles at different velocities and with different suspension rheological conditions. As shown in the figure, the stable-turbulent (S-T) flow regime lies above the transitional deposition boundary defined by the red line .

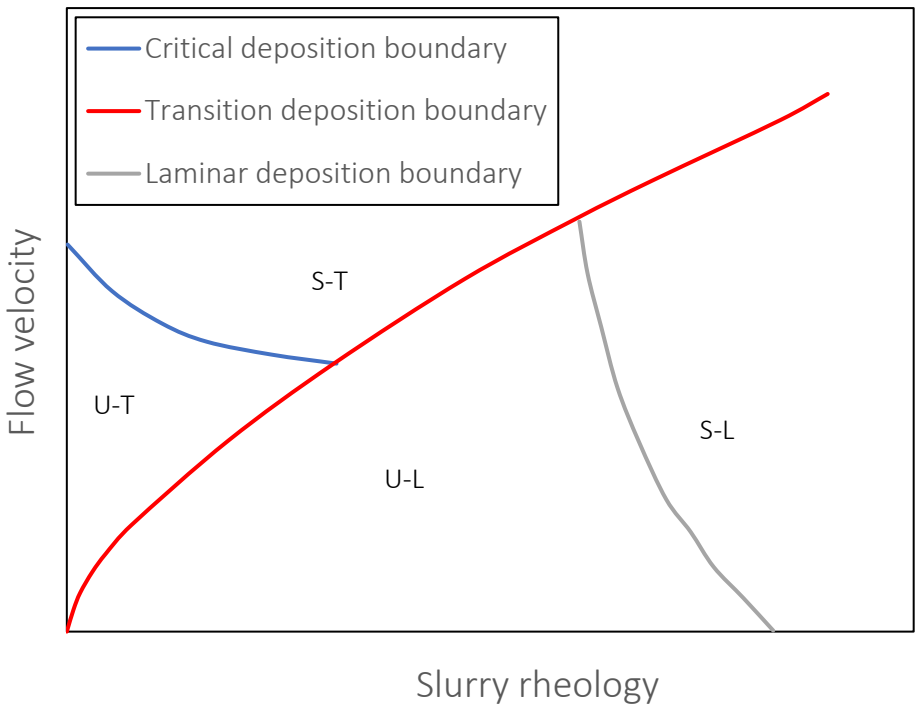

Figure 1-4: Flow regime plot for coarse particle transport in suspension (Adapted from Poloski et al. [17]).

The determination of the velocities on this boundary strongly depends on the rheology of the mixture, i.e. the fine-coarse particle suspension. This boundary velocity, which is often referred to as laminar-to-turbulent transition velocity (V_t) can be estimated indirectly using the Wilson-Thomas turbulent flow model [19] or from the Bingham plastic transition Reynolds number [18]. In these equations, the mixture's yield stress is a key input parameter. Below the transition boundary lies the laminar flow regimes. It is known that under laminar flow conditions, coarse particles settle [3], but as yield stress increases coarse particles are suspended by dispersive yield-stress forces [18] hence, providing flow stability.

To ensure that the tailings treatment for dewatering and drying MFT addresses tailings placement challenges, it is important that the coarse and fine solids are totally transported and discharged to the DDA. Therefore, transporting these suspensions under stable flow conditions in the pipeline is essential. As discussed above, this condition can be achieved under both laminar and turbulent flow regimes, but the mixture yield stress must be known. Additionally, the mixture yield stress affects DDA capacity and performance.

1.2 Problem Statement

The importance of yield stress in pipeline transport and placement of bimodal suspensions has been discussed in Section 1.1. The determination of yield stress for fine particle suspensions (< $44\mu m$) is a relatively straightforward process because particle settling is not an issue. Fine particle suspension rheology depends on many variables such as particle size, particle size distribution, pH, mineralogy, water chemistry, previous shear condition, and solid concentration [13, 20, 21]; consequently, predictions of yield stress are nearly impossible and thus experimental measurements are heavily relied upon. However, with a comprehensive rheological measurement program, correlations can be developed to predict the yield stress of fine particle suspensions for a specific operation [4].

In the case of bimodal suspensions, the presence of fast-settling coarse particles further complicates the rheological measurements. For instance, if coarse particles settle too quickly, uniform solid distribution of the bimodal suspension is altered which can significantly affects rheological measurements [22]. Therefore, there is a need to scalp (i.e. remove) the coarse

particles before conducting rheological characterization, but this process is tedious and time-consuming. In addition, alternative approaches to obtaining rheological parameters through pipe-loop testing is costly since large sample volumes are required [4]. These rheological measurements are very difficult, and costly [23]. Evidence showing the difficulty in making these types of rheology measurement is provided in Figure 1-5. This figure shows a comparison of Bingham yield stress ratios, which is the yield stress of a bimodal suspension to that of the corresponding fine particle suspension, obtained by different researchers. This figure shows significant data scatter. For instance, Paulsen's data [11] show a significant difference in the magnitude of yield stress ratio at $C_s = 0.2$ even in the same dataset.

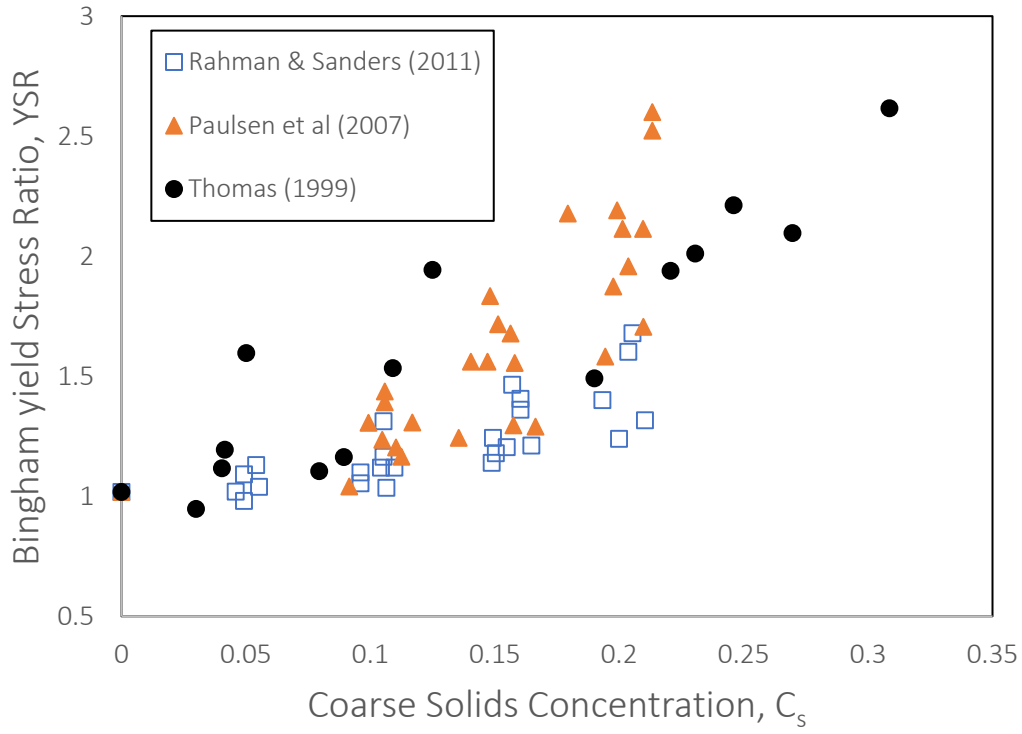

Figure 1-5: Comparison of Bingham yield stress ratios obtained by different researchers (Adapted from Rahman [13]).

The challenges of determining the yield stress of this suspension from rheological measurements could be addressed by predicting the yield stress, but available semi-empirical correlations rely upon experimentally determined fitting values. Therefore, reliable data are required to improve upon the predictive capacity of these correlations.

1.3 Research Objectives

If a correlation exists that can accurately predict the yield stress of these fine-coarse particle suspensions, then fewer measurements of, at least, the fine-particle suspensions will be needed to make accurate predictions. The challenge, however, remains that available semi-empirical correlations cannot accurately predict the yield stress of bimodal suspensions. One of the reasons limiting the predictive performance of these models/correlations is due to the inadequate understanding of the interaction mechanisms of coarse particles in a fine-particle suspension [24], and the effects of coarse particle properties(e.g. size, shape) on the bimodal suspension yield stress. Therefore, the main aim of this work is to answer the following questions:

- *What is the actual increase in yield stress of a fine suspension by the addition of coarse particles? and how can this be measured accurately?* This information is vital for the development of physical models to accurately predict the yield stress of bimodal suspensions. To have an accurate and general model, the fundamental physical interaction mechanism between constitutive coarse and fine fractions of the bimodal suspension is required. However, this interaction is yet to be fully understood [24], which leads to:
- *How do solids (coarse and fines) interact in a bimodal suspension to augment yield stress?* The interaction mechanism strongly depends upon the coarse particle concentration and properties (e.g. size, shape, particle size distribution).

In an attempt to answer these questions and to accurately predict the yield stress of bimodal suspensions, three shear yield stress correlations (Thomas [25], Deltares [26], and Lim et al. [23]) were tested to investigate their predictive capabilities. These correlations were chosen because the Deltares [26] and the Lim et al. [23] models have assumed that the coarse particles do not contribute directly to the rheology of bimodal suspension, hence, providing at least some explanation by which the coarse particles augment yield stress of fine-particle suspension.

1.4 Thesis Outline

Chapter 2 provides information about the rheological models used to describe the flow behaviour of suspensions and the rheometry techniques used to obtain the yield stress. It also discusses the context needed to understand the mechanisms and the contributions of different particle types to rheology. The gaps from previous works are also highlighted in this chapter. Lastly, the three models tested in this study are introduced.

In Chapter 3, the experimental materials, equipment, and procedures used in this work are covered, and the methods adopted for validating the procedures and results are discussed. The materials section provides information about the properties and sources of the sands, kaolin clay and MFT used. The equipment used for particle characterization, mixing and shear conditioning of suspensions, as well as the rheometer used for rheological measurements are described. In addition, information about the test matrices, procedures for estimating the key parameters of the Lim et al. [23] model and validation protocols are discussed in this chapter.

Chapter 4 contains the results obtained from the experiments conducted and subsequent analyses. In this chapter the contributions to yield stress augmentation by coarse particle size and shape as well as the performance of the correlations tested are described. Chapter 5 provides the conclusion and recommendations based on the experiments and analyses that were conducted during this research project.

1.5 Research Contributions

This study has contributed to the existing knowledge on the yield stress augmentation of bimodal suspensions, and these contributions are listed below:

- The study provides additional information about the significance of coarse particle size and substantiates the effect of coarse particle shape on yield stress augmentation.
- A shear sensitivity protocol was developed when producing the coarse and fine particle suspension tested in this study; a step missing from previous works.
- The study further emphasizes the value of using the vane viscometer for reliable yield stress measurements.

- It provides relevant information on the performance of the three correlations tested, and more importantly, the Lim et al. correlation was applied on oil sands material. In contrast to the previous application were the key parameters (i.e. the gel point and close packing fraction of fines) were assumed, here, these parameters were experimentally estimated.
- It provides new streams for future work to further improve upon the knowledge of yield stress augmentation of fine particle suspension by coarse particle addition in existing literature.

1.6 Author's Contributions

While the bulk of the experimental work and analysis was conducted independently by the author, many other people made important contributions. For instance, to ensure the contribution to yield stress increase associated with coarse particle shape and size is clearly studied, the selection of sands and the formulation of an experimental matrix was completed by the author with the assistance of Nitish Ranjan Sarker and Dr. Sanders.

Also, to ensure accurate yield stress augmentation measurements are made, an improved experimental program, which involves the preparation of suspensions as well as improved rheological measurements using the vane viscometer, were completed by the author with the assistance of Ghassan Khan and Erin Bundy. Other experimental measurements and analyses to determine the gel point and close packing fraction of kaolin were completed by the author. The author also completed the data analyses which tested the performance of the three semi-empirical correlations. In addition, SRC provided experimental data for this analysis.

The organization of thesis content was completed by the author through invaluable reviews and contributions from Dr. David Breakey and Dr. Sanders.

Chapter 2 LITERATURE REVIEW

2.1 Rheological Models

Rheological models describe the flow behavior of fluids and in rheological context, fluids are broadly classified as either Newtonian or non-Newtonian. Newtonian fluids obey Newton's law of viscosity expressed as:

$$\boldsymbol{\tau = \mu\dot{\gamma}} \tag{2.1}$$

where a linear relationship exists between the shear stress (τ) and the time rate of shear strain (commonly referred to as a shear rate) ($\dot{\gamma}$) and the viscosity (μ) is the slope of the linear relationship [27].

Fluids whose flow behavior cannot be described by the relationship given in Equation (2.1) are said to be non-Newtonian. Unlike Newtonian fluids, they are not characterized by a constant slope of μ, and usually viscosity alone is insufficient to describe their flow behavior because it is dependent on shearing conditions and/or shear history. The flow behaviour of these fluids is predictable and can be described by time-independent fluids models.

The focus in this work is on time-independent non-Newtonian fluids, specifically the viscoplastic class: fluids that require a certain minimum value of shear stress to induce their flow. The suspensions investigated in this work showed this flow behavior and have also been described with time-independent non-Newtonian viscoplastic models by several researchers e.g. [13,24, 27]. Although there are several models to describe viscoplastic fluids, clay suspensions have often been modeled using any of the Bingham fluid models [24], since it closely approximates the flow behavior. The Bingham model takes the form

$$\boldsymbol{\tau = \tau_B + \mu_B\dot{\gamma}} \tag{2.2}$$

The Bingham fluid model, given in Equation (2.2), and it is a two-parameter model with yield stress and viscosity terms. These terms can be determined from a flow curve (rheogram) given by the relationship between shear stress and shear rate as shown in Figure 2-1. The rheogram allows for comparison of different types of models. The estimated yield stress from the flow curve of a

Bingham fluid is referred to as Bingham yield stress and this is directly used in pipeline design and operation.

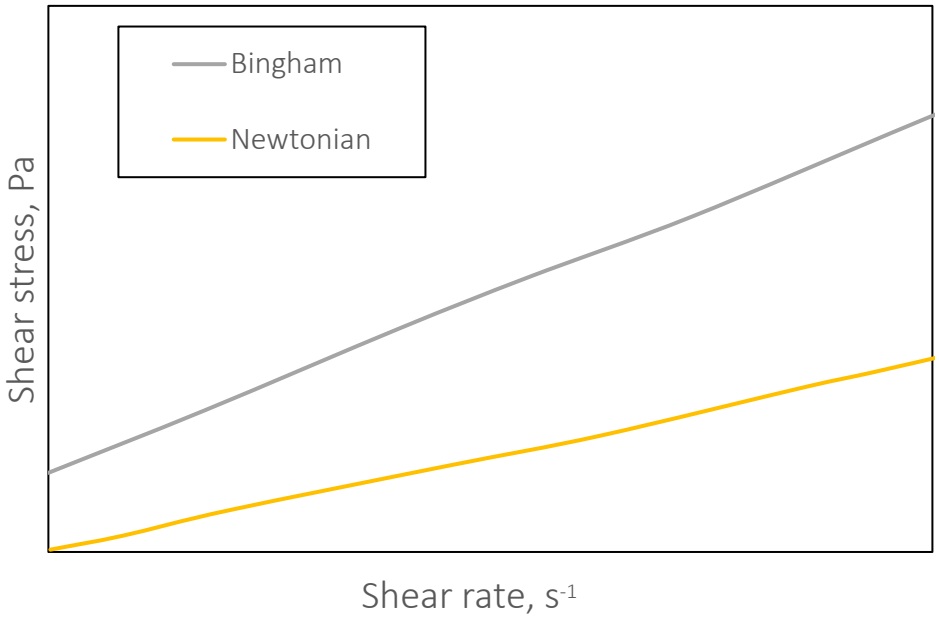

Figure 2-1: Rheogram for fluids satisfying typical rheological models.

Yield stresses are commonly seen with fluid-particle systems where ultra fine solids are dispersed in liquids under conditions favoring particle-particle attraction [28]. These fluid particle systems (often referred to as suspensions or slurries) exhibit both pseudosolid and liquid-like behavior when subjected to different stress thresholds, and the critical stress threshold where a transition exists from pseudosolid to liquid-like behavior is termed the yield stress [28]. The yield stress in Figure 2-1 is the y-intercept of the flow curve. Many other materials, such as ointments, paints, and grease show yield stress (viscoplastic) behavior [28].

Yield stress as a flow parameter is a critical suspension property in the storage and transport of thickened tailings. Thickened tailings as discussed in Chapter 1 contains clay, sand and coagulant/polymer flocculant, and the clay component constitutes the fine particle fraction of the suspension. The fine particle fraction of a typical bimodal suspension has been reported to be responsible for the non-Newtonian yield stress behavior [13] since it consists mostly of clay particles that are known to have a high surface area-to-volume ratio [29].

2.2 Rheometry

In a simple term, rheometry is the process of determining the rheology of a material. Fluid rheology is often measured with a rotational viscometer [17], and many previous investigations have collected rheological information for their bimodal suspensions with a concentric cylinder viscometer [11, 14]. The device gives the Bingham yield stress and plastic viscosity from the flow curve analysis which can be used directly in pipeline calculations [27, 30, 31].

In this study, the vane viscometer has been used exclusively to measure the yield stress of bimodal suspensions, although some yield stress measurements for kaolin-only suspensions were also completed using the concentric cylinder geometry. These measurements were required in determining the close packing fraction of kaolin using Liu's model [32] (see Chapter 3, Section 3.5). The working principles of the vane rheometers will be discussed in the following sections, since it was the primary technique to measure rheology of suspensions in this study.

2.2.1 Vane Viscometer

In this study, the vane geometry was used to directly measure the yield stress of all fine particle and bimodal suspensions. The vane itself consists of six sets of thin blades equally spaced around a shaft as shown in Figure 2-2. The vane viscometer is always operated at a very low shear rate (i.e. < 0.1 RPM) when immersed in a fluid or suspension. The torque is measured over a set time and the stress corresponding to the maximum torque reached before a subsequent decline is defined as the true or vane yield stress [28] as shown in Figure 2-3.

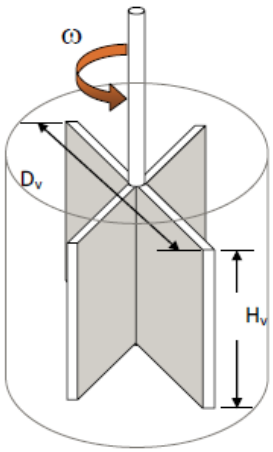

Figure 2-2: Schematic of the vane geometry [9]

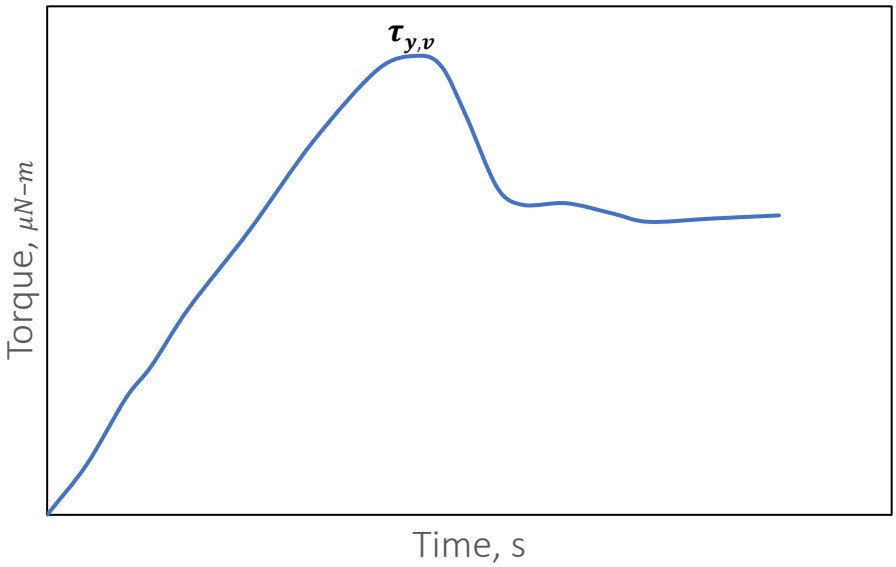

Figure 2-3: Graph showing yield stress in a rate-controlled mode.

The vane yield stress is estimated using [20]:

$$\boldsymbol{\tau_{y,v} = T_{max}/K_v} \tag{2.3}$$

$$\boldsymbol{K_v = \frac{\pi D_v^2}{2}\left(\frac{H}{D_v} + \frac{1}{3}\right)} \tag{2.4}$$

where K_v is the vane constant defined by the vane dimensions,$\tau_{y,v}$ is the vane yield stress, and T_{max} is the maximum torque.

The development of this relationship is based on the assumptions that [28, 33]:

- The fluid is sheared along an imaginary cylindrical surface created by the vane blades
- The stress distribution is uniform along this imaginary cylindrical surface.

The vane technique was adopted from soil science where it was first used for soil shear strength characterization [34, 35, 36]. It was adopted to address common issues and limitations associated with operating the rotational rheometers at low shear rate such as wall slip [20]. Since its adoption for measuring the yield stress of concentrated suspensions, it has been widely used by many researchers for different materials including: pulp, grease, and inorganic colloidal suspensions such as clay, mud, iron-oxide, alumina, titanium oxide, zirconia [33]. It has also been

used for poly-dispersed systems of fine-and coarse-particle suspensions. For example, Koehler and Fowler [30] have used the vane together with other rotational rheometers to measure the rheological parameters of concrete and mortar suspensions. In other investigations, it has been used on fine suspensions and sand mixtures [30, 37, 38] . Overall, these works have reported satisfactory results using this device for poly-dispersed systems.

The issue of wall slip commonly associated with the concentric cylinder is not a concern using the vane, because, unlike the concentric cylinder, where the suspension is sheared against the walls of the cup and rotor, with the vane sensor, the shearing occurs within the suspension layers [28]. Therefore, the vane was adopted in the present investigation because it provides more direct, easier, and quicker measurements than the concentric viscometer. Concerns about the settling of coarse particles are minimized with the vane because it is operated at very low spindle speeds. Also, annulus blockage that can occur when the coarse particles are large compared to the viscometer gap width is circumvented using the vane viscometer.

To appreciate how coarse solids augment the yield stress of a non-Newtonian bimodal suspension, the origins of yield stress in fine particle suspensions need to be understood. Likewise, the independent contributions by the coarse and fine solids of a bimodal suspension to rheology need to be understood. In the following sections, the individual particle-particle interaction and particle-fluid interactions by these solids are discussed.

2.3 Fine-Particle Suspensions: Particle Interaction and Rheology

The rheology of fine particle suspensions has been studied by different researchers, e.g. [14, 28, 37, 39]. When clay particles are dispersed in a fluid such as water, their interaction in this system is governed by surface forces [39]. This interaction is dictated by the combination of attractive van der Waals and repulsive electrostatic double layer forces [37, 40]. Depending on the order of magnitude of each of these forces, the resultant particle-particle interaction can either be attractive or repulsive and this net interaction largely determines the rheology of the clay suspension.

For a clay suspension where the resultant surface force is repulsive, particles are not strongly attached to each other and they remain dispersed in the colloidal suspension [39] as

illustrated in Figure 2-4 (a). At this condition, the suspension will not have a yield stress or a very low one. At high concentrations a small yield stress is inevitable

Conversely, if resultant surface force is attractive, the clay surface charge favors net attractive force and clay particles attach to each other to form flocs, which are defined as clusters of particle with enclosed water by Michaels and Bolger [41] (see Figure 2-4 (b)), and groups of flocs called aggregates can form a network structure as shown in Figure 2-4 (c). Depending on the concentration of fine particles at this condition, a spanning networked system of aggregates and flocs can exist. This network can form as long as the concentration is higher than a critical concentration called the gel point or percolation threshold [42], which is the minimum concentration required for the onset of a yield stress. This networked structure is responsible for the yield stress of a clay suspension system.

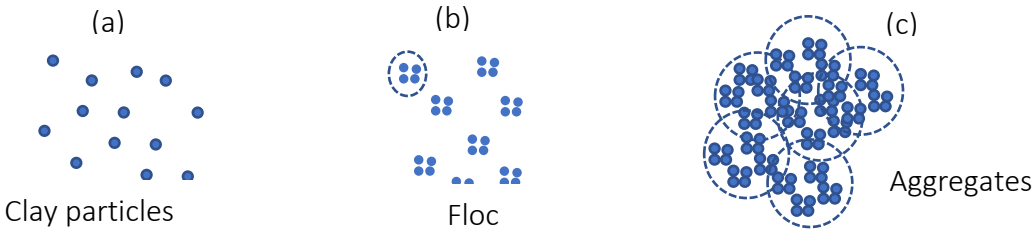

Figure 2-4: Illustration of fine particle association (a) Clay particle (b) Flocs (c) Aggregate. The dotted lines show a group of primary particles becoming a floc in (b) and group of flocs becoming aggregates in (c).

Since several studies have shown that kaolin is an abundant clay mineral found in oil sands [42] and because kaolin has been used by many oil sands researchers e.g. [37, 42] who showed that its rheological behavior closely matches that of mature fine tailings (MFT) [37], kaolin is therefore used in this work as an analogue. Kaolin is a clay mineral with charged plate-like surfaces [24, 40]. When dispersed in water, the surface charge distribution can be altered by the ionic species and concentration as well as pH. Low pH promotes kaolin particle aggregation which in turn increases the yield stress. When the ionic species and concentration are increased, electric double layer is decreased to promote particle-particle interaction. The attractive interaction produces flocs and aggregates.

In a flocculated kaolin suspension, the flocs structures enclose and trap a portion of the continuous phase, which reduces the volume of the unbounded free water. The reduction of the free-water volume fraction leads to an increase in the viscosity and yield stress of the suspension.

2.3.1 Effect of Particle Size and Concentration on Yield Stress of Fine Suspensions

The fundamental work of Thomas [43] shows that particle size plays a significant role in determining a suspension's yield stress. Zhou et al. [44] investigated the effect of size of four differently sized aluminum oxide (Al_2O_3) particulates on yield stress. They showed that, approximately, $\tau_y \propto 1/d_p^2$, which indicates that the surface area of particle is important for the development of a yield stress.

The effect of the concentration of fine particle on yield stress has been investigated by many other researchers, e.g. [14, 43, 45, 46]. With increasing concentration of fines, particle-particle interactions are increased, which has a direct relationship to the suspension yield stress [14, 43, 45, 46].

2.4 Coarse-Particle Suspensions: Particle Interaction and Rheology

Unlike fine particle suspensions, water-continuous coarse-particle suspensions exhibit Newtonian behavior. The rheology of these settling slurries is determined by body forces such as hydrodynamic forces, frictional forces and particle-particle collisions [47]. This contrasts with what is seen for fine particle suspensions, whose rheology is determined primarily by surface forces. For coarse particle suspensions, there is no evidence that coarse particles contribute to the development of a networked structure that can account for a yield stress [14].

The underlying concepts of how the particles interact in this system to increase viscosity for neutrally buoyant suspensions might be useful to understand how coarse particles contribute to a yield stress increase in a fine particle suspension. In addition, it is useful to explain possible misconceptions about the proposed interaction mechanisms of coarse particles in a yield stress fluid.

The addition of non-interacting coarse particles to a Newtonian fluid such as water contributes to an increase in the Newtonian viscosity, provided that the particles remain

suspended [47]. This increase in viscosity was first explained by Einstein [48] for the case of monosized, non-interacting spheres for dilute suspension with concentrations < ~ 0.02 (v/v) . The viscosity change is known to be caused by different mechanisms, the magnitudes of which are determined by the solids concentration. The mechanisms include the hydrodynamic effect, particle-particle interaction, and frictional effect. The hydrodynamic effect includes the excluded volume and lubrication contact [16]. For the case of excluded volume effect which manifest at low concentration, coarse particles occupy space originally filled with fluid to reduce the layer of sheared fluid to increase viscosity. In the case of lubrication contact, which exist at a higher solids concentration, the viscosity of the suspension increases because fluid forces between adjacent particles increases. At high coarse concentration, the viscosity increase is predominantly due to particle-particle and frictional force effects. Table 2-1 below summarizes these effects.

Table 2-1: Coarse particle concentration and interaction mechanism in Newtonian carrier fluid [16]

Concentration of coarse particle, C_s	Particle -particle /particle-fluid interactions mechanisms
0.05-0.1 (v/v).	Excluded volume: Reduced fluid sheared layer
≥ 0.1 (v/v)	Lubrication contact: Increased fluid force due to reduced distance
$C_s \rightarrow C_{max,s}$	Collison, jamming, friction: Direct particle contact

Besides particle concentration, the effect of coarse particle shape also contributes to viscosity increase and this is summarised in the following section.

2.4.1 Effect of Coarse Particle Properties on Viscosity of Coarse Suspensions

Thomas [49] and Sumner et al. [13] investigated the effect of coarse particle shape on viscosity. Generally, angular or rounded particles produce higher viscosity than spherical particles for suspensions at the same solids concentration.

Landel et al. [50] incorporated the maximum solid concentration, $C_{max,s}$, which is the maximum packing fraction of solid in the system to account for the effects of shape and particle size distribution on rheology of their coarse particle suspensions. Also, Thomas [25] and Chong et

al. [51] have included $C_{max,s}$ to their model to account for the contribution caused by coarse particle shape. Schaan et al. [52] also proposed a semi-empirical model that suggests the mechanism of interaction of coarse particle is strongly determined by linear concentration, which also considers the effect of shape. Based on their investigation, the relative viscosity is given by:

$$\frac{\mu_m}{\mu_L} = 1 + 2.5C_s + 0.16\lambda^2 \tag{2.5}$$

$$\lambda = \frac{1}{\left[\left(\frac{C_{max,s}}{C_s}\right)^{1/3} - 1\right]} \tag{2.6}$$

where λ is the linear concentration of coarse particles. It is the ratio of particle diameter to distance between adjacent surfaces and it approaches infinity as the concentration particle approaches the maximum packing concentration, $C_{max,s}$. Results from these works showed that the ratio, $C_s/C_{max,s}$, reasonably captures the effect of coarse particle shape and shows that it has relevance to coarse particle suspension rheology.

2.5 Bimodal (Fine-Coarse Particle) Suspensions

Both fine- and coarse-particle suspensions have been discussed independently in the previous sections, and the fact that contributions to mixture viscosity from each of these constituent solids are governed by different forces. A number of studies have been conducted to understand the rheological behavior of bimodal suspension systems containing both fine and coarse particles, e.g. [24, 25, 37, 41, 50]. The general conclusion drawn from these studies is that the addition of coarse particles to a fine suspension augments the rheology of the system. However, the authors of these studies have provided different mechanistic descriptions of how rheology augmentation develops with coarse particle addition, and they have also reported different magnitudes of augmented yield stress [12]. The implication of this discrepancy, i.e. in mechanism and data, is that actual physics and contributing physical parameters may not be captured in models or correlations.

Several issues prevent current models or correlations from being effective. The main issues are described in the following sections.

2.5.1 Proposed Mechanisms for Rheology Augmentation

The mechanism for the rheology augmentation of fine particle suspensions by coarse particles remains a debatable topic [11]. Understanding the physical interaction of the coarse particles with flocs in a fine suspension system is essential, not only to explain how the increase in yield stress is developed with coarse particle addition, but to know the factors contributing to the augmentation process.

Past researchers have frequently proposed different mechanisms of interaction, for example, Coussot and Piau [46] suggested three reasons that could explain the increased yield stress observed in their investigation: (a) increased dry solid surface of coarse particles, which consequently reduces the water content; (b) friction caused by particle–particle contact; and (c) *crowding effect*, the concept that coarse particles occupy the space originally filled by the fine suspension and then reduces the distance between aggregates to promotes interaction.

Another possible mechanism, based on the investigation of Sengun and Probstein [53] on coal particles, is the concept of *excluded volume*, which applies up to moderate coarse concentrations of 0.3 (v/v). In this description, it is suggested that coarse particles in the clay suspension act independently in the clay-water system and only take up space to reduce the sheared volume occupied by the fine suspension (carrier fluid). At higher concentrations, a lubrication contact effect is proposed, where the carrier fluid within the matrix of the coarse particles is "squeezed". Hence, according to Sengun and Probstein [53], coarse particles did not participate in any form of attractive association with the clay particles and act in similar fashion as it would in a Newtonian fluid as previously discussed in Section 2.3.

The explanation of Sumner et al. [13] of the augmentation mechanism is also based on the *crowding effect*. They assumed that the increase in yield stress results from an increase in the effective concentration of 'rheologically-active' clay particles and that the coarse particles are inert, with no attractive or repulsive forces influencing the rheology of the suspension [11]. Since their proposed relationship underestimated the results, their work suggests that the crowding effect is insufficient to explain the interaction at higher concentration. The difference was ascribed to the shape of the coarse particles, specifically that there is an increase in the effective solid volume

fraction of non-spherical particles as compared to spherical particles when placed in a shear field. This higher effective solid volume fraction results in a higher yield stress at high solids concentration.

2.5.2 Measurement of Yield Stress Augmentation

Traditional rheological measurements of non-Newtonian suspensions containing some portion of settling particles are difficult and several studies have reported the inaccuracies in obtaining these measurements using a rotational viscometer [22, 23, 54, 55]. Some researchers have adopted the redesign of the concentric cylinder viscometer to circumvent measurement challenges due to the presence of fast-settling coarse particles in a fine suspension. For example, Gustafsson et al. [22] used modified concentric viscometer to determine the rheology of magnetite. According to this investigation significant data scatter was observed as shown in Figure 2-5. The data scatter was pronounced and non-systematic at high solids concentrations, which suggests particle jamming due to gap limitations of the device. This finding is indicative of the difficulty generally experienced using this device and the very tedious task to make accurate measurements with the conventional couette viscometer.

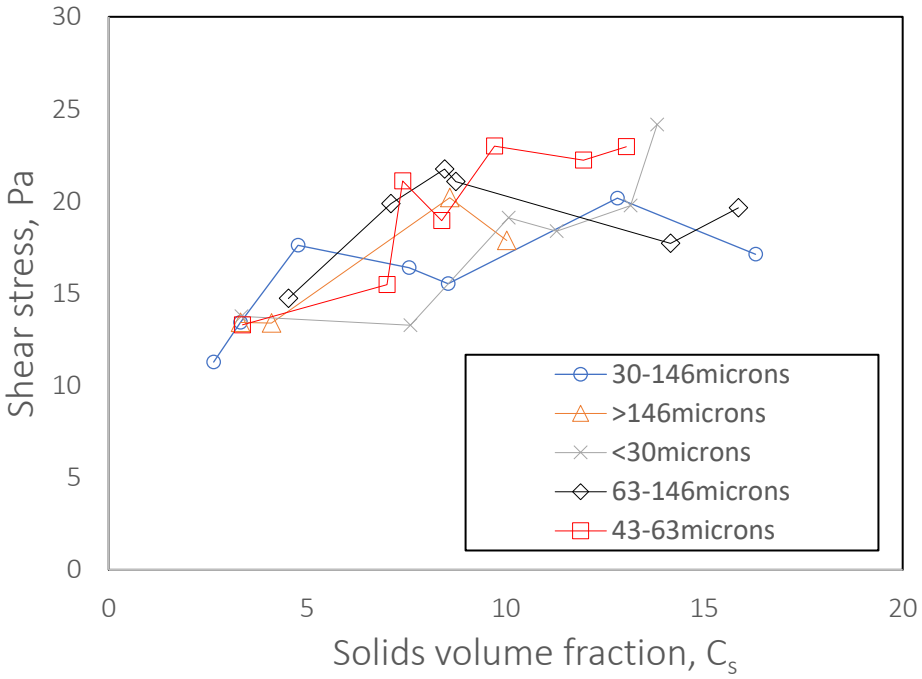

Figure 2-5: Shear stress at different solids volume fraction for five different sands (Adapted from Gustafsson et al [22]).

In other recent investigations significant disparity exists in the magnitude of yield stress measured for suspensions containing clay and coarse particles [14]. The disparity is partly because of the difficulty encountered using the concentric viscometer with issues such as settling of coarse particle during high speed rotation (a condition that changes the uniform distribution of solids), wall slip, and annulus blockage. Again, the disparity in the augmented yield stress measurements is exemplified by comparing the Thomas [25], Paulsen [11] and Rahman [14] data which was earlier discussed and shown in Figure 1-5. It can be inferred from this comparison that the measured magnitude of the yield stresses of these bimodal suspensions disagree, even for similar material and similar solids concentrations. This disparity in augmented yield stress data makes the use of correlations based on these data highly suspect. In other words, to accurately predict the augmented yield stress of a bimodal suspension, accurate rheological measurements are essential.

In more recent rheological investigations of settling suspensions, vane viscometers have been used to obtain augmented yield stress [12, 23, 26]. A few vane yield stress ratio measurements made by Rahman [14] present less scattered data compared to the counterpart concentric cylinder measurements as shown in Figure 2-6 for the limited data collected.

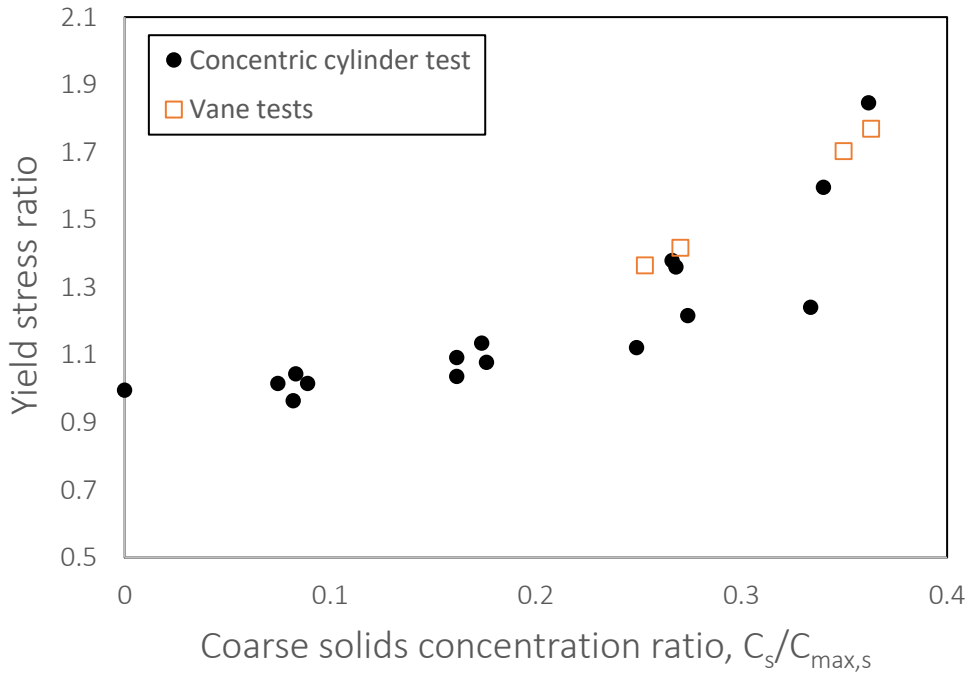

Figure 2-6: Comparison of data scatter between yield stress ratio obtained from concentric cylinder and vane viscometers [14].

Although the Bingham yield stress is the actual parameter used in pipeline design, taking vane measurements was found to be appropriate in this study. The reason is that a recent study conducted by Spelay at al. [12] shows an excellent agreement between the vane and Bingham yield stress ratios (obtained from concentric cylinder viscometer measurements) for low concentrations of coarse particles. The comparison is reproduced in Figure 2-7. Vane yield stress values are always less than Bingham yield stress than (48% lower in one particular study [11]), but in terms of their ratios, these quantities are similar as shown Figure 2-7.

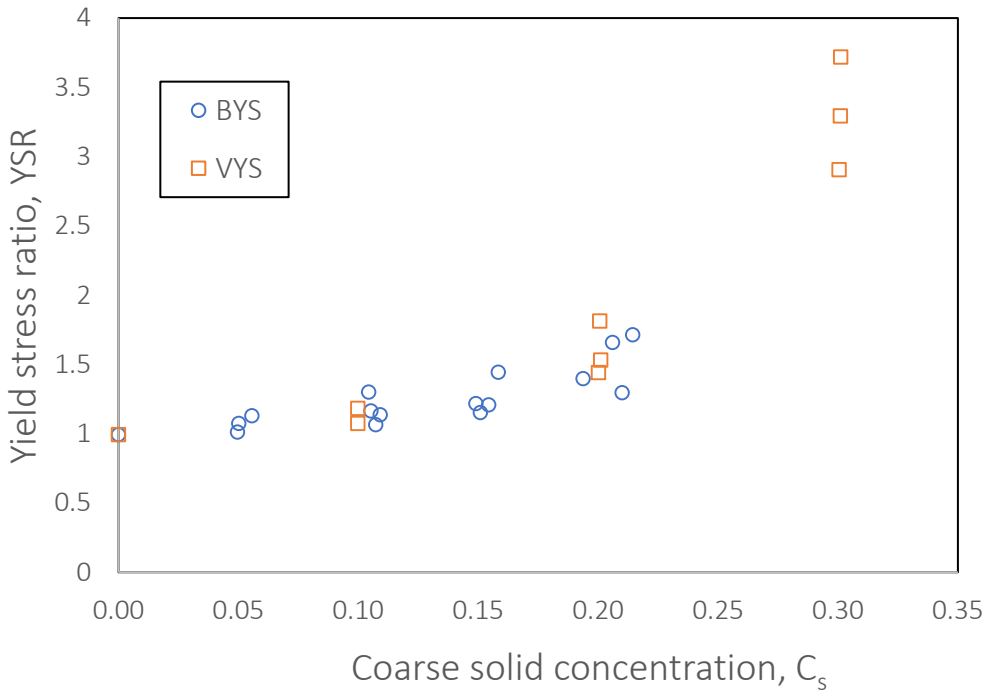

Figure 2-7: Comparison of vane and Bingham yield stress ratios of kaolin-sand mixtures at low concentration of coarse particles [12]. VYS-vane yield stress sand BYS-Bingham yield stress.

2.5.3 Influence of Coarse Particle Properties

Paulsen [11] and Rahman [14] have contributed to the available knowledge of the rheological augmentation of bimodal suspensions by investigating the effect of shape and size of the coarse particles. For instance, Paulsen [11] studied the effect of coarse particle concentration and shape on the rheological augmentation of kaolin suspensions. In his work, three different coarse particles of similar particle size distribution, but of different shape were studied. From this investigation, angular particles were found to increase the yield stress of the fine suspension more than rounded

particles, and this strongly suggests that the effect of the shape of the coarse particles is significant. Also, investigation of the effect of coarse particle concentration and particle size was undertaken by Rahman [14], who used two different sands with different particle sizes (d_{50}) and different shapes (angular and non-spherical rounded sands). From those results, it appears that, for the size range of coarse particles tested in his study, coarse particle size did not cause a significant increase in the yield stress of the kaolin suspension. But since he did not study a broad range of particle sizes, the effect of size cannot conclusively be considered insignificant for all cases.

Therefore, there is a need to further investigate the effect of coarse particle shape and size. The need remains because the trend observed by Rahman [14] does not fully eliminate size as a factor, since just two coarse particle types were considered, and these sands differ in both shape and size. Also, the limit of the coarse volume concentration investigated in that work was 0.20 (v/v), which is relatively low and does not allow a better understanding of the augmentation at higher concentration. This limit was imposed by the choice of measurement device in his work.

Considering the difficulty in identifying the correct interaction mechanisms, and in the light of other challenges discussed above i.e., measurement difficulties and the contributions to yield stress increase by coarse particles properties, performance of correlations to describe the yield stress of a bimodal suspension system, the data available are insufficient. It is evident that to have accurate correlations, accurate rheological measurements are required.

Having discussed some of the works done and highlighting the challenges and gaps in this field of study, some of the available yield stress correlations will be briefly discussed in the following section.

2.6 Semi-Empirical Shear Yield Stress Correlations

Past researchers have developed many semi-empirical correlations to describe the yield stress of bimodal suspensions such as kaolin-sand suspensions. Here, some of the correlations that have been used are presented. The semi-empirical correlations discussed here are those of Thomas [25], Deltares [26], and Lim et al. [23]. Two of these models, Thomas [25] and Deltares [26], have been selected since the effect of coarse particle shape and concentration are captured with the concentration ratio, $C_s/C_{\max,s}$, which is expected to improve the predictions and accuracy of these models. These models also find application in the oil sands industry. For the Lim et al. [23] correlation, it provides a microstructural analysis for yield stress development and increase with addition of coarse particles.

2.6.1 Thomas [25] Correlation

Thomas [25] used the analogy of the viscosity expression formerly used by Landel et al. [50] to fit the yield stress measurements of narrowly sized sand and mine tailings mixtures. The mixture-to-carrier yield stress ratio was expressed as a function of coarse solids concentration and it is given by:

$$\frac{\tau_{y,m}}{\tau_{y,f}} = \left(1 - \frac{C_s}{AC_{max,s}}\right)^{-2.5} \tag{2.7}$$

where $\tau_{y.m}$ is the yield stress of fine-coarse suspension, $\tau_{y,f}$ is the yield stress of fines-only suspension, A is an empirical constant, C_s is the coarse solid volume concentration and $C_{max,s}$ is the maximum coarse solid concentration. The value for $C_{max,s}$ was assumed to be 0.6, and $A = 1.5$ as the value that gave the best fit to the measured values of Bingham yield stress.

This semi-empirical expression has also been used by other researchers [11, 14,56] to fit their experimental data, but in all cases, the values of A obtained to best fit their Bingham yield stress data were different. For instance, Paulsen [11] obtained a value of 1.9, while Rahman [14] used 2.9. This variation suggests there is a difference in the magnitude of yield stress obtained from these investigations, even when similar coarse particle concentrations and particle properties were studied (e.g. by Paulsen [11] and Rahman [14]). It should be noted that Rahman

collected a very limited number of vane yield stress measurements, and for the vane measurements, the value of A =1.9 provided the best fit. According to Rahman [14] comparative analysis of the Bingham and limited vane yield stress data fit to the Thomas model, a single value of A described the vane data, but the Bingham yield stress data fall between A = 4.2 and 1.9 as shown in Figure 2-8. As this figure shows, the fitting constant obtained with the vane data overpredicted most of the Bingham yield stress ratio data, even though the data scatter spanned between the two fitting values. Similarly, the lower bound fit underpredicted the vane data. If the actual magnitude of the augmented yield stress is captured in this measurement, then a single fit would be sufficient to predict these data sets. This argument further supports the collection of more vane yield stress measurements. Paulsen [11], who compared the accuracy of different models, concluded that this expression closely described the augmented behavior for a coarse concentration up to 40% of $C_{max,s}$.

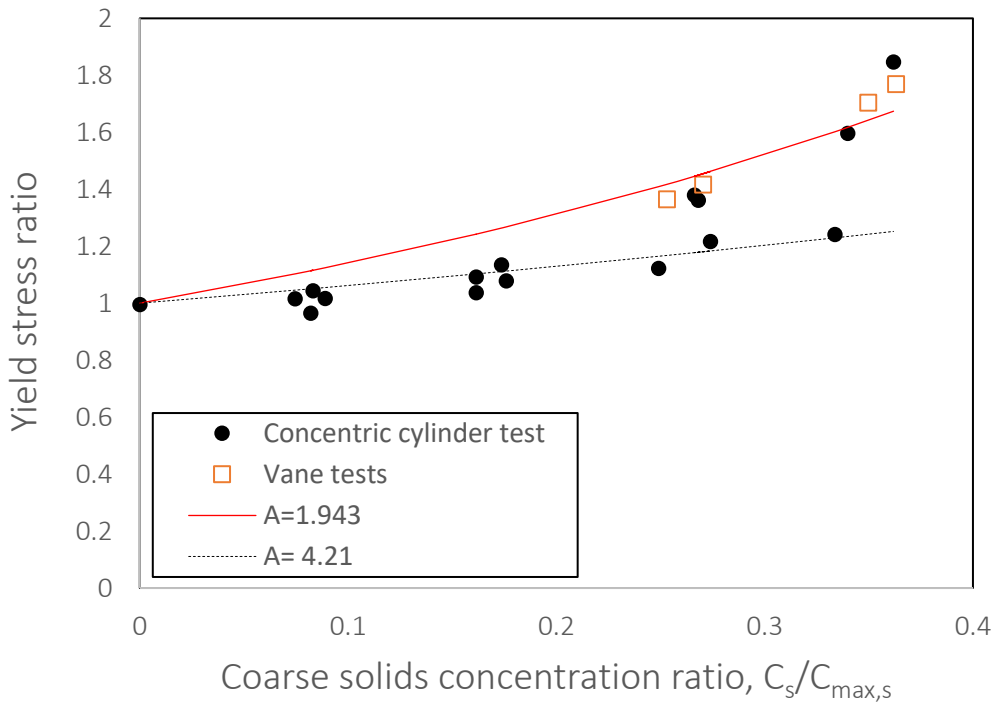

Figure 2-8: Comparison of different yield stress measurements and performance of the Thomas correlation with different fitting values of A (Adapted from Rahman [14])

This semi-empirical correlation is more widely used in the oil sand tailings industry [57] and it does not require the determination of any other physical quantity for its application. To apply this model, the expression is fit to yield stress data of a bimodal suspension to obtain the fitting parameter, A,

analytically. The predictive performance is then tested using the value obtained on the yield stress measurements of other bimodal suspensions containing different type of sand.

2.6.2 Deltares [26] Correlation

This semi-empirical correlation was introduced by Jacobs et al. [58]. They modelled the rheology of slurry based on water content to fines ratio. This water content to fines, $\boldsymbol{W_f}$, is practically identical to the ratio of water content, W and plasticity index, PI, which is a function of solids and clay volume [26]. This correlation finds application in the oil sands tailings industry. From works recently completed under the umbrella of Deltares, the vane yield stress of suspensions has been predicted by:

$$\boldsymbol{\tau_{y,m} = A'(W_f)^{\beta} e^{\alpha\lambda}} \tag{2.8}$$

where A' (coefficient of yield stress), β (power coefficient), and α (friction coefficient of sand influence) are empirical constants, λ is the linear concentration, and W_f is the water content to carrier fluid which can be obtained with the following relations:

$$\boldsymbol{W_f} = (weight\ of\ fine / weight\ of\ water) * 100 \approx W/PI \tag{2.9}$$

To apply this correlation, the friction coefficient,α, is obtained from the plot of yield stress ratio (i.e. $\boldsymbol{\tau_{y,m}/\tau_{y,f}}$) against λ . The coefficient of λ from the exponential fit of this plot gives the value of friction coefficient,α. For the power coefficient, β, it is obtained as the slope from the plot of $\boldsymbol{\tau_{y,m}}$ against W_f when $\lambda = 0$,i.e. fines-only suspension [26]**.** These fitting values obtained for a fine-coarse mixture can then be used to predict the vane yield stress measurements of other fine-sand mixtures. It should be noted that this expression does not necessarily require any extra measurements, since W_f can be obtained with Equations (2.9).

Van de Ree, [26], Hanssen [57] and Jacobs [58] are among the researchers that have described the vane yield stress of their bimodal suspensions using Equation (2.8), and obtained a reasonably accurate fit using this correlation. The accuracy of this expression can be attributed partly to the presence of the concentration ratio, $C_s/C_{\max,s}$,which accounts for the contributions of coarse particle concentration and shape on the augmented yield stress. This ratio is a part of the linear concentration expression given by λ. The linear concentration contributes to yield stress increase based on concept of lubrication contact.

2.6.3 Lim et al. [23] Correlation

In 2013, Lim et al. [23] presented a constitutive shear yield stress equation which accurately predicted the shear rheology of their bi-dispersed suspensions comprising fines and coarse sand particles. This expression was earlier used by Shane et al. [59] to determine the compressive yield stress of suspension in a thickener system. The relationship is given by:

$$\boldsymbol{\tau_{y,v}} = \left(\frac{\boldsymbol{a}\left(\boldsymbol{C_{cp,m}} - \boldsymbol{C_m}\right)\left(\boldsymbol{b} + \boldsymbol{C_m} - \boldsymbol{C_{g,m}}\right)}{\left(\boldsymbol{C_m} - \boldsymbol{C_{g,m}}\right)}\right)^{-\boldsymbol{c}} \tag{2.10}$$

where $C_{cp,m}$ is the close packing fraction of the mixture, C_m is the total solids volume fraction, $C_{g,m}$ is the gel point of mixture, b = 0.02, and a and c are empirical fitting parameters.

This correlation is applicable over a range of solids concentrations spanning between the gel point and the close packing fraction of the mixture, and this model is valid for suspensions exhibiting a shear yield stress [23].

The first term in the brackets, ($C_{cp,m}$ - C_m), shows how far the total solid volume fraction, C_m, is from the mixture's maximum solid volume fraction; which is how much more solid loading to reach the maximum concentration. This term measures the degree of freedom of particle movement. The second term, (C_m - $C_{g,m}$), which also appears in the denominator show how far the mixture's solid concentration is from the mixture gel point. The mixture gel point defines concentrations of solids, coarse and fine, which allows fine aggregates to stay connected within the matrices of the coarse particles.

According to their work, mixture gel point model is given by:

$$\boldsymbol{C_{g,m}} = \frac{\boldsymbol{C_{g,f}}}{\boldsymbol{1 - S + SC_{g,f}}} \tag{2.11}$$

where, $C_{g,f}$ is the gel point of fines-only suspension and S is the coarse solid fraction calculated as:

$$\boldsymbol{S} = \frac{\boldsymbol{C_s}}{\boldsymbol{C_s + C_f}} \tag{2.12}$$

Therefore, $C_{g,m} = f(S, C_{g,f})$ and when $S = 0$, then $C_{g,m} = C_{g,f}$.

For the close packing fraction of the mixture, $\boldsymbol{C_{cp,m}}$, the analogue of Equation (2.11) is used but the gel point of fines, $C_{g,f}$ is replaced with the close packing fraction of fines:

$$\boldsymbol{C_{cp,m} = \frac{C_{cp,f}}{1 - S + SC_{cp,f}}} \tag{2.13}$$

where $C_{cp,f}$ is obtained either directly from filter press experiments or estimated using appropriate models such as the YODEL presented in Equation (3.8). In this study, the gel point and close packing fraction values have been determined experimentally and the details are presented in Chapter 3.

In this study, Equation (2.10) is re-cast in a power law form. If

$$\boldsymbol{X = \left(\frac{(C_{cp,m} - C_m)(b + C_m - C_{g,m})}{(C_m - C_{g,m})}\right)} \tag{2.14}$$

then Equation (2.10) can be re-written as

$$\boldsymbol{\tau_{y,v} = a' X^c} \tag{2.15}$$

This was done to simplify the model using a power law function which also provides a convenient path to possibly ascribe a set of single fitting parameters (a' and c) for the whole data set, since in Lim et al.'s [23] work, the fitting parameters were a function of coarse fraction.

The theory behind the correlation of the Lim et al. [23] assumes that the coarse particles are 'rheologically inert', which means that the coarse particles take up space and reduce the distance between adjacent aggregates without participating in any form of particle-particle attraction or repulsion. This reduction in space between aggregates promotes the attraction between aggregates through van der Waals forces and hence an increase in the strength of the formed network. This strength is observed as the augmented yield stress as illustrated in Figure 2-9. Although the total solid concentration increases, the yield stress contribution comes from the increased effective solid volume fraction of aggregates within the spaces between the coarse particles.

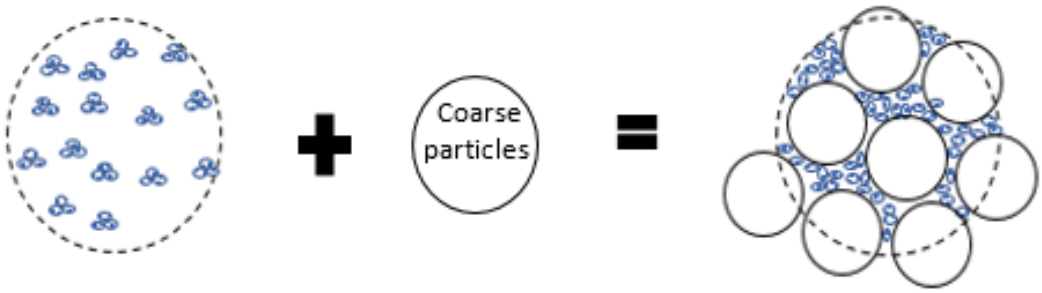

Figure 2-9: Influence and mechanism of coarse particle interaction in augmenting the yield stress of bimodal suspension

It should be noted that no further discussions were made concerning the interaction mechanism of coarse particles in the fine particle suspensions system, but the assumption of sand inertness supports many of the previous works conducted.

In their work, the effect of coarse particle shape and size was not considered, and the close packing fraction of sand, which partly characterizes the shape, was assumed to be 0.64. Compared to other correlations where the effect of coarse particle shape is captured, for the Lim et al. [23] correlation, the limit where it captures the effect of shape is at a very high coarse concentration which is highly difficult and unlikely to be reached.

2.7 Summary

This chapter provides background information necessary to understand the scope of this study. Fundamental concepts on the rheology of kaolin and bimodal suspensions pertaining to the present investigation are described. Here, the semi-empirical correlations often used to describe the flow behavior, as well as the development of yield stress in a typical colloidal suspension are highlighted.

The vane viscometer principles, operations, and advantages over the concentric viscometer are presented. This helps to understand why it is preferred over the concentric viscometer and exclusive chosen for collecting rheological data in current investigation.

Independent contributions of the solids (fine and coarse) to rheology are discussed as these fundamentals to help explain the behavior of a more complex suspension containing fine-coarse particles. Contributions from previous works are also highlighted in this chapter. It was shown that despite great efforts from researchers of like Paulsen [11] and Rahman [14], additional yield stress augmentation measurements are needed to determine if available correlations have any ability to be predictive , or if they can be used for interpolation within a set of measurements.

2.8 Research Scope and Objectives

The aim of this study is to predict the yield stress of two types of bimodal suspensions: industrial MFT and model oil sands tailings samples produced from kaolin clay. The rheological investigation in this work is limited to the yield stress parameter because it is the more important parameter for tailings transport and placement.

To this end, the objectives of this study are:

1. To make high-quality, reproducible vane yield stress measurements of the two types of bimodal suspensions: kaolin-sand and MFT-sand mixtures.
2. To predict the yield stress of bimodal suspensions, by testing the semi-empirical shear yield stress correlations and comparing their predictive ability and accuracies.
3. To investigate the effect of coarse particle shape and size in augmenting fine particle suspension yield stresses.

Chapter 3 EXPERIMENTAL METHOD

3.1 Introduction

Experimental programs conducted to fulfil the objectives of this study are discussed in this chapter. Section 3.2 provides the information such as the properties and sources of the sands, water, kaolin clay and industrial MFT used for preparing the suspensions. In Section 3.3, the equipment and set-up for sample preparation, rheology measurements and particle classification are discussed. In Section 3.4, the experimental procedures and matrices are detailed. Lastly, the experimental methods for preparing suspensions as well as obtaining key parameters for the Lim et al. [23] model are provided in Section 3.5. This section provides a confidence level on the methods adopted and the results obtained in this work.

3.2 Materials

3.2.1 De-ionized Water and Coagulant

De-ionized water from an installed Elix Advantage Milli-Q water system (by Millipore) was exclusively used for all experiments. All glassware, mixers, and viscometer sensor systems used were thoroughly washed with detergent and rinsed using de-ionized water to ensure the consistency of water chemistry, and to avoid the introduction and dissolution of foreign ions that may affect the rheology of the tested suspension. Calcium chloride dihydrate, $CaCl_2.2H_2O$, (Fisher chemical) was used as a coagulant. This was added to the kaolin suspension at a fixed coagulant-to-kaolin mass ratio of 0.001 following the procedures of Rahman [14].

3.2.2 Kaolin Clay

The kaolin used in this investigation was manufactured by the Kentucky Tennessee Clay Company, and supplied by Plainsman Pottery, Edmonton, AB, Canada. The average particle diameter according to the supplier is 1.0-1.2 μm, and the density is 2696 kg/m^3 according to the Saskatchewan Research Council (SRC) data base [14]. Since the mineralogy and/or ion composition of kaolin can vary from batch to batch, all primary investigations and a few repeated tests were completed using kaolin collected from a single batch. For most of the repeated tests, rheological measurements were made on kaolin suspensions made at different concentrations using kaolin from a new batch. Results obtained from the new batch were then compared with rheological measurements obtained from the first batch for suspensions of similar volume concentration. This

was performed to ensure the rheological measurements of kaolin suspensions from different batches were comparable before conducting the repeated tests. Comparable results were obtained from the batches as shown in Chapter 4 and in Appendix A.

3.2.3 Lane Mountain (LM-50) Sand

Lane Mountain sand was obtained from Lane Mountain Company (Valley Washington, USA). LM-50 sand used was collected from a single 22.7 kg bag as supplied. Prior to its use, a sieve analysis was conducted to determine the particle size distribution. The result is reported in Chapter 4**.** The Lane Mountain sand has been used by other researchers as the coarse particle component of bimodal slurries [47, 60] and the density of Lane mountain sand is 2650 kg/m^3 according to the SRC [60]. In this study coarse particles have been selected based on density, shape, and size and the mass median diameter (d_{50}) from particle size distribution analysis is 300 µm. The maximum solid concentration, which is also referred to as the close packing fraction of sand is taken as $C_{max,s} = 0.49$ [12]. The $C_{max,s}$ gives an indication that the shape of the LM-50 sand is angular [61, 62].

3.2.4 Sil-1 Sand

Another type of sand used in this experiment is Sil-1 sand produced by SIL Industrial minerals, Edmonton, AB, CA. This coarse-particle sand has a density of 2650 kg/m^3, and it is a rounder grain sand compared to the Lane Mountain sand as shown in the particle image analysis reported by Sarker [63]. Sil-1 sand has a maximum solid concentration of $C_{max,s} = 0.59$ as obtained from batch setting test, and the mass median diameter (d_{50}) from particle size distribution analysis is 290 µm.

3.2.5 Sil-325 Sand

The third type of sand used in this investigation is Sil-325 sand (silica flour) which is finer than the other types of sands. It was obtained from the SIL Industrial Minerals, Edmonton, AB, Canada. This sand was selected because of its size, and has a density of 2650 kg/m^3 [62]. The maximum solid concentration obtained from settling experiments and the mass median diameter (d_{50}) were reported to be 0.469 and 28 µm respectively [62]. Figure 3-1 shows a picture of the 3 types of sand used in this study.

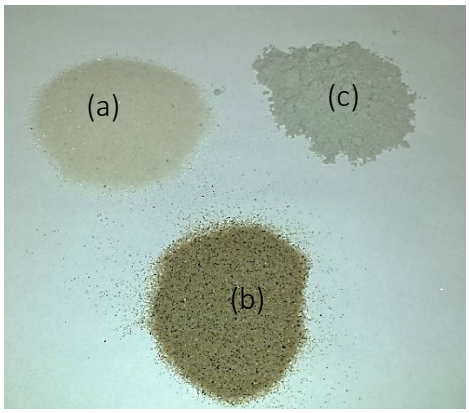

Figure 3-1: Coarse particle types and sizes (d_{50}) used in this work (a) Sil-1= 290 μm (b) LM-50 = 300 μm, and (c) Sil-325 = 28μm.

3.2.6 Industrial Samples

The MFT used in this work was supplied by Syncrude Canada Limited. It is a mixture of clay, silt, bitumen, and water and has a medium-to-dark grey colour. The details according to the supplier's material safety data sheet are shown in Table 3-1. The reported solids concentrations by weight were 26.9 and 32.5% (w/w) for the two samples supplied, and the pH is between 8-9. Tests were limited to these concentrations due to the unavailability of additional process water. Prior to the preparation of the MFT-sand mixtures, the received MFT samples were sieved with the 106μm screen to remove the coarse solid fraction, and to reduce the bitumen content in the slurry.

Table 3-1: MFT composition information (Source: Syncrude MSDS for MFT)

Ingredient	Composition
Bitumen	1-2 Wt. %
Naphtha	< 0.1 Wt.%
Clay	30-60 Wt. %
Water	37.9 -68.9 Wt.%

3.3 Equipment and Set-Up

3.3.1 Sample Preparation

All weighing measurements were conducted using an FX-3000 electronic balance scale from A&D, Japan. This scale has a precision of 0.01 g and can measure up to a maximum mass of 3000 g. Specific concentrations of kaolin suspensions were made by mixing a predetermined amount of kaolin clay in an appropriate volume of de-ionized water using the IKA RW 20 overhead mixer (IKA Werke GmbH & Company, Germany) which can be operated over a wide range of speeds between 280 to 2000 RPM. For this work, a 45^{o}, 3-bladed axial, pitched blade turbine (PBT) was used for preparing the kaolin suspensions and conducting the shear conditioning of the kaolin and MFT suspensions. The off-bottom clearance is 33 mm which is half the diameter of the impeller and mixed in a 79 mm diameter Pyrex beaker.

The pH and conductivity measurements of the suspensions in this work were taken with a dual-purpose meter (Mettler Toledo Seven-Multi system). To ensure accuracy of the measurements, the pH probe was calibrated daily before use.

The addition of kaolin particles to water (or the addition of water to kaolin) introduces air bubbles in the suspension. The hydration process causes the swelling and the break-up of kaolin particles, thus simultaneously liberating and trapping air bubbles. With the introduction of mixing, significant amounts of air bubbles are introduced into the suspension, especially when mixing is done at high speed. Also, by increasing the concentration of kaolin the suspension yield stress increases, which in turn makes the release of trapped air bubbles more difficult. Therefore, the revised de-aeration set-up used by Rahman [14] was considered necessary to help liberate air bubbles trapped in the kaolin/MFT suspensions. Removing as much trapped air as possible greatly improves the quality of the measurements taken.

The de-aeration set-up consists of the following: A 15 L bucket; a submersible pump manufactured by Gast Manufacturing Inc., model 5-MSP; a Nalgene vacuum aspirator pump manufactured by Nalgene Company; Master-flex tubing; a retort stand; a flat-bottom vacuum flask, and stopper. The schematics for this set-up is shown in Figure 3-2, and a more detailed picture can be found in Appendix C.

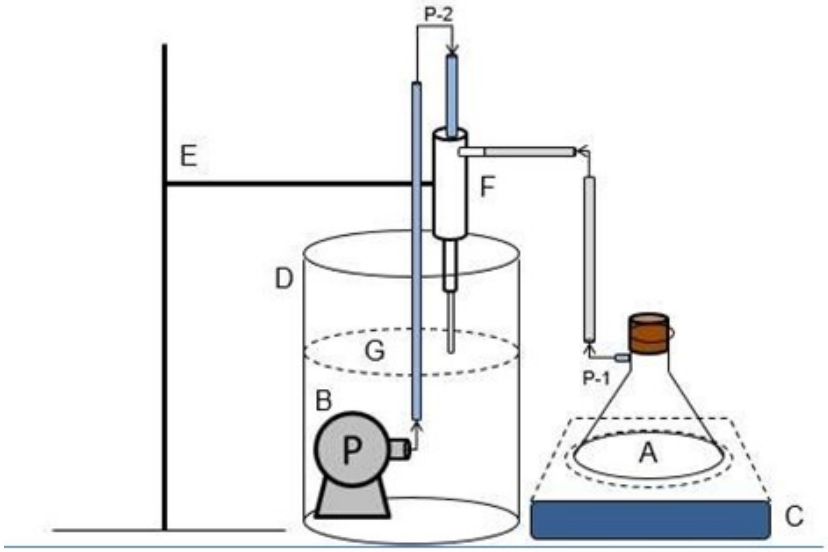

Figure 3-2: Schematic of kaolin suspension de-aeration set-up.

In Figure 3.2, the components are labelled as follows:

A – Flat bottom vacuum flask

B – Submersible pump

C – Magnetic stirrer and hot plate device. Provides the stirring for the second part of the vacuuming operation

D – Plastic bucket.

E – Retort stand: This supports or hold in place the vacuum aspirator.

F – Nalgene Vacuum aspirator

G – Reservoir water for the vacuuming operation

P-1– Connection point of vacuum flask inlet and aspirator, and

P-2- Connection point of the vacuum aspirator inlet and the submersible pump.

3.3.2 Viscometry Measurements

In this investigation, all rheological measurements were taken using the Haake VT550 Viscometer (Thermo Fisher Scientific, Waltham, MA, USA). This viscometer can be used with both vane and concentric cylinder sensor systems. It is equipped with a temperature control unit used together with the concentric cylinder sensor system, see Figure 3-3. The temperature of the concentric cylinder sensor is controlled by this unit, supplying de-ionized water through the temperature jacket encasing the cylinder-sensor systems. For concentric cylinders operation, the volume of sample loaded into the cup is determined by the type of concentric cylinder sensor. There are three different rotor sensors based on the diameter of the cylinders: MV-I, MV-II, and MV-III. The cup and rotor sensors are shown in Figure 3-4. A limited number of Bingham yield stress and plastic viscosity measurements of kaolin-only suspensions were taken using the MV-I sensor. To estimate the Bingham yield stress and plastic viscosity, the viscometer is used with the concentric cylinder geometry system and operated under laminar conditions (details about the concentric viscometer and Bingham yield stress estimation can be found in Appendix D). It measures torque over a wide range spindle speed between 0-800 RPM and has a torque resolution of 0.17 nNm. A S60 CANNON standard oil (CANNON instrument company) was used to check the system's calibration.

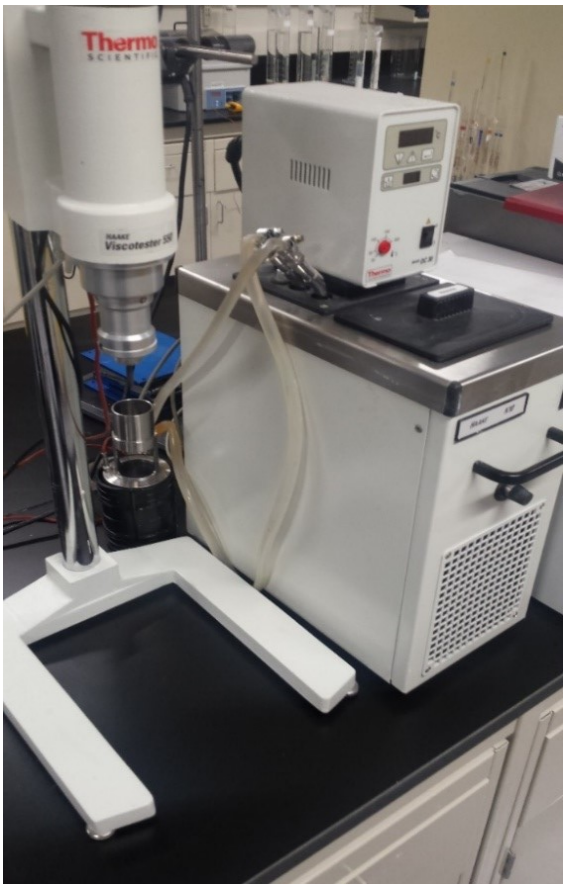

Figure 3-3: The Haake VT550 viscometer and temperature control unit.

Figure 3-4: Cup and rotor sensors of the Haake VT 550 Viscometer.

3.3.3 Vane Viscometer

Most of the rheological measurements in this study were taken using the vane sensor system. The vane sensor was exclusively used to measure the yield stress of all bimodal suspensions. The vane sensor system provides a more repeatable and robust yield stress measurement, particularly for bimodal suspensions, when compared to the Bingham yield stress estimated from the use of the concentric cylinder geometry. The vane sensor used in this study is the FL-100; it has 6 blades as shown in Figure 3-5, and its diameter and height are 22 mm and 16 mm respectively. The dimensions of the vessel are important for the satisfaction of the sample volume and vessel selection criteria. In this work, about 220 mL was the smallest volume of suspension tested for a vessel dimeter of about 79 mm, which satisfies the selection criteria [20]. According to the recommendation by Nguyen and Boger [20] the minimum sample volume should be twice the diameter and twice the height of the vane sensor dimension. These conditions are necessary to minimize errors such as wall effect using the vane. The set of criteria provided below shows the relationship between vane diameter and vessel selection and the minimum immersion depth is known from the relationship where:

$$D_v \leq 0.5D_c \tag{3.1}$$

$$Z_{above} \geq D_v$$

$$Z_{below} \geq 0.5D_v$$

where D_c is the diameter of vessel, D_v is the vane diameter, Z_{above} is the distance from the suspension surface to the top of vane, and Z_{below} is the bottom of the vessel to the bottom of the vane.

The vane sensor used in this study is grooved to easily detect the minimum depth for correct measurement. Although the Haake VT 550 viscometer has an FL-10 sensor (see Figure 3-5) which is a larger vane, the FL-100 was chosen due to the smaller sample size required to make measurement. This allowed the completion of all the experimental matrices from a single batch of kaolin. The vane was operated at 0.01 RPM, which is a very low shear rate, therefore it was not necessary to control the temperature since this rotational speed did not increase the suspension's

temperature by viscous heating. All suspensions were prepared and stored at room temperature and the approximate temperature during the vane measurements was 22 ^{o}C.

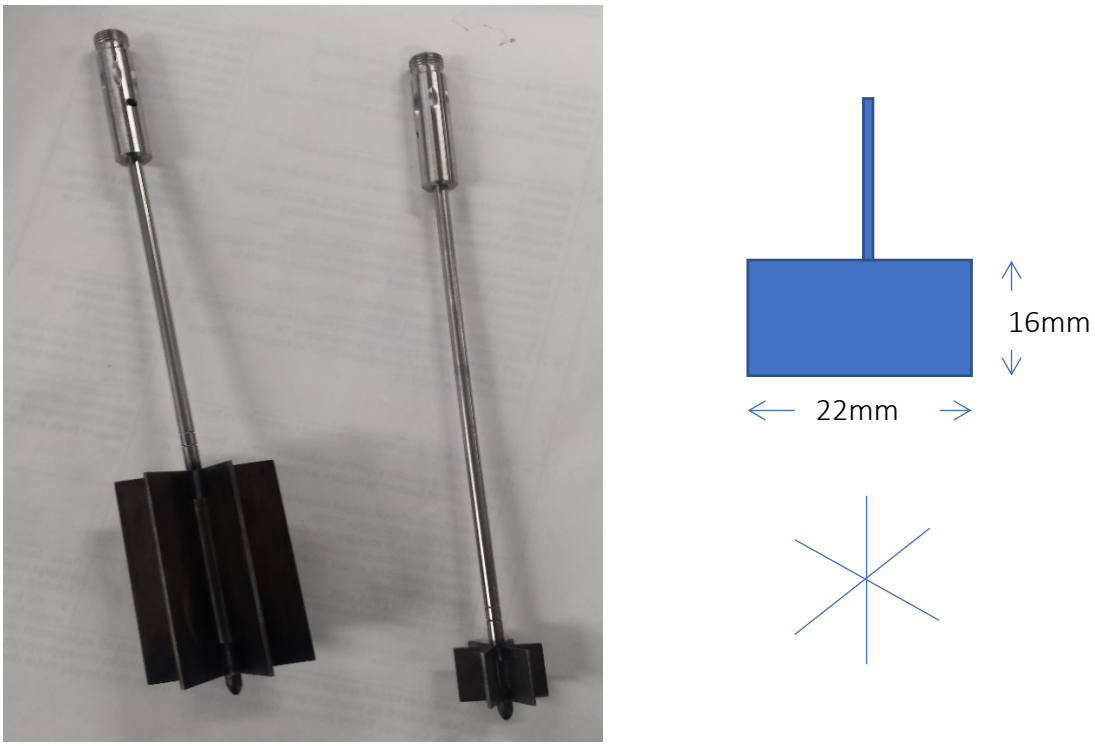

Figure 3-5: Vane sensors of the Haake VT 550 viscometer. Left to right is the FL-10 and FL-100.

3.3.4 Particle Classification

Particle size distribution analysis is an important tool required to study and understand the interaction mechanism of different particle sizes in suspension. For classifying coarse particles, the Ro-Tap RX-29 mechanical shaker (W.S. Tyler) was used in this study (see Figure 3-6). This shaker is adjustable to accommodate a maximum of six vertically stacked-sieves. To perform a sieving operation, sieves are stacked from largest screen opening at the top to the lowest at the bottom, followed by the pan. The largest screen used in this work is the ASTM standard sieve #40 (425 µm) while the smallest screen opening is the #325 (45 µm) sieve. The mechanical shaker was operated over a set period of 20 mins. The shaker imparts both vertical and horizontal vibration to the stacked sieves, thus allowing the gradation of loaded sand samples through each of the stacked sieves based on linear dimension [20].

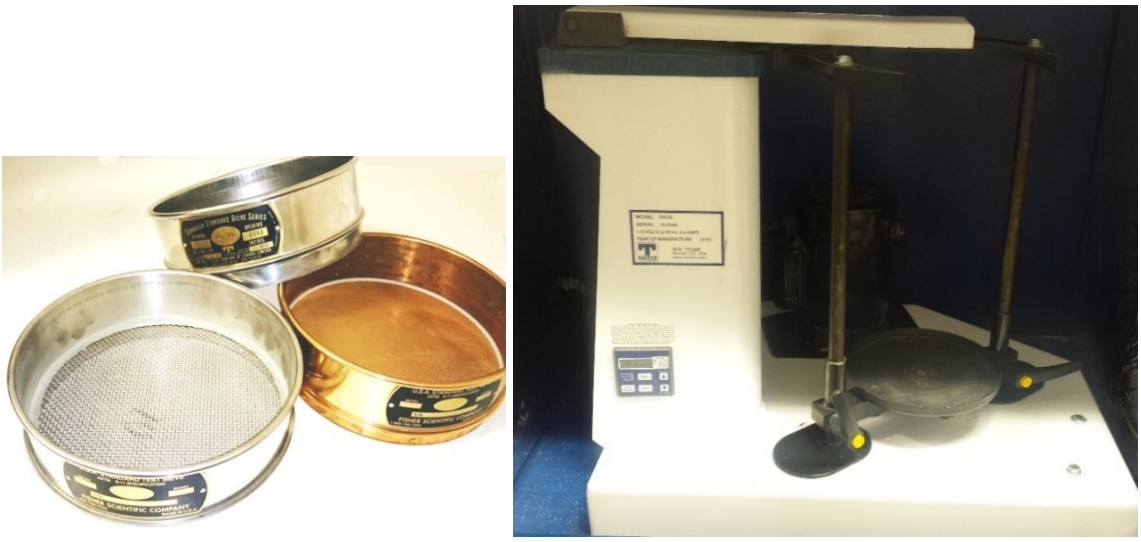

Figure 3-6: (a) ASTM US Sieves (b) Ro-Tap RX-29 mechanical shaker.

3.4 Experimental Procedure and Matrices

3.4.1 Overview and Test Program

This section provides the details of the experimental works completed to fulfil the objectives of this study. First, particle size distribution (PSD) analysis and classification was completed for the coarse particles using the sieve technique. In the second step, the coarse particles were washed using de-ionized water, dried and sieved with the ASTM Screen #325 to remove contaminants and particles less than 45µm. Before preparing the bimodal suspensions, preliminary experiments were conducted on kaolin-only suspensions to develop a shear conditioning protocol to ensure the suspension is time-independent before taking the vane yield stress measurements.

Next, experiments to investigate the effect of sand addition on carrier fluid rheology were conducted. This was done by measuring the pH, conductivity, and yield stress of kaolin suspension before the addition of coarse particles, after the addition of coarse particles, and after scalping the coarse particles by sieving. This was needed to determine if the introduction of coarse particles significantly affects the chemistry and rheology of the kaolin suspensions.

Experiments were then conducted to measure yield stress of fines-only and bimodal suspensions, and to investigate the effect of shape and size of coarse particles on the

augmentation mechanism. Details of the suspension preparation and rheology measurement steps are clearly itemized in the subsequent sections, and Table 3-2 – 3.3 present the experimental matrices for this study.

Table 3-2: Experimental matrix for bimodal suspensions of kaolin and sands mixtures.

Coarse particle types	Kaolin volume concentration (v/v)	Coarse particle volume concentration (v/v)
LM-50	0.12	0.03*
Sil-1	0.15*	0.1*
Sil-325*	0.2	0.25*
	0.24*	0.35*
		$0.80C_{max,s}$

*Tests completed for Sil-325 sand.

Table 3-3: Experimental matrix for MFT bimodal suspensions.

Coarse particle types	MFT volume concentration (v/v)	Coarse particle volume concentration (v/v)
LM-50	0.11	0.03
Sil-1	0.14	0.1
		0.25
		0.35
		$0.80C_{max,s}$

The particles were selected to investigate the effect of shape and size on yield stress augmentation, and particles of similar density, different shapes with comparable sizes, and different sizes with comparable shapes were chosen. The concentration of both the fine and coarse particle fractions were also selected to cover a wider range when compared with the previous works of Paulsen [11] and Rahman [14]. The comparison of the test range covered here with previous investigations is

shown in Figure 3-7 where C_s is the volume concentration of coarse particles and C_f is the volume concentration of kaolin-only suspension. To optimize the number of tests, four concentrations were chosen. For the Sil-325, the highest concentration of coarse particle was not completed because it was very difficult to prepare, and only two fine concentrations were tested to reduce the number of tests.

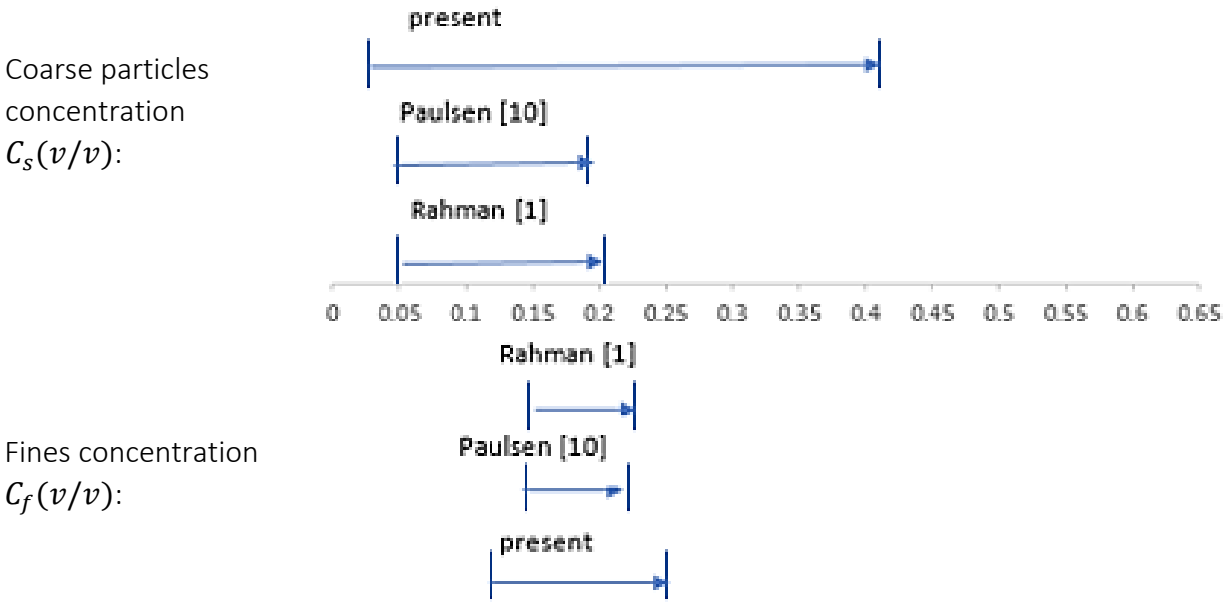

Figure 3-7: Comparison of test range

3.4.2 Particle Characterization

The following procedure was used to determine the particle size distribution of sands, and to remove sand particles smaller than 45µm so that they do not add to the flocculating characteristics of kaolin suspensions.

Procedure:

1. To prepare the sieves; brush each sieve's screen to remove particles that may block the sieve openings. Clean the metal sides (in and out) of the sieves with clean paper towel to remove any dust from previous use.

2. Measure and record the weight of the clean sieves, pan and lid to be used.
3. Stack the sieves with the largest screen opening on top and smallest at the bottom, then the pan. The pan should come last to collect smallest particle size.
4. Pour sand from bag into a big bucket and mix thoroughly then
5. Measure 1000 g of sand into a clean and dry 1 L beaker.
6. Empty the beaker of sand into the topmost sieve using a spatula, that is the sieve with the largest opening, and tightly cover with the lid.
7. Place stacked sieves of sand in the mechanical shaker and set timer to 20 mins.
8. Press start to begin and shut the doors properly to partially contain the noise.
9. At the end of the set time, the mechanical shaker stops. Remove the stacked sieves and gently unstack the sieves to measure the retained mass of sand on each sieve.
10. Carefully measure retained sand on each sieve and then discard the pan contents (i.e. solids that are less than 45µm).
11. Use the recorded values to determine and plot the particle size distribution curve.

The particle size distribution curves for the sands are presented in Chapter 4.

3.4.3 Particle Pre-treatment

All coarse particles used (LM-50, Sil-1, and Sil-325) were thoroughly washed, dried, and sieved before they were added to kaolin/MFT suspensions. The steps, as shown below, eliminate possible changes to the flocculating characteristics of the kaolin suspension that may be caused by the introduction of fines (-45 µm) from the coarse particles and/or trace minerals to the kaolin sample.

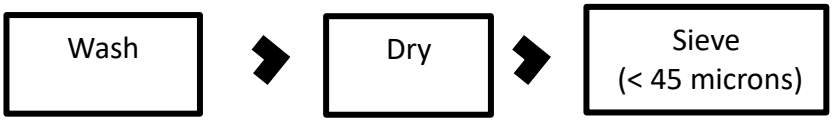

Figure 3-8: Coarse particles treatment steps

Step 1: Washing procedure

1. Carefully measure out the amount of sand to be washed into a clean 1L beaker. To conveniently wash, measure about 300 g into a 1L beaker.
2. Add about 700 mL DI-water to the 300 g of sand in the 1L beaker.
3. Gently stir the sand-water mixture using a spatula for about 1 -3 mins.
4. Take pH and conductivity measurements of the mixture and record values.
5. Carefully stir the sand-water mixture to re-suspend settled sand particles, then pour gently into a clean #325 mesh sieve.
6. Carefully wash the particles retained on the sieve with deionized water into a 1L beaker.

Step 2: Drying procedure

The following steps were used to dry the wet sand:

1. Conduct vacuum filtration on the wet sand to extract a significant amount of water from the sand-water mixture obtained from Step 1 above . A photograph of the set-up can be found in Appendix C).
2. Spread the vacuum-dried sand in an aluminum pan and allow to dry in fume hood overnight (18-21 hrs).
3. Further dry the sand using a vacuum oven for 6-8 hrs at 60 ^{o}C, and 0.14 bar.

Step 3: Sieving

This follows the same procedure in Section 3.4.2, but in this case only the 45micron screen is used to screen off any particles less than this size, particles greater than 45microns are kept for the preparation of bimodal suspensions of kaolin/MFT suspensions.

3.4.4 Shear Sensitivity Protocol

The dispersion of kaolin into water results in floc formation because the water chemistry condition favours particle-particle attraction. The initial floc structure formed when this mixture is freshly made changes when the suspension is subjected to shear. For a constant applied shear over a certain time, floc re-structuring attains an equilibrium condition when the rate of breakage and formation of flocs is the same. Beyond this time, the suspension becomes shear independent,

since any further shearing at the same shear rate does not cause a significant change in the flocs structure.

When shearing stops, floc connectivity is re-established primarily through Brownian motion and particle-particle collision [64]. This continuous motion and collision of particles/flocs result into an increasing yield stress as a function of time, a thixotropy effect that changes the properties of viscoplastic fluids [65]. In this work all yield stress measurements were taken immediately after shearing the suspension.

Shear sensitivity of the suspensions can be obtained by measuring the torque as a function of time. Direct torque can be measured using the Haake viscometer with any of the MV sensors. However, the challenge with the use of this device is that the volume required for vane measurement is much greater than the maximum sample size for the MV-III sensor (which provides the largest volume for the MV sensor series). It was therefore necessary to devise a means to detect the prevalent rheology of the suspension at different shear periods indirectly. As a result, an overhead mixer was used with the 45° PBT axial impeller to provide a uniform and fully sheared suspension.

Since the overhead mixer is not equipped with a torque measurement device, fine suspension samples were stirred at lowest speed (280 RPM) for different durations and at the end of these periods, vane yield stress measurements were taken. This gave the shear sensitivity (i.e. the change the yield stress) as a function of time. The results of the shear sensitivity measurement investigation, which were obtained at different mixing times for the highest kaolin concentration test in this study (i.e. $C_f = 0.24$) are reported in Chapter 4, and the MFT results are reported Appendix A.

3.4.5 Kaolin Slurry Preparation

The general steps for the preparation of suspensions (kaolin-only and bimodal slurry), and rheology measurements are presented in Figure 3-9. A similar procedure was adopted for the MFT suspensions except there is an additional step that involves sieving the MFT (see Figure 3-10). This figure highlights the steps involved and the preliminary experiments conducted to develop a reproducible procedure and to produce high-quality measurements in this investigation.

Kaolin suspensions were made at different solid volume fractions according the matrix in Table 3-2. To prepare the suspension, kaolin is dispersed in de-ionized water, then deaerated to remove trapped air bubbles, and then allowed to rest for a day to establish chemical equilibrium. Following this rest period, the suspension is shear-conditioned to prepare it for rheological measurement, and for bimodal suspension preparation. The steps for the preparation are reported below:

Step-1: Kaolin suspension preparation

1. Determine the amount of kaolin required to make a specific solid volume fraction of kaolin suspension using Equation (3.1).
2. Measure out the required quantity of kaolin and de-ionized water using the weighing balance.
3. Firmly attach the shaft-impeller onto the IKA RW 20 overhead digital mixer.
4. Place beaker of deionized-water underneath the overhead mixer and carefully lower the height of mixer until the off-bottom distance is half the diameter of impeller, then firmly secure the overhead mixer onto the clamp at this height. The diameter of Pyrex beaker is 130 mm and that of the impeller is 66 mm.
5. Switch on the mixer and gently pour the kaolin into the mixing deionized-water slowly. After fully dispensing the measured kaolin clay into the deionized-water, weigh 0.001 times the kaolin mass of $CaCl_2.2H_2O$. For example, if 150.0 g of kaolin was measured and dispersed, then weigh 0.15 g of $CaCl_2.2H_2O$ and pour the measured $CaCl_2.2H_2O$ into the mixing slurry. Although it is hygroscopic, the measurement was quick, so water adsorption is negligible. Allow mixing to continue for 30 mins.
6. After 30 mins of mixing, stop mixer and carefully adjust height of the impeller to remove the suspension in the beaker for pH and conductivity measurements using the Mettler Toledo meter.
7. Insert clean probes (pH and conductivity) into the suspension and take measurements.
8. Rinse probes and clean with paper towels, then repeat 2-3 times until the measurements are stable and repeatable.
9. De-aerate the suspension following steps 9 -13.

10. Prepare a reservoir of water in a 15 L bucket up to a sufficient level to cover the submersible pump.
11. Firmly connect the submersible pump's outlet to the inlet of the vacuum aspirator (Point A) with a Masterflex tube as shown below.
12. Firmly secure the vacuum aspirator with a retort stand such that the outlet (Point B) is directly above the bucket as shown Figure 3-2.
13. Connect point F of the aspirator pump to the tapered inlet (P-1) of the vacuum flask as shown Figure 3-2.

The amount of kaolin and water required for a specific solid volume fraction of kaolin suspension can be calculated using :

$$C_f = \frac{\forall_f}{(\forall_f + \forall_l)} \tag{3.2}$$

where $\forall_f$ is the volume of fines, $\forall_l$ is the volume of water and C_f is the solid volume fraction of fines. The volume of fines can be calculated using :

$$\forall_f = \frac{M_f}{\rho_f} \tag{3.3}$$

here ρ_f is fines density and M_f is the mass of fines calculated as shown below:

$$M_f = \frac{C_f \forall_l \rho_f}{(1 - C_f)} \tag{3.4}$$

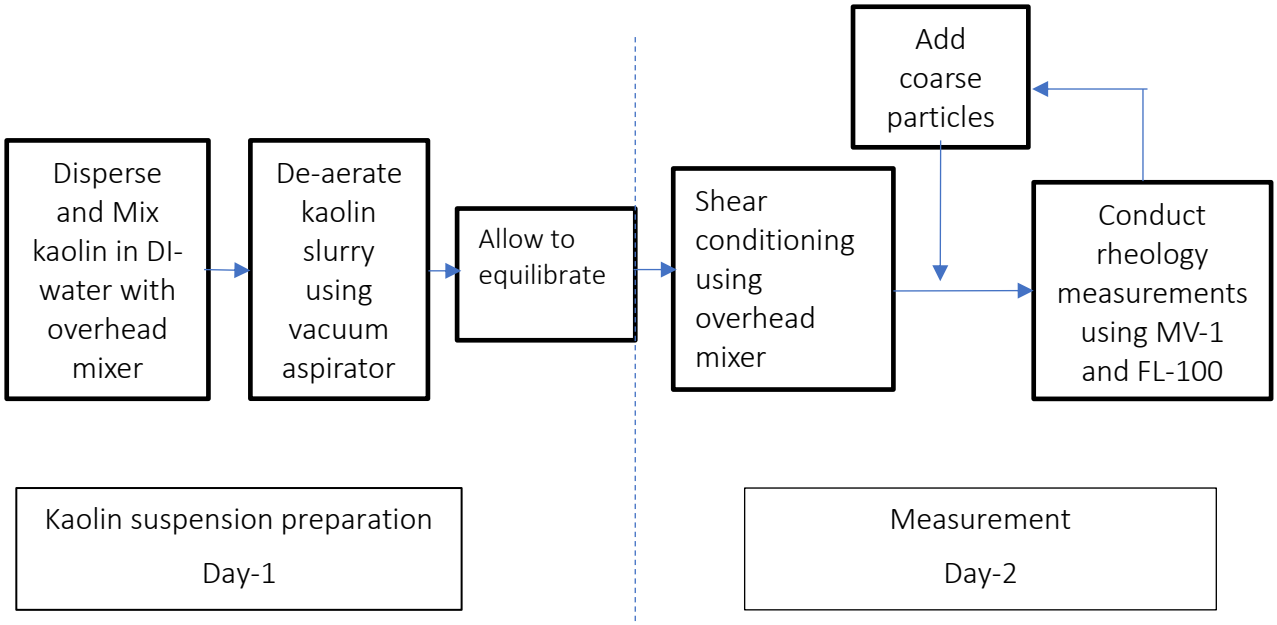

Figure 3-9: General test procedure for the model oil sands tailings suspension preparation and measurements.

In the case of MFT, the 'as-is' samples were sieved using the 106 µm screen; to allow thicker mixture pass through the screen, and to reduce the potential of screen blockage, and mixed thoroughly for 30 mins using the overhead mixer of a 66 mm diameter impeller, then de-aerated and shear conditioned in a similar fashion as the kaolin-only suspension as shown in Figure 3-10.

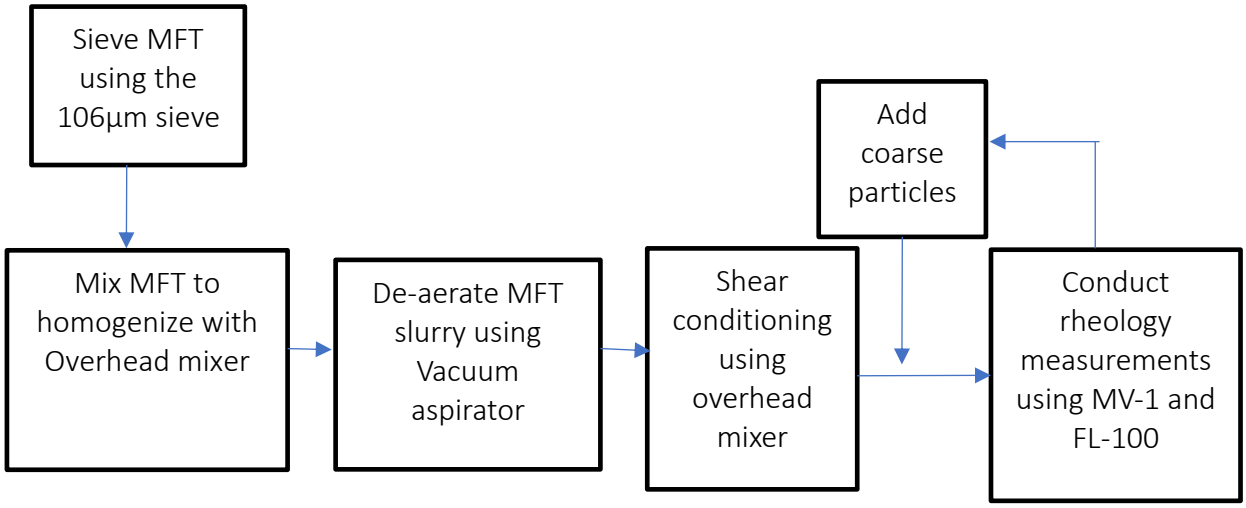

Figure 3-10: General test procedure for MFT suspension preparation and measurements.

Step 2: De-aeration of kaolin and MFT suspensions

The suspension prepared, in Step 1 above, is vacuumed in the de-aeration set-up discussed in Section 3.3.1 as follows:

1. Gently pour about 500 mL kaolin/MFT suspension into a 1L flat bottom vacuum flask. Insert a clean magnetic bar and tightly cover with cork.
2. Place the vacuum flask on a magnetic stirrer and turn the stirring knob to the lowest RPM.
3. Start the pump and switch on the magnetic stirrer and gradually increase the speed of the magnetic stirrer until an appropriate speed is reached which does not create a vortex.
4. Stop the magnetic stirrer and the pump after 25 mins.
5. Repeat procedures 1- 4 until all the suspension gets de-aerated.
6. Pour the suspension back into a beaker and cover with parafilm. Set covered suspension aside in designated area to equilibrate overnight before conducting the shear conditioning and rheology measurement steps.

Step 3: Shear conditioning and bimodal suspension preparation

The following procedure was developed to ensure that the kaolin suspension prepared and the supplied MFT attain a time and shear-independent state before conducting the vane yield stress measurement. In addition, this protocol also ensures that the additional stirring of the fine suspensions (kaolin and MFT) by hand after an initial vane measurement does not cause a significant change in the flocs/aggregate structure. A significant change in the flocs/aggregate structure would affect the vane yield stress measurements made thereafter. The additional hand stirring step was found necessary since the bimodal suspensions were made by adding the coarse particles to the kaolin/MFT suspensions.

The following procedure is conducted on the kaolin suspension prepared and left to equilibrate from Step 2 above:

1. Gently stir to resuspend the suspension using a clean spatula for about 2-3 min.
2. Carefully pour about 220 mL of kaolin suspension into a 500 mL Pyrex 1060 beaker.
3. Insert a clean and dry 3-blade axial impeller into the IKA RW 20 overhead mixer.

4. Place the beaker of kaolin suspension under the impeller and carefully adjust the height of the overhead mixer such that the off-beaker bottom distance is half the diameter of impeller. The diameter of Pyrex beaker is 79 mm and that of the impeller is 66 mm.
5. Adjust the mixer speed knob to the lowest speed (280 RPM) and switch on the mixer
6. Stop mixing after 40 mins and to take the vane yield stress measurement of the kaolin suspension.
7. After taking the vane yield stress measurement, stir the kaolin suspension by hand for 5 mins before re-taking the vane measurement.
8. To make the bimodal suspension, in step-7 while stirring, gently add the pre-determined and measured quantity of sand to the kaolin and mix for 5mins before taking the vane measurement.

The mass of coarse particles to add for a specific coarse-solid concentration by volume can be calculated using

$$C_s = \frac{\forall_s}{(\forall_f + \forall_l + \forall_s)} \tag{3.5}$$

where $\forall_s$ is the volume of coarse particle $\forall_l$ is the volume of water, $\forall_f$ fines volume, and C_s is the coarse volume concentration.

To validate these shear conditioning and mixing methods, the vane yield stress measurements of similar kaolin-only and kaolin-sand suspensions similar to those studied in a previous investigation at SRC, where a standardized paint mixer was used, are compared with suspensions made following the shear and mixing methods described above. Before preparing the bimodal suspensions, the particle size distribution for the Lane Mountain sand (LM-125) used was compared with the SRC reported PSD (see Figure 3-11). This was necessary to ensure the results were not affected by variation in PSD. The vane yield stress ratio comparison obtained shows a comparable result which will be presented in Chapter 4.

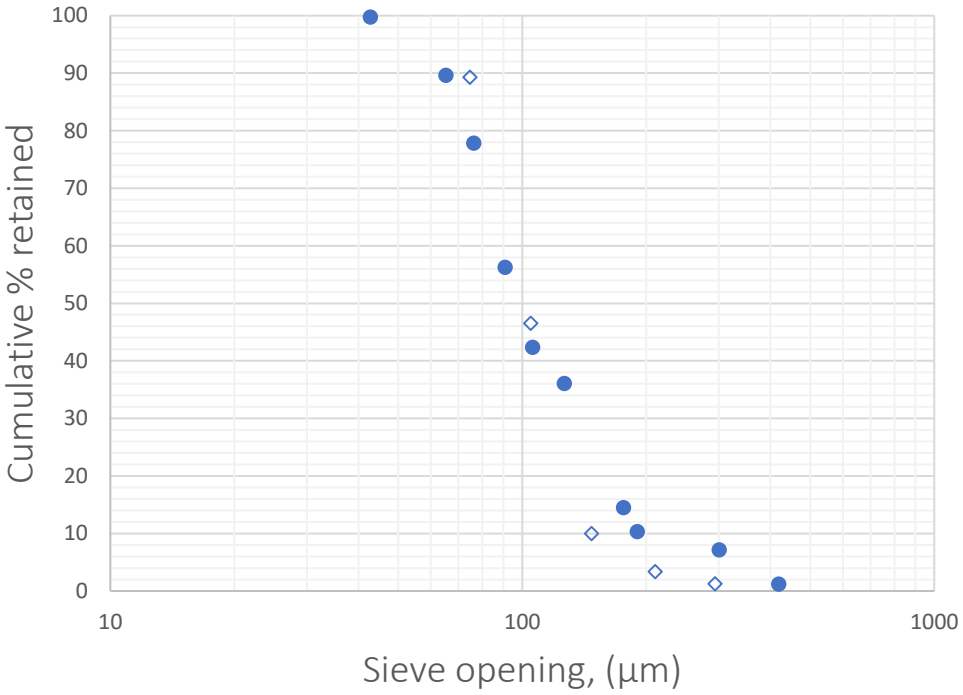

Figure 3-11: Comparison of the particle size distribution of Lane Mountain 125 (LM-125) used in present preliminary investigation and by the SRC [8].

Step 4: Rheological measurements.

Rheology measurements were conducted immediately after the shear-conditioning step. For kaolin-only suspensions, the FL-100 and MV-1 sensors were both used to collect the vane yield stress measurements, and the Bingham yield stress and viscosity respectively. However, in the case of the bimodal suspensions, only the vane yield stress measurements were taken, and the vane was operated in rate-controlled mode at constant speed of 0.01 RPM.

3.4.6 Determination of Gel point for Kaolin Suspensions

Gel point is a material property that can be obtained from equilibrium batch settling test. As discussed earlier, it is the minimum solid volume fraction in which a spanning network of flocs forms in a suspension [66, 67]. In a batch settling test, at this critical solid concentration, the integral network pressure of the interacting floc system is transmitted from the top of the sediment through the networked structure to the base of the sediment zone as shown in Figure 3-12. Therefore, a relationship exists between gel point and the exerted base pressure, and the

gel point can be estimated by extrapolating the experimental data obtained from simple equilibrium batch settling tests to a base pressure of zero [68]. Different researchers have also determined the gel point from batch settling experiment by using a simple averaging method [66, 67]. The method requires the determination of the final average solid volume fraction, C_{avg}, from a set of equilibrium batch settling experiments using the following expression:

$$C_{avg} = \frac{\sum_i^n \left(\frac{C_o h_o}{h_f}\right)_i}{n}, \tag{3.6}$$

where C_{avg} is the average solid volume fraction; C_o is the initial solid volume fraction; h_o is the initial suspension height; h_f is the final suspension height and n is the number of tests. The average solid volume fraction is plotted against the base pressure, P_{base} :

$$P_{base} = C_o \Delta\rho g h_o \tag{3.7}$$

where $\Delta\rho$ is the density difference between solid and liquid, g is the gravitational force and h_o is the initial suspension height.

Two methods were used to obtain the average solid volume fraction from the batch settling experiments, viz. the constant initial solid volume fraction method and the constant initial suspension height method [59]. With the constant initial solid volume fraction method, a

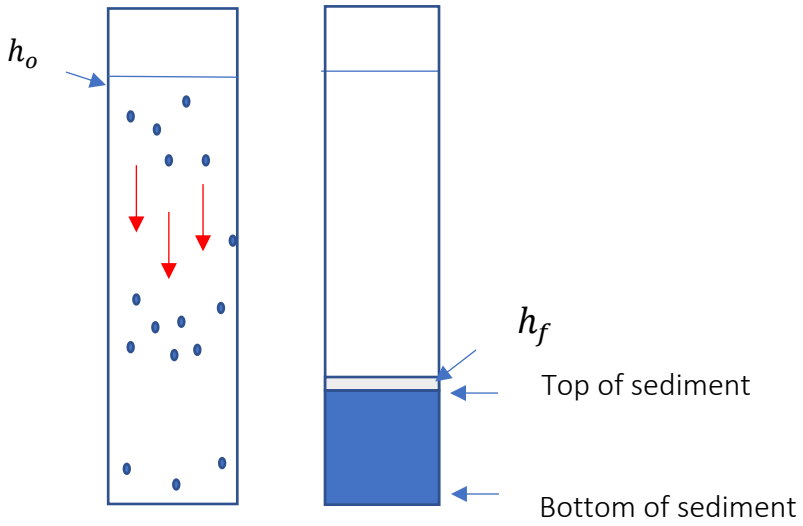

Figure 3-12: Settling of fine-particle suspension to equilibrium condition from an initial suspension height h_o to final suspension height h_f.

suspension of fine particles is made at a specific low concentration (C_o), but at different initial suspension heights in settling columns of similar geometry and then allowed to rest to attain an equilibrium state. In the case of the constant initial height method, suspensions of different initial solid volume fractions are prepared but at equal initial height in a similar set of settling columns and then allowed to attain equilibrium state. Experiments completed by Usher [68] to evaluate the gel point of zirconia used these methods and very similar values of $C_{g,f}$ = 0.04 and 0.045, respectively, were obtained for the constant initial height and the constant initial solid volume fraction methods (see Figure 3-13). Between these two methods, the constant initial solid volume fraction method is found to be less tedious and it requires less material when compared to the constant initial height method. Therefore, the constant initial solid concentration was adopted in the present investigation.

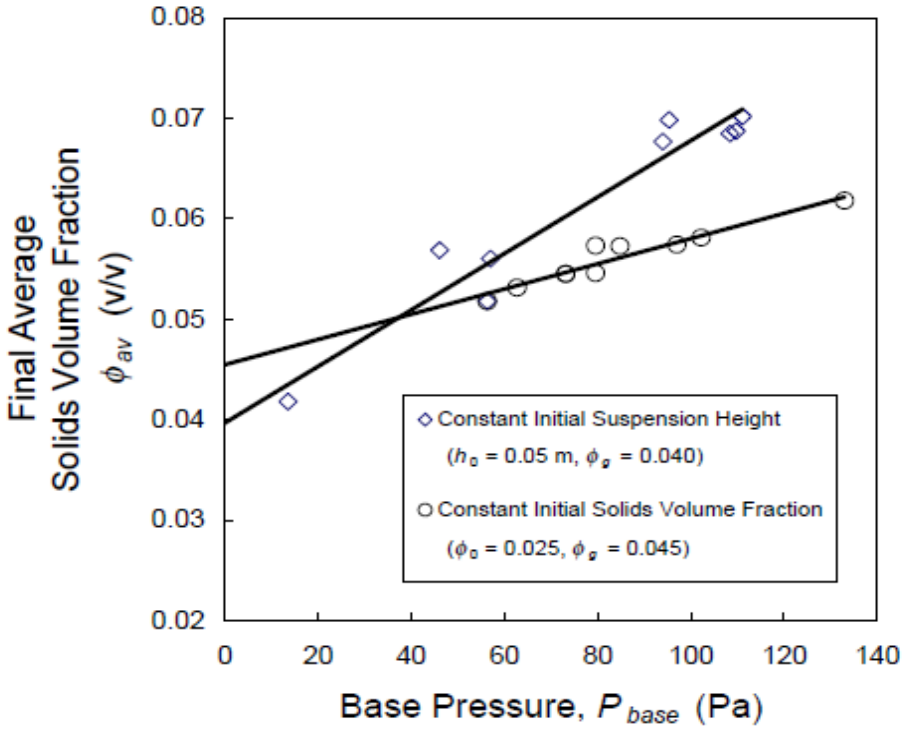

Figure 3-13: Graph showing the extrapolated gel point of zirconia suspension using both the constant initial height and constant initial solid volume fraction methods. Reproduced from [69].

Other researchers have also determined the gel points of zirconia (Green [70]), and kaolin clay [71] using the equilibrium batch settling test method. In the literature, the value for the gel point of kaolin suspensions ranges between 0.04 - 0.10 (v/v).

The gel point in this study was obtained by conducting equilibrium batch settling tests using the constant initial solid volume fraction method [68]. The general steps involved are listed below, and the procedures adopted for completing each of these steps are further explained. To ensure the initial solid volume fraction of kaolin chosen was appropriate, several preliminary batch-settling tests were completed at different initial solid volume fractions, and the most conservative concentration (0.02) was used. The details of these preliminary tests are provided in Appendix A.

The general steps include:

A. Determine an appropriate initial solid volume fraction (see details in Appendix A).
B. Prepare suspension at a pre-determined initial solid volume fraction and conduct equilibrium batch settling test using the constant initial solid volume fraction method [68].
C. Estimate the average solid volume fraction from the simple average equation (Lim et al. [23])
D. Estimate the gel point by approximation [68].

Procedure

1. Prepare $C_f = 0.02$ kaolin suspension following steps 1-6 in Section 3.4.5.
2. Prepare the graduated 250 mL flat bottom cylinders for batch settling, by pasting a clearly marked scale on the outside wall of the cylinders using a clear cello-tape. The settling columns used for the gel point determination are a set of 250mL Pyrex graduated cylinders (see Figure 3-14).
3. Mark different initial suspension heights (h_o) on the graduated cylinders with a thin-pointed pen or marker.
4. Re-suspend the prepared suspension (Step 1 above) and dispense the suspension carefully into the cylinders to reach different marked heights on the cylinders.

5. Cover the cylinders with parafilm to avoid loss of fluid to evaporation then place the filled cylinders on a vibration-free and flat surface.
6. Allow suspensions to settle to an equilibrium state, which might take several days (5-10 days) as observed and reported by Usher [68].
7. Determine the average solid volume fraction, C_{avg} using Equation (3.6) for the different initial suspension heights (h_o) tested and plot solid volume fraction against base pressure.
8. Extrapolate the linear regression of the plotted data to zero base pressure to determine the gel point of the fines from the intercept.

In this work, gel point determination was limited to the kaolin clay suspension, since the MFT used was provided at two concentrations and no process water was available to prepare different concentrations.

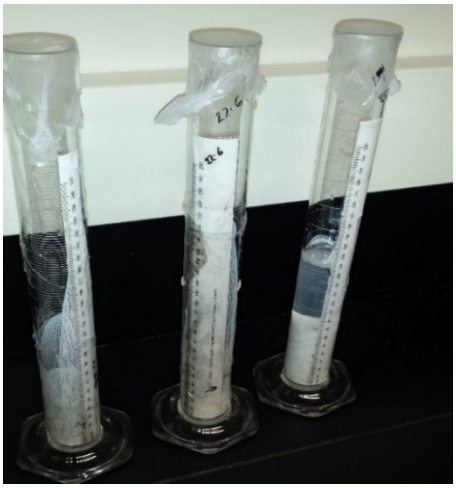

Figure 3-14: Image of a settling suspension progressing to equilibrium and settling columns used for gel point estimation.

3.4.7 Determination of Close Packing Fraction for Kaolin Suspensions

The close packing fraction of solids, otherwise referred to as the maximum solids concentration, [23] is an important parameter of the Lim et al [23] model that needs to be estimated experimentally. For hard monodispersed spherical particles, the random close packing value is 0.64 [72]. In the case of hard incompressible solids such as coarse sand particles, this value can be obtained from batch sedimentation experiments [62] . Though various methods are available, such as pipe loop, concentric cylinder viscometry and settled bed tests, or estimated using appropriate

models [62], the batch sedimentation experiment presents a simple and direct approach. Values used in this study have been reported by SRC and other researchers [62].

Suspensions of fine particles such as kaolin in water are compressible and to estimate the close packing fraction of such materials, rheological data over a range of solids concentration is required. For instance, Flatt and Bowen [73] estimated the close packing fraction of AKP-50 to be 0.56 using a yield stress model called YODEL from a set of vane yield stress measurements. This value was further compared with filter press experimental results and it was found to have an excellent agreement. In this study, the YODEL model was employed to estimate the close packing fraction of kaolin suspensions, as given by:

$$\tau_y = \frac{mC_m(C_m - C_{g,f})}{C_{cp,f}(C_{cp,f} - C_m)} \tag{3.8}$$

where m and $C_{cp,f}$ which is the close packing fraction of fine are fitting parameters.

Therefore, the general steps shown in Figure 3-15 were used to estimate the close packing fraction of kaolin suspensions. It should be noted that although other models can be applied to estimate the close packing fraction, the YODEL [73] was chosen for this study.

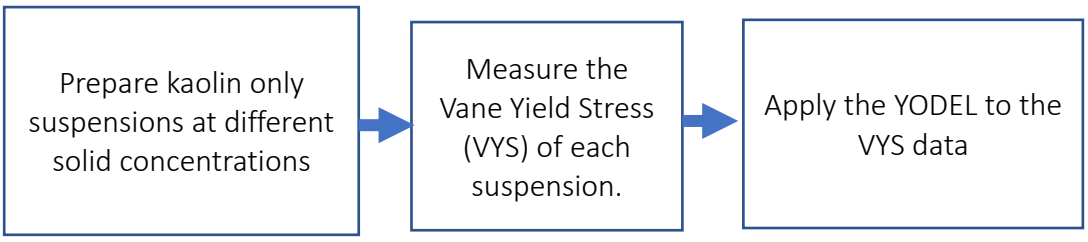

Figure 3-15: Steps for estimating close packing fraction of kaolin.

The procedures for each of these steps are highlighted as follows;

1. Prepare kaolin suspensions at different solid volume fractions and take the vane yield stress measurements following the procedures detailed above in Section 3.4.5.
2. Plot the measured yield stress values against solid volume fractions.

3. By using Equation (3.8), fit the model to the data using the least squares method to obtain the close packing fraction of fines, $C_{cp,f}$, as a fitting parameter.

The results obtained for the close packing fraction of a kaolin suspension are presented in Chapter 4. The constitutive equation (2.13) developed by Lim et al. [23] was used to determine the close packing fraction of bimodal suspensions containing fine and coarse particles, and the value of close packing fraction obtained here is used in as input parameter.

To validate the close packing fraction obtained for the kaolin-only (fines) suspension, it was compared with Liu's model [32] given by:

$$1 - \eta_r^{-\frac{1}{n'}} = \dot{a}C_f + b' \tag{3.9}$$

where, η_r is the relative viscosity of kaolin-only suspensions, C_f is the solid volume fractions of kaolin, $\dot{a}$ is the slope of linear regression and b' is the intercept, n' is a fitting parameter which is flow dependent and suspension specific. The result from using this model provided a very similar value to that obtained using the YODEL which is presented in the next chapter.

3.5 Verification of Experimental Methods

To ensure the methods for preparing the suspensions led to high-quality vane yield stress measurements, the kaolin-Sil-1 suspensions made in this study are compared with kaolin-Sil-4 suspensions made by Spelay et al. [12] at SRC at similar kaolin concentrations. Also, some of the measurements have been repeated according to Table 3-4 for the repeated test matrix, to check their repeatability.

Table 3-4: Repeated test case

		Kaolin concentration (v/v)		
Repeat test	Sil-1	0.12	0.15	0.20
	LM-50	0.12	0.15	0.20
	Sil-325	-	0.15	-

Tests were repeated for the concentrations of kaolin according to Table 3-4, and in all cases, for the three sands, the same concentration of sands detailed in Table 3.2 were re-tested. Results for the kaolin-sand comparison, vane yield stress measurements and analyses, and results for the repeated test cases are provided in following chapter.

The results obtained for the close packing fraction and gel point of kaolin which are communicated in the next chapter were verified by using a different semi-empirical model to estimate the close packing fraction of both kaolin and AKP-50 suspensions. For the gel point estimate, AKP-50 was ordered from the same source as Lim et al. [23], prepared and then left to establish equilibrium just like the kaolin used in the current study. After establishing equilibrium, the gel point of AKP-50 was estimated following the same procedure for the kaolin as described earlier in Section 3.4.6. The gel points of AKP-50 and kaolin obtained and detailed in the following chapter were compared to the value reported by Lim et al. [23] and in the literature respectively. Since the value for the gel point of kaolin is within reported ranges in literature, and because the estimated AKP-50 gel point is close to the value reported by Lim et al. [23], satisfactory results are expected for the present investigation.

The results obtained using the experimental methods described here have been compared with those used in previous studies and similar outcomes are observed, as is discussed in greater details in the following chapter.

Chapter 4 RESULTS AND ANALYSES

4.1 Introduction

Recall that the objectives of this study are: (1) to make high-quality and consistent vane yield stress measurements; (2) to investigate the effect of coarse particle shape and size on yield stress augmentation; and (3) to test the performance of a number of yield stress augmentation correlations.

Hence, to provide the necessary context of how each section presented here contributes to these objectives, the sections in this chapter are first outlined here. First, to show the reliability of the measurement methods used in this study, the following issues are addressed:

Classification of coarse particles for yield stress analysis: The PSD analysis of the Sil-1 and LM-50 sands are presented in Section 4.2. In addition, information about the Sil-325 and LM-125 used in this work and other types of sands such as the Sil-4, LM-70, GS-5010, LM-125 from a recent study are presented. It should be noted that the LM-125 is a common sand tested, and in this work, it was only used for preliminary analysis to justify the shear conditioning protocol. This classification provides the information required to properly interpret the vane yield stress results and to help understand the interaction mechanisms when coarse particles are added to a fine particle suspension.

Shear conditioning of fine particle suspensions: As discussed in the previous chapter, it is necessary to ensure the suspensions attain a shear-independent state before taking rheological measurements. Therefore, in Section 4.3, the results from the parametric study for the shear conditioning of kaolin and MFT suspensions are presented.

Sand inertness: To show that the chemistry and rheology of the carrier fluid (fine particle suspension) are not significantly affected by the addition (and subsequent removal) of coarse particles, results from the investigations of sand inertness are presented in Section 4.4.

Repeatability test: The repeatability of the procedures followed, and measurements obtained in the current work is reported in Section 4.5. Following this, in Section 4.7, the results for the gel point and close packing fraction of kaolin are reported as well as the methods used to validate the

results obtained. The gel point and close packing fraction of fines are key input parameters for the Lim et al. correlation, since these values are needed for the mixtures gel point and close packing fraction model, i.e. Equations (2.11) and (2.13).

Comparing vane yield stress measurements from different sources: By comparing the vane yield stress results from current study with other recent investigations, the consistency of the vane yield stress measurement is established. This is discussed in Section 4.6. This comparison also supports the reliability of the suspension preparation procedures discussed previously.

Once reliable data were obtained, the results and analysis conducted to fulfill the project objectives included the following:

Evaluation of shear yield stress models: In Section 4.8, three semi-empirical correlations are tested to show the most suitable model to reasonably predict the yield stress of a bimodal suspension based on vane yield stress measurements. In addition to performance, the effect of coarse particle shape and its importance in improving correlations predictive ability are discussed.

Effect of coarse particle size on yield stress augmentation: Here, results obtained using angular and rounded sands as part of the present study are compared with results where several other sands were used in a similar investigation by Spelay et al. [12]. This comparative analysis provides a better idea of the role of coarse particle size on yield stress augmentation, and a better understanding of the mechanisms of interaction of coarse particles with fine-particle suspensions.

4.2 Classification of Coarse Particles for Yield Stress Analysis

Particle characterization provides the information necessary to understand the physics and interaction mechanisms of particles in a fluid-particle system. One of the objectives of this study is to investigate the effect of coarse particle shape and size in yield stress augmentation. Therefore, it is essential to have the information of the size and shape of the coarse particles used in this investigation, and any other coarse particles selected for comparative analysis. By comparing the vane yield stress results for the suspensions containing similar concentration of kaolin and sands, it is expected that the effect of coarse particle shape in yield stress augmentation will be observed with the Sil-1 and LM-50 (since the sizes are similar). Likewise, the effect of size can be investigated

by comparing the data obtained for the Sil-1 and the Sil-325 bimodal suspensions (since the shapes are similar).

The Sil-1, LM-50 and LM-125 sands were classified using the sieve technique to obtain the mass median particle size (d_{50}) of these sands. For the Sil-325 sand, a value of d_{50} = 28μm reported by Gillies [62] has been used because the Sil-325 was obtained from the same source and the careful measurements of Gillies [62] were validated by Smith [74]. Figure 4-1 shows the cumulative particle size distribution (PSD) of the LM-50 and Sil-1 sands. The two sands have very similar mass median sizes: 290 µm for Sil-1 and 310µm for LM-50. But the shapes of these sands are quite different based on their close packing fractions, $C_{max,s}$, as reported in Table 4-1. Since $C_{max,s}$ depends of shape and size distribution of particles [61], in this study it gives an indication of the shape because the size distribution of the sands are similar. More information about the sands used in this work is provided in Chapter 3, Section 3.2.

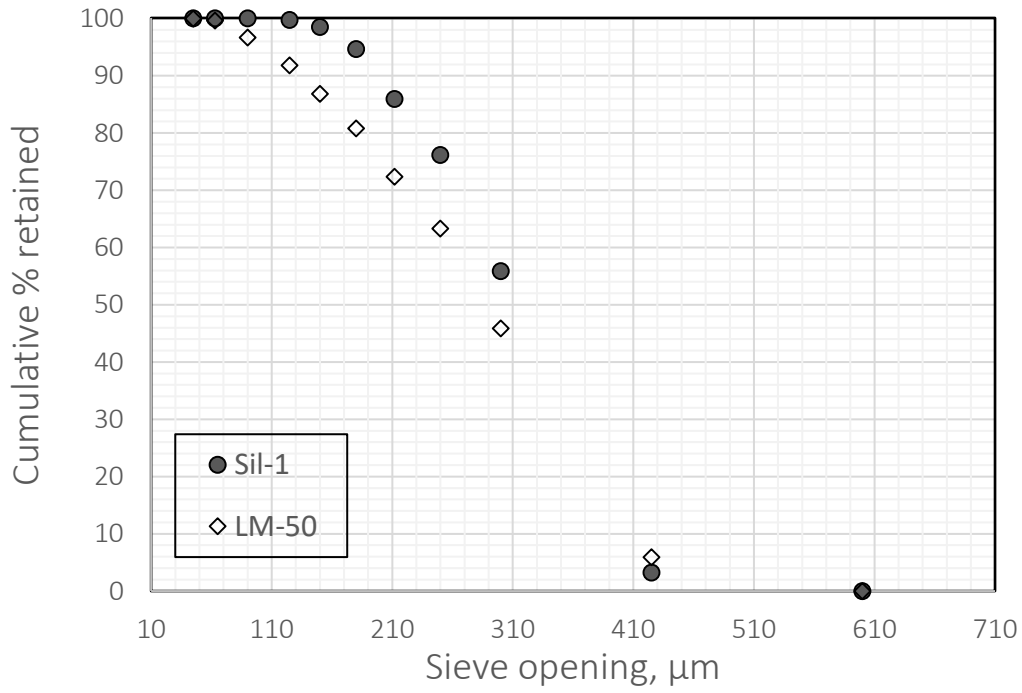

Figure 4-1: Cumulative particle size distribution of the LM-50, LM-125 and Sil-1 sands.

The mass median diameter (d_{50}) and $C_{max,s}$ of the sands used in a similar study by Spelay et al. [12] are also presented in Table 4-1. These sands have varying sizes but can be grouped into two shape categories (angular and rounded sands) based on their respective values of $C_{max,s}$.

Table 4-1: Classification of coarse particles

Types	Shape	$C_{max,s}$	Size $d_{50}(\mu m)$	d_{90}/d_{10}
*Sil-4**	Rounded	0.59	430	0.85
Sil-1	Rounded	0.59	290	0.50
LM-50	Angular	0.49	300	0.34
*GS-5010**	Rounded	0.58	190	0.66
LM-125**	Angular	0.49	100	0.74
LM-70*	Angular	0.48	160	0.38
Sil-325	Rounded	0.62	28	-

*Particles used by Spelay et al. [12].**Particles used in this study and by Spelay et al. [12] **Bolded**: Rounded sands.

4.3 Shear Conditioning of Fine Particle Suspensions

Before taking the vane yield stress measurements of all the suspensions, fines-only suspensions (kaolin-only and MFT) prepared and mixed following the procedure described in Section 3.4.5 were subjected to a shear sensitivity protocol to ensure they attained a time-and shear-independent condition. Figure 4-2 shows the vane yield stress of a 0.24 (v/v) kaolin-only suspension plotted as a function of mixing time. For the MFT, a similar trend is seen, and the plot is provided in Appendix A. This figure shows that the kaolin suspension becomes shear insensitive after a mixing period of 40 mins. Therefore, the mixing period must be at least greater than 40 minutes for accurate results for the mixing conditions selected for this study. Although not shown here, a similar observation was made for the MFT suspensions (see Appendix, Figure A-1).

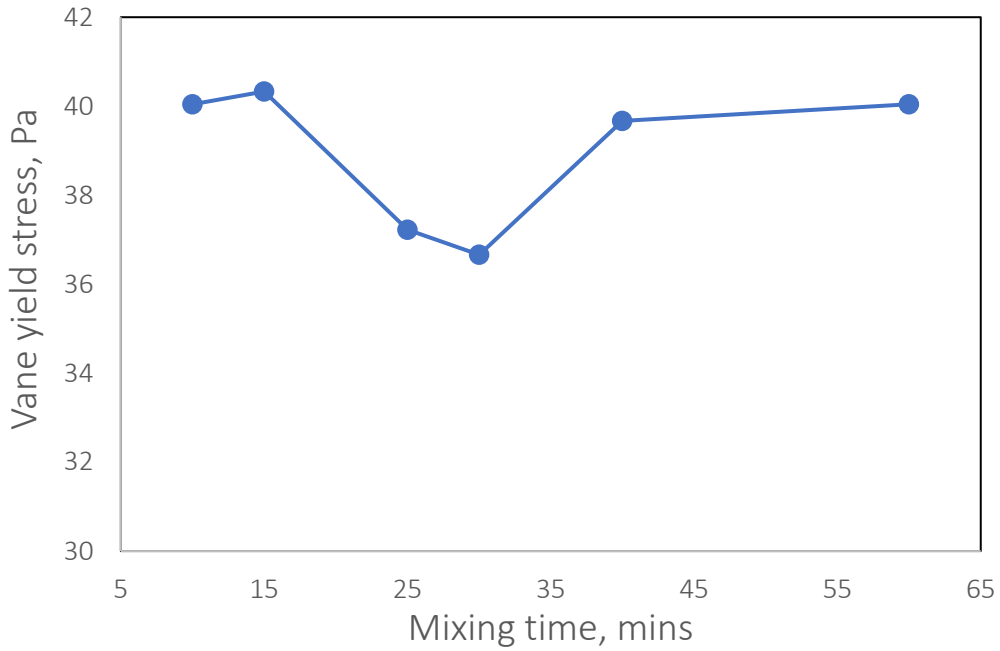

Figure 4-2: Shear sensitivity plot for kaolin-only suspension, $C_s = 0.24$ (v/v). Mixing is done using the overhead IKA RW 20 mixer at $N = 280$ RPM and pH $= 3.63$.

For each of the mixing periods, after taking the vane yield stress measurement of the kaolin and MFT suspensions with the overhead mixer as described above, these suspensions were further stirred by hand, and the vane yield stress measurements were re-taken to investigate:

1. If additional hand-stirring significantly caused a change to the flocs structure; and
2. The appropriate initial mixing time for which the yield stress was least affected by additional hand mixing. Initial mixing time represents the respective mixing periods using the overhead mixer as shown in Figure 4-2.

This investigation was necessary to reduce error associated with the hand-mixing procedures when measuring the vane yield stress of bimodal suspensions. It should be noted that several past investigations have not considered possible errors associated with this step.

Figure 4-3 presents the normalized vane yield stress results for the kaolin and MFT suspensions as a function of initial mixing time. The normalized vane yield stress is the ratio of the vane yield stress measurements made immediately after stirring the suspension by hand to that made after mixing with the overhead mixer; thus, if hand-mixing has no effect, then the vane measurements should be the same. Deviation from the reference case for the kaolin and MFT suspension is lowest

between 30 - 40 mins mixing period. For the kaolin, the maximum estimated error is less than ± 10% seen before the 30mins mixing time. Observation of the MFT suspension deviation is as much as 20%, suggesting the MFT is more shear sensitive with the additional hand stirring when compared to the kaolin suspension.

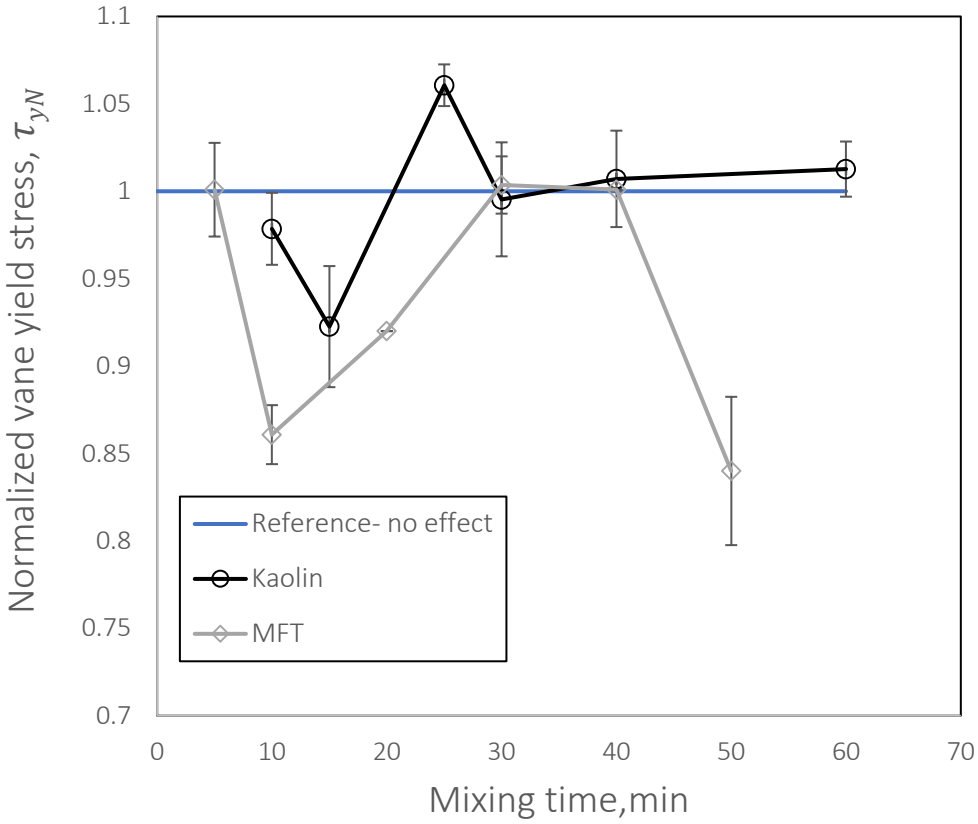

Figure 4-3: Normalized vane yield stress-time response after additional hand-mixing for $C_s = 0.24$ (v/v) and 0.14 (v/v) and pH = 3.63 and 8.17 for kaolin and MFT suspensions respectively. The reference line represents the vane measurements made after mixing with the overhead mixer.

These results show that the additional hand stirring did not significantly affect the rheology of these fine suspensions between 30-40 mins mixing period. Therefore, for the preparation of all model and industrial suspensions tested here, 40 mins mixing time using the overhead IKA RW 20 mixer at a speed of $N = 280$ RPM was chosen, and all additional hand stirring was performed for 5 mins.

4.4 Inertness of Sand

The effect of adding sand particles to the fine suspension was investigated. If there is a significant change to the chemistry and/or the amount of water content, the rheology of the initial fine suspension can be significantly affected. The rheology and water chemistry of the fine particle suspension were tested to determine if a significant amount of water is adsorbed onto the surfaces of sand particles, and if the water chemistry of the fine particle suspension is considerably altered.

The pH, conductivity and the vane yield stress of the initial kaolin-and MFT-only suspensions were taken. Sand was then added to create a bimodal suspension. After about 18 hours, the coarse particles were screened (scalped) out of the bimodal suspension to re-create a fines-only suspension. The pH and conductivity of the resulting suspension was then measured. The results obtained are presented in Figure 4-4.

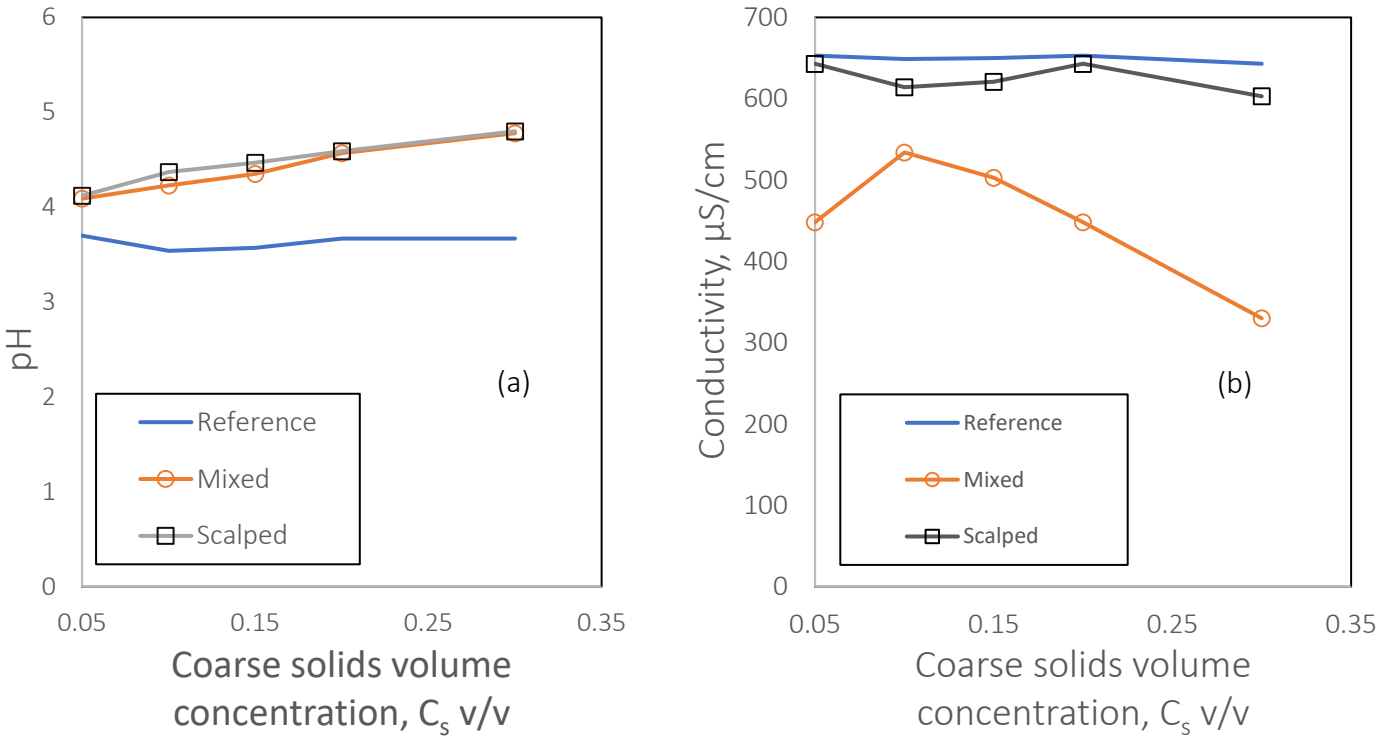

Figure 4-4: Effect of sand particle addition on a kaolin suspension of $C_s = 0.12$ (v/v) using Sil-1 sand at different coarse solid concentrations. (a) mixture pH (b) mixture conductivity. The reference case is the kaolin-only suspension, and mixed is kaolin-Sil-1.

Figure 4-4 shows the pH and conductivity measurements for each of these cases (kaolin only suspensions, kaolin-sand and scalped suspensions). Figure 4-5 presents the vane yield stress measurements as a function of coarse concentration for the kaolin and MFT cases. As shown in Figure 4-4 (a), a slight but irreversible increase in the pH of the kaolin-only suspension is observed with the addition of coarse particles. Figure 4-4 (b) shows that the conductivity of the binary suspension changed from that of the initial fines-only suspension, but when the sand was removed, the conductivity values returned approximately to the initial values. The same trends were observed with the MFT suspension (shown in Appendix B). Although the pH was not returned to the original value, the effect on the yield stress of the kaolin-only suspension was not significant as can be seen Figure 4-5 (a). This figure shows that the yield stress of the scalped kaolin and MFT suspensions were similar to the initial values, suggesting the change in pH that occurred when coarse particles were added did not alter the rheology of the fine suspensions.

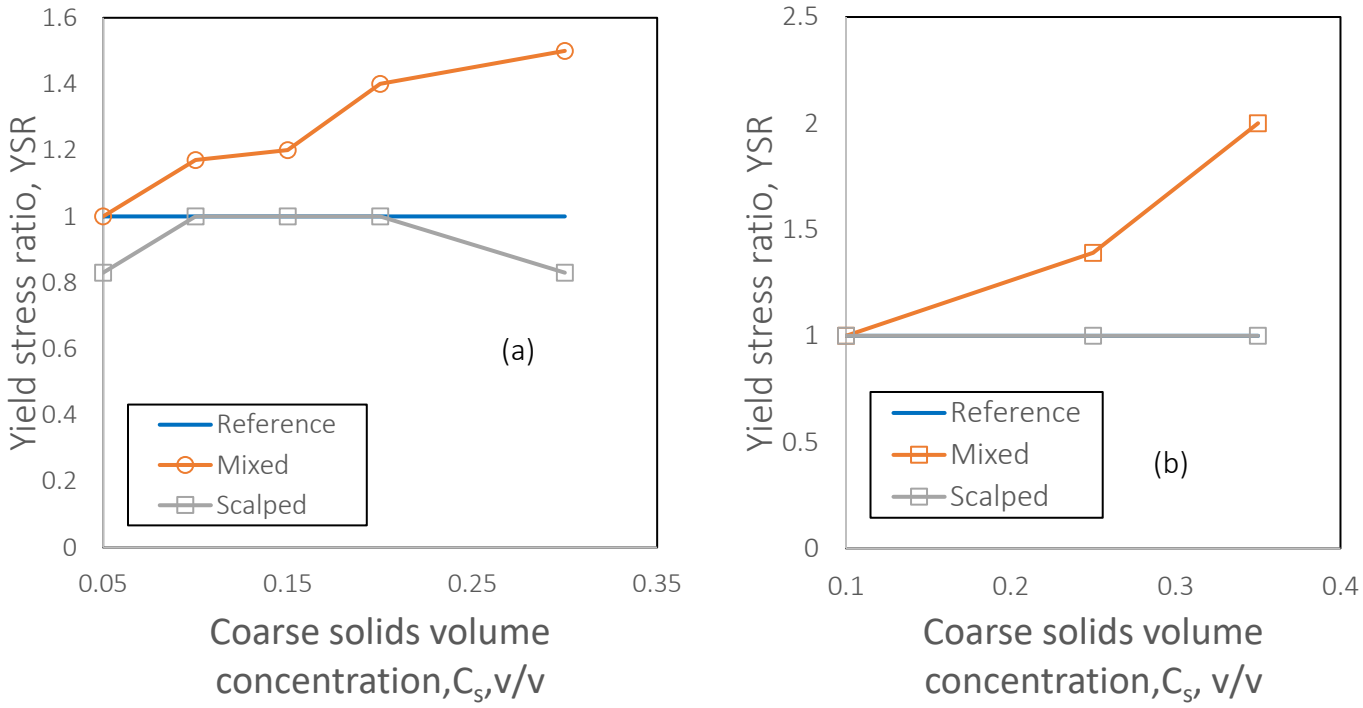

Figure 4-5: Effect of sand particle addition on (a) mixture's yield stress for kaolin suspension of C_s = 0.12 (v/v) using Sil-1 sand at different concentrations and (b) MFT of C_s = 0.11 (v/v). The reference cases are kaolin and MFT only suspensions.

In general, this reversible rheology suggests that the chemistry and floc structure of the kaolin and MFT only suspensions were not significantly altered by the introduction of sand. It also strongly indicates that the coarse particles did not change the water content (amount) of the initial fines-only suspensions through adsorption.

4.5 Repeatability Tests

Here, repeated experiments as discussed earlier in Section 3.5 are presented to check the variability between the vane yield stress measurements. The result presented here is for the case of C_f = 0.15 kaolin concentration because it is a common concentration repeated for all three types of sands tested in this work, while other results are given in Appendix A.

The vane yield stress ratio measurements for kaolin-sand suspensions are presented in Table 4-2 to Table *4-4* . The low errors shown in these tables indicate that the repeatability of the vane yield stress measurement is generally high, and this high repeatability is observed with other repeated cases, as reported in Appendix A.

The results indicate that the procedures adopted for preparing the bimodal suspension along with the vane yield stress measurement method give consistent and repeatable results when determining the increase in yield stress of bimodal suspensions.

Table 4-2: Repeatability for Sil-325

C_s	Vane yield stress ratio (Initial)	Vane yield stress ratio (Repeated)	% Error
0.00	1.00	1.00	0.00
0.03	1.06	1.10	3.77
0.10	1.23	1.22	-0.80
0.25	2.29	2.54	10.9
0.35	6.90	7.01	1.59

Table 4-3: Repeatability for Sil-1

C_s	Vane yield stress ratio (Initial)	Vane yield stress ratio (Repeated)	% Error
0.00	1.00	1.00	0.00
0.03	1.06	1.00	-5.66
0.10	1.09	1.11	1.83
0.25	1.45	1.36	-6.21
0.35	2.45	2.18	-11.02
0.46	7.50	7.90	5.33

Table 4-4: Repeatability for LM-50

C_s	Vane yield stress ratio (Initial)	Vane yield stress ratio (Repeated)	% Error
0.00	1.00	1.00	0.00
0.03	1.00	0.98	-2.00
0.1	1.01	1.09	7.92
0.25	1.59	1.63	2.51
0.35	3.59	3.82	6.40
0.4	8.55	8.29	-3.04

4.6 Comparing Vane Yield Stress Measurements from Different Sources

To ensure that the shear conditioning and mixing methods employed in this study are effective and that the results are consistent, the vane yield stress measurements for the bimodal suspensions containing kaolin and LM-125 sands used in this study and in Spelay et al. [12] are compared. This was done because the LM-125 sand used is known have comparable PSD as shown in Figure 3-11. As mentioned in Chapter 3, unlike the overhead mixer plus hand-mixing steps used

in this work, a paint-mixer was employed by Spelay et al. [12] for mixing and preparing their bimodal suspensions. If the choice of mixing process (shaker vs. hand stirring) did not affect the quality of measurements, it is expected that the magnitude of increased yield stress is the same for both datasets.

In Figure 4-6, the vane yield stress ratios plotted against sand volume concentration is presented for kaolin volume concentration of 0.15 (v/v) for the LM-125 sand cases. A comparable magnitude in the yield stress ratio is shown in this figure which means that the methods adopted for mixing, as well as the rheology measurement techniques are consistent. This is a very important result, since consistent rheological measurements between datasets are essential to develop a general model to accurately predict the yield stress of a bimodal suspension.

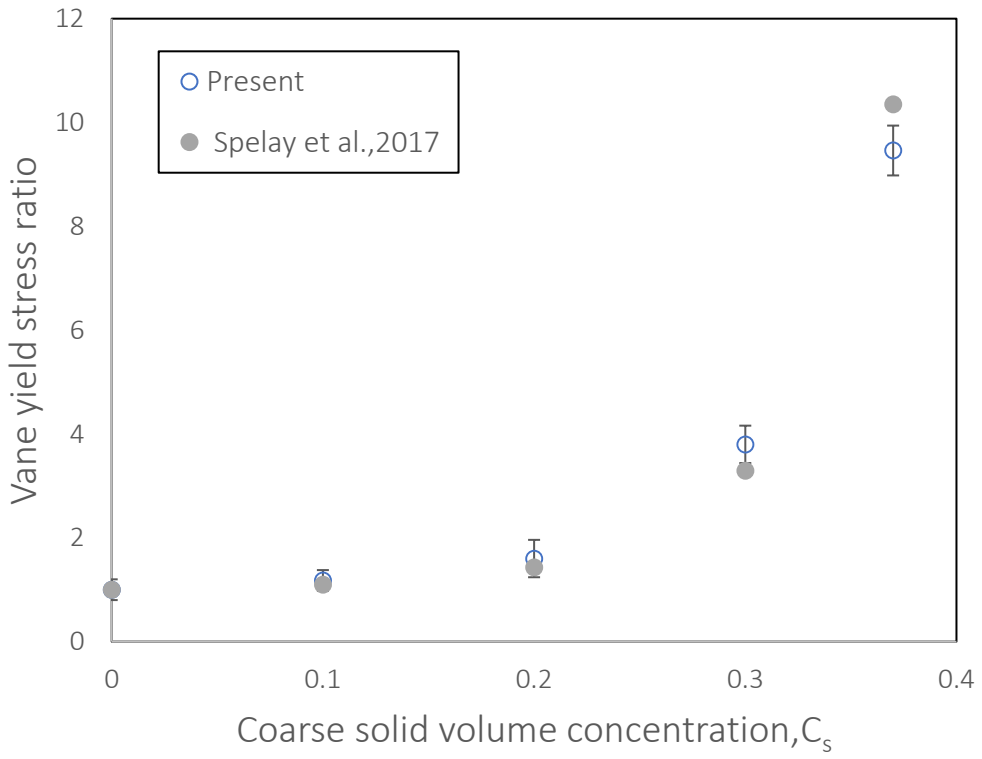

Figure 4-6: Comparison of the vane yield stress measurements for similar fine and coarse concentration from different sources using the LM-125 sands.

4.7 Measurements of Basic Parameters of Kaolin-only Suspension

The estimation of the gel point and close packing fraction of fine particle suspensions is essential because these parameters are required inputs for the Lim et al. [23] model.

4.7.1 Gel Point

As discussed in Chapter 3, the gel point of kaolin was determined using equilibrium batch settling tests. Although many batch settling tests were completed during this process for different initial solid volume fractions, the results shown here are for an initial solids volume fraction of 0.02. This value was selected for presentation here because the constant initial solids concentration provided a more accurate result than the higher initial solid volume fractions tested. The detailed results from these initial tests are summarized in Appendix A. As shown in Figure 4-7, the gel point is obtained by plotting the average solid volume fraction, C_{avg}, against the base pressure, P_{base}.

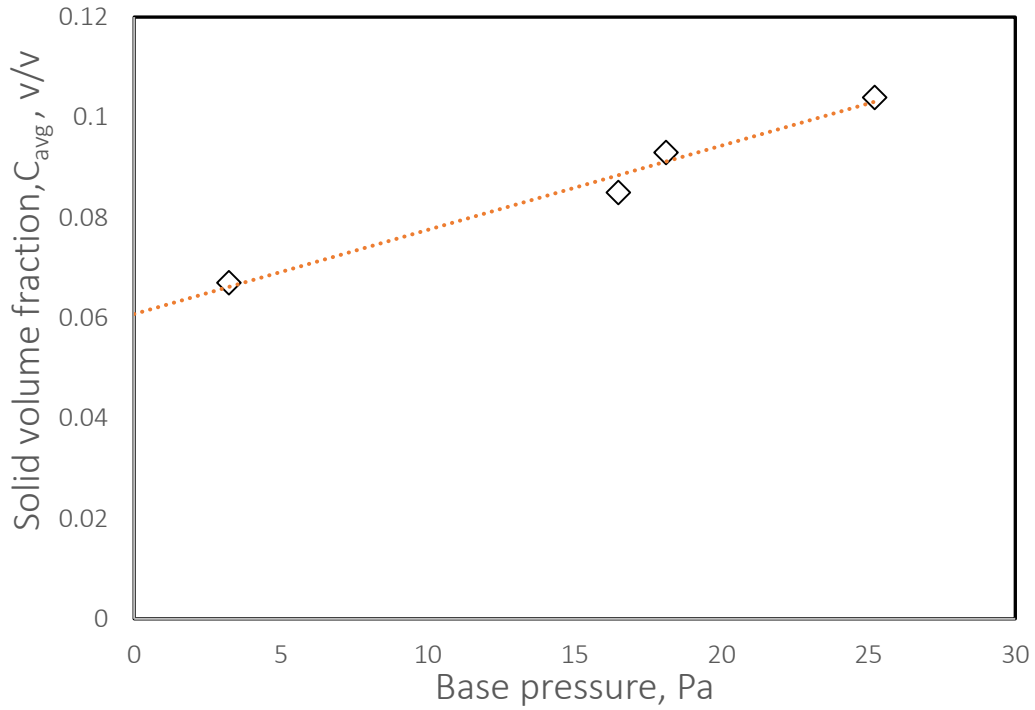

Figure 4-7: Estimated gel point of kaolin at a constant initial solid volume fraction of 0.02 (v/v) using flat bottom settling columns.

The intercept obtained from the linear regression of these data gives the gel point of kaolin which, as shown in Figure 4-7, is estimated to be $C_{g,f} = 0.06$. With this estimated value for the kaolin-only suspension, the gel point of mixtures containing both fines and sand can be evaluated using

the constitutive mixture gel point model, Equation (2.11). Also, the determination of the gel point of the fines-only suspension partly fulfils the objective to experimentally determine the key parameters of the Lim et al. [23] model. Lastly, the gel point of kaolin becomes an input parameter in the YODEL model used, which is to determine the close packing fraction of kaolin.

As discussed in Chapter 3, the gel point procedure was validated using AKP-50 as a reference material and Figure 4-8 presents the gel point of AKP-50 following the methods used for the kaolin. The initial solids volume fraction of AKP-50 was taken as $C_o = 0.04$ for the batch settling experiments and the gel point of AKP-50 is 0.071 as indicated on the graph. The gel point obtained compares favorably with the 0.06 value reported in the literature [23]. Furthermore, the gel point of kaolin in this work also compares favorably with literature values ranging between 0.04 -0.1 [71, 75]. Therefore, the method gives reasonable results for both kaolin and AKP-50.

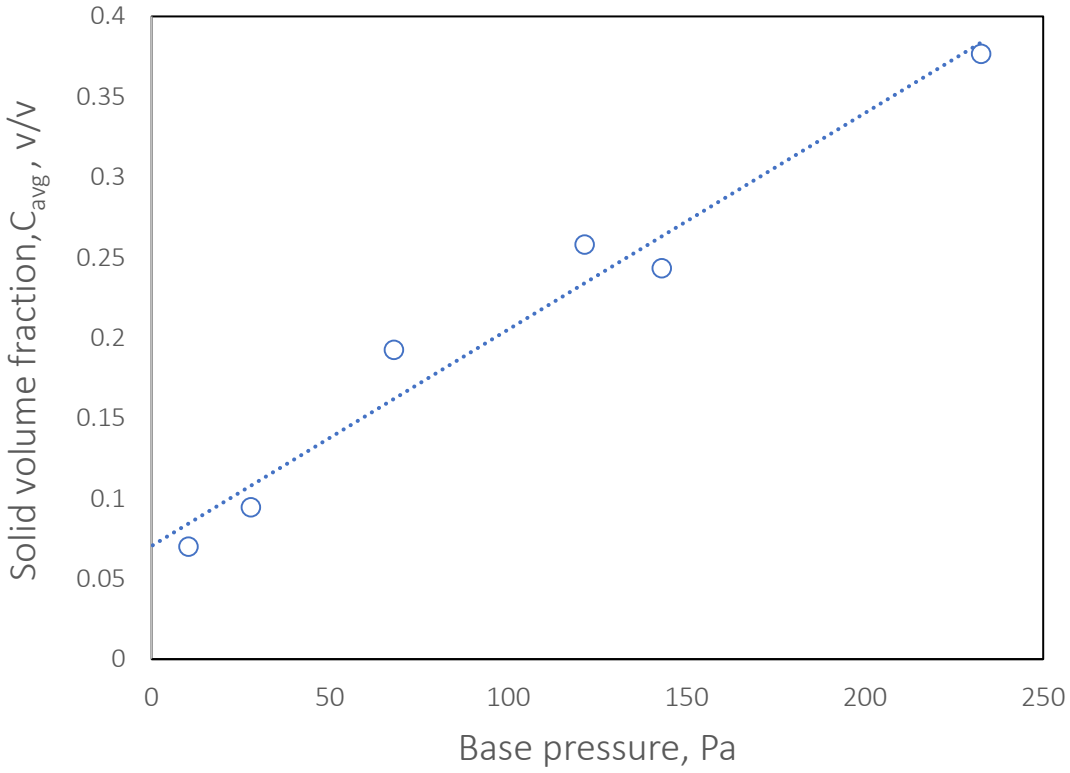

Figure 4-8: Solid volume fraction against base pressure to estimate the gel point of AKP-50 using initial solid volume fraction of 0.04 (v/v).

4.7.2 Close Packing Fraction

The close packing fraction of kaolin was estimated using the YODEL [73] model, given earlier as Equation (3.8). Figure 4-9 shows the graph obtained by fitting the measured vane yield stress data for solid volume fractions of kaolin between 0.08 - 0.22 with the YODEL model [73]. The close packing fraction of kaolin, $C_{cp,f}$ is the fitting parameter and was estimated as 0.52 using the least squares method. This was done by setting the percolation threshold parameter [42] (the gel point) to 0.06, which was the value obtained from the batch settling tests described in the previous section.

Again, with this estimated value for the kaolin-only suspension, the close packing values for mixtures containing fine and sand can be evaluated using the constitutive mixture close packing fraction model, Equation (2.13). Again, this partly fulfils the objective to experimentally determine the key parameters of the Lim et al. [23] model.

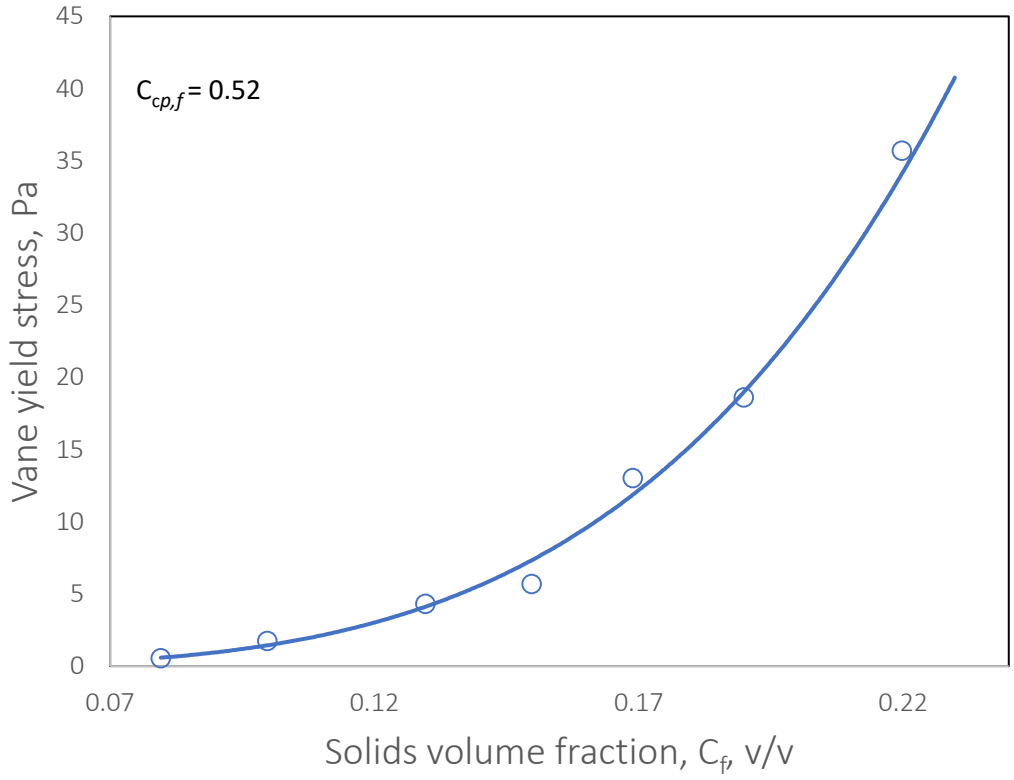

Figure 4-9: Determination of kaolin close packing fraction using the YODEL model [67].

The close packing fraction of kaolin was validated using Liu's model as discussed in Section 3.4. Figure 4-10 shows the plot of $1-\eta_r^{-1/n'}$ against the solid volume fractions of kaolin, C_f ,for n' = 4.2. The analytical solution shown in the graph below shows that when the y-axis value is 1, the corresponding value of the x-axis, which gives the close packing fraction of kaolin is 0.509. This value is in excellent agreement with the value obtained using the YODEL.

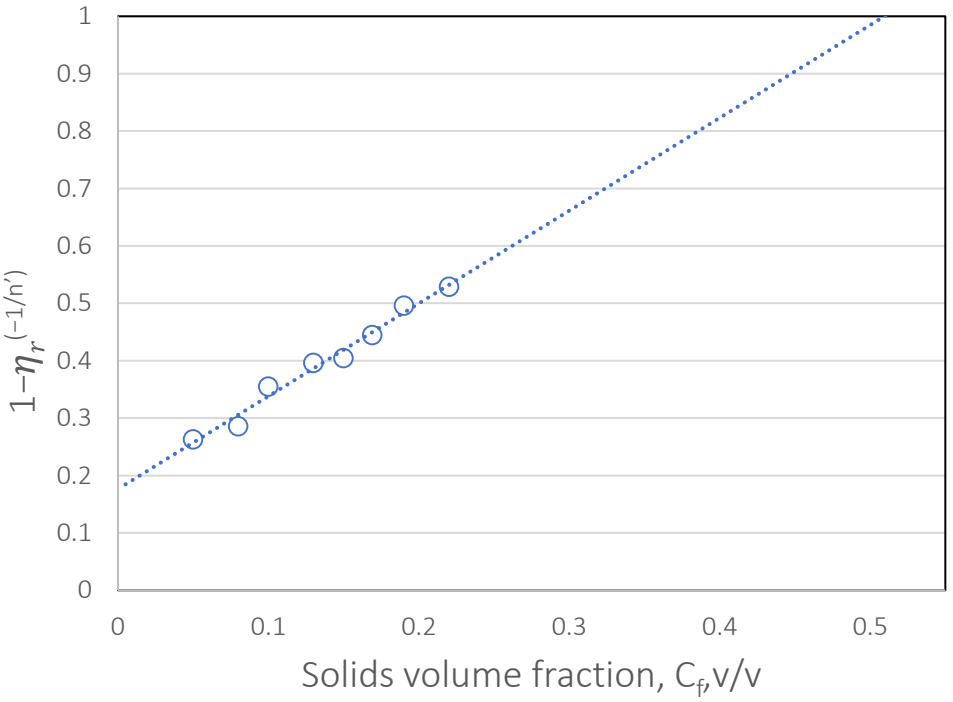

Figure 4-10: Well fitted linear correlation for the relative viscosity data of kaolin suspensions using Liu's model [65].

4.8 Rheology of Bimodal Suspensions: Evaluation of Three Semi-empirical Shear Yield Stress Correlations

In this section, the performance of the semi-empirical correlations is evaluated and discussed for both the industrial and idealized bimodal suspensions.

4.8.1 Lim et al. Correlation Performance – All data

To show the model's performance for a single suspension type, the vane yield stresses of kaolin-sand mixtures are first plotted for the kaolin–Sil-1 suspension. Note that any of the other sands, i.e. LM-50 or Sil-325, used in this study could have been considered at this point, i.e. there was no specific reason to study the Sil-1 mixtures first. The vane yield stress data for the Sil-1 tests

$\left(0 \leq C_s \leq 0.8\, C_{max,s}\right)$ are presented in Figure 4-11, where the vane yield stress is plotted against "X" which again is the compound term defined as:

$$\boldsymbol{X = \left(\frac{\left(C_{cp,m} - C_m\right)\left(b + C_m - C_{g,m}\right)}{\left(C_m - C_{g,m}\right)}\right)} \tag{4.1}$$

These data were fit with the power form of the Lim et al. [23] model discussed in Chapter 2, to obtain the fitting parameters a' and c. The values of a' and c for all suspension types are also presented in Table 4-5. Figure 4-11 shows that overall, the fit for the Sil-1 data is reasonably good, even as shown by the goodness-of-fit in Table 4-5. The fitting parameters obtained from the kaolin–Sil-1 tests for the full data set (i.e. $0 \leq C_s \leq 0.8\, C_{max,s}$) are then used to predict the vane yield stress of other kaolin-sand suspensions.

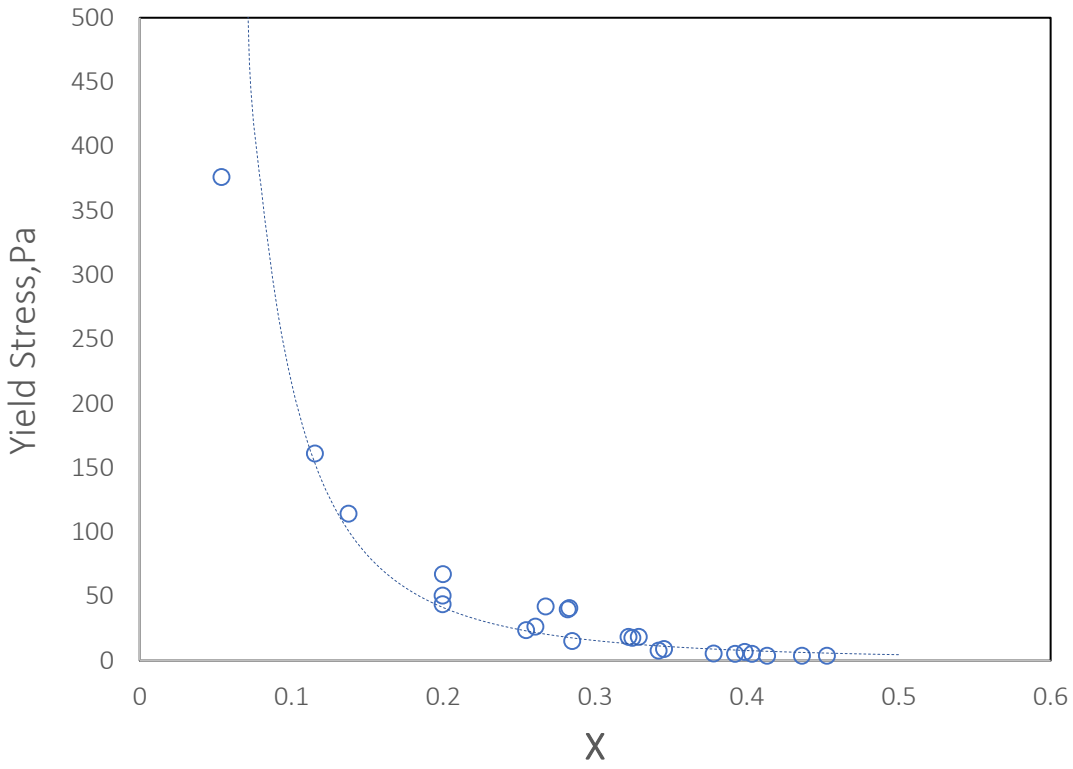

Figure 4-11: Lim et al. [21] correlation fit for the kaolin–Sil-1 suspensions data using all coarse particle concentrations.

Table 4-5: Comparison of the Lim et al. [21] correlation fit for kaolin–Sil-1 and LM-50 at different sand concentrations

$C_s/C_{max,s}$	R^2		a'		c'	
	Sil-1	LM-50	Sil-1	LM-50	Sil-1	LM-50
0	0.99	0.99	0.01	0.01	-6.39	-6.66
≤ 0.5	0.91	0.97	0.13	0.10	-4.21	-4.51
≤ 0.8	0.86	0.97	1.76	0.40	-2.04	-3.19

This is shown with the parity plot in Figure 4-12 (b); a subset of Figure 4-12 (a). Since the fitting parameters have been obtained for the Kaolin – Sil-1 sand, the generality and predictive capacity of the model can be tested on other sand types using this set of parameters.

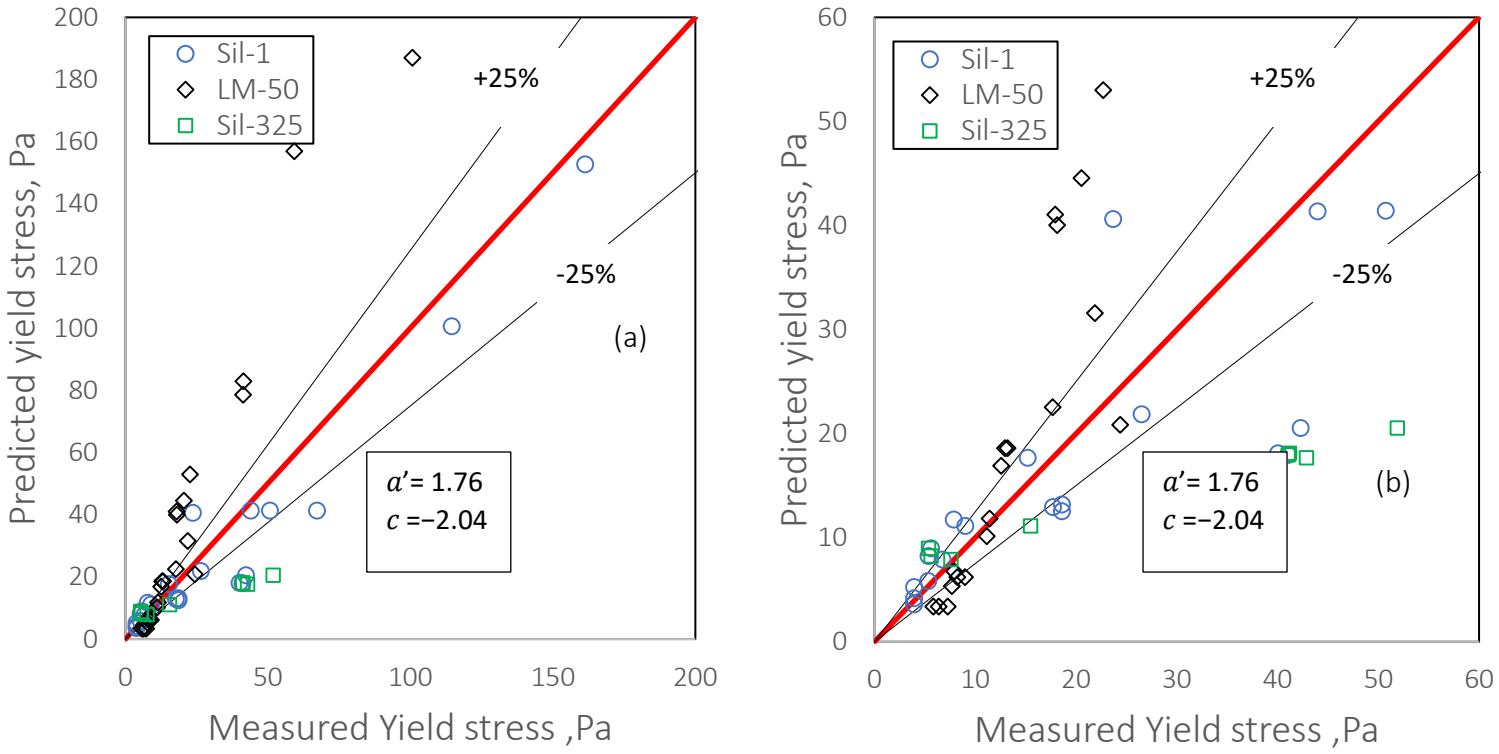

Figure 4-12: Parity plot for the bimodal suspensions of kaolin-sands. The predicted vane yield stress values are obtained with the Lim et al. [21] correlation showing: (a) full data set and (b) the subset of (a).

Figure 4-12 (a) presents the parity plot for all the three sands tested in this study. Here the predicted vane yield stress data are obtained using the values of a' and c for the Sil-1 data (i.e. $a' = 1.76$, $c = -2.04$). The predicted data are plotted against the measured values for $0 \leq C_s \leq 0.8\, C_{max,s}$. (i.e. the "full" data set). Figure 4-12 (b) is a subset of Figure 4-12 (a) which shows the low coarse concentration values. In this study, "low coarse concentration" values defined arbitrarily as $0 \leq C_s \leq 0.5\, C_{max,s}$. These figures show that the predictions made for the Sil-325 and LM-50 data deviate from the parity line significantly and systematically.

This strongly suggests that the fitting parameters of the Lim et al. [23] depends on coarse particle properties such as shape and size. For the case of coarse particle shape, the LM-50 and the Sil-1 sands have comparable sizes as shown in Figure 4-1, but their shapes (as indicated by the $C_{max,s}$ values) are different. For the Sil-325 sand, the deviation is apparently related to particle size since the size of the Sil-325 is much smaller compared to other sands but has a similar $C_{max,s}$ to the Sil-1 sand.

The accuracy of these predictions is also estimated using the absolute relative error:

$$\%E = \left(\frac{|Y_m - Y_p|}{Y_p}\right) * 100 \tag{4.2}$$

where Y_m is the measured vane yield stress and Y_p is the predicted vane yield stress. The two absolute relative errors used for quantitative analysis in this study are the maximum (E_{max}) and average (E_{avg}) errors:

$$\%E_{max} = max(E_i),\ i = 1\ to\ N \text{ and,} \tag{4.3}$$

$$\%\boldsymbol{E_{avg}} = \frac{\sum_{\boldsymbol{i}}^{\boldsymbol{N}}(E_i)}{N} \tag{4.4}$$

where N is the number of data points used for the analysis. The maximum and average errors for the kaolin-sand suspensions with the Lim et al. correlation is provided in Table 4-6.

Table 4-6: Absolute errors for the Lim et al. correlation predictions for the kaolin-sands suspensions

Error	Sil-325	Sil-1	LM-50
$\%E_{max}$	840	128	164
$\%E_{avg}$	87.9	36.9	64

The significant error values shown in Table 4-6 further indicates the poor predications obtained using the Lim et al. correlation.

A similar trend was also observed for the case of the industrial MFT suspensions using the LM-50 and the Sil-1 sands. In Figure 4-13, the experimental data for these two sands and the different best fits are shown.

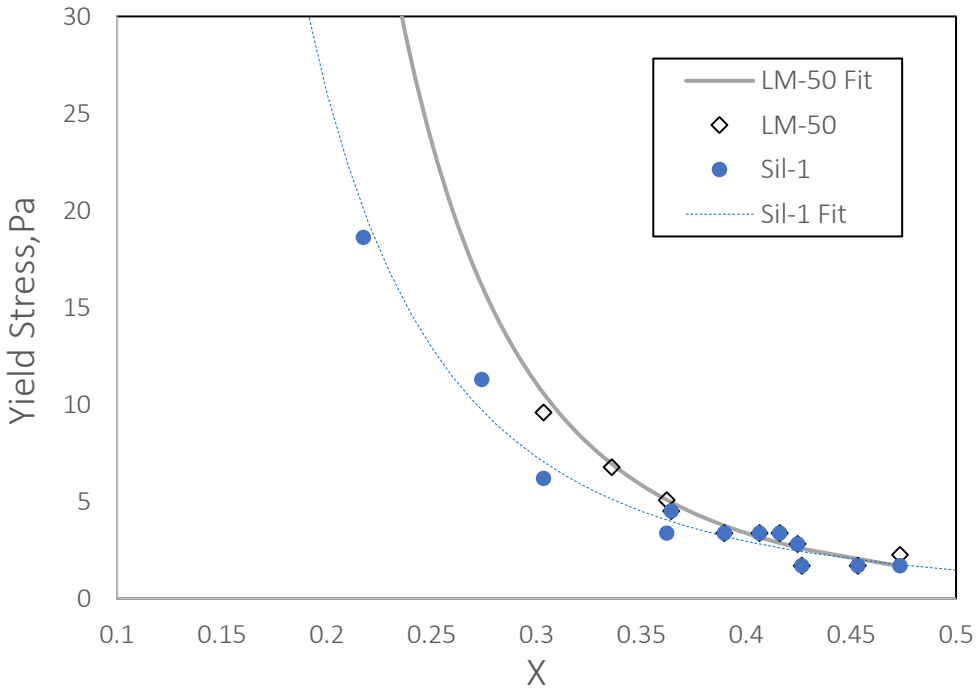

Figure 4-13: Lim et al. [21] correlation fit for the industrial MFT suspensions with LM-50 and Sil-1 sands. The best-fit parameters are given in Table 4.5.

These best fit lines for these MFT-sands suspensions have been obtained using different fitting parameters as shown in Table 4-7. This difference strongly suggests that for these data, the fitting

parameters also are affected by the shape of the coarse particles, just as seen with the idealized bimodal suspensions.

Table 4-7: Comparison of the Lim et al. [21] correlation fit for the MFT- Sil-1 and LM-50 sands

Sand type	a'	c	R^2
LM-50	0.08	- 4.03	0.93
Sil-1	0.17	- 3.14	0.97

The parity plot in Figure 4-14 shows the prediction and accuracy of this model on the MFT-sand suspension systems. The plot presents the prediction of the vane yield stress measurements for the MFT– LM-50 suspension using the set of fitting parameters obtained with the Sil-1 sand.

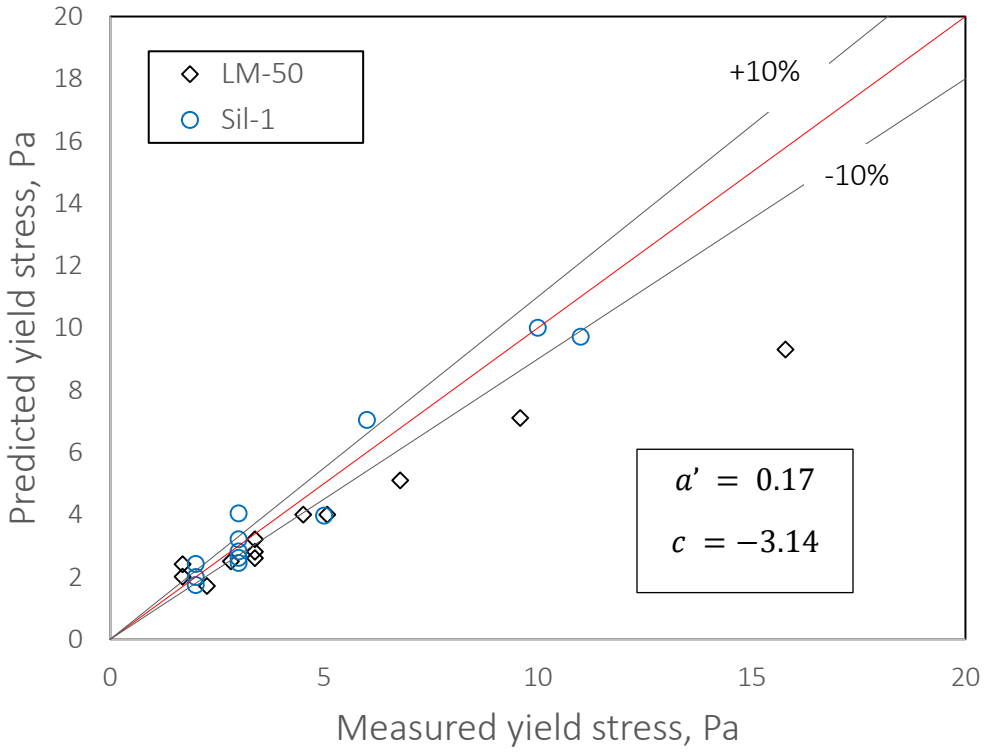

Figure 4-14: The Parity plot for bimodal suspensions (MFT-sands) using the fitting parameter obtained for the MFT–Sil-1 data.

Compared to the kaolin case where many data points fall beyond the ± 25% error boundary, with the MFT, a reduced error for the Sil-1 fit is seen within a ± 10% error margin, and the deviation of LM-50 is equally reduced. Again, the maximum error values for the LM-50 and Sil-1 suspensions are 41.8 and 34.6 and average errors are 22.1 and 12.9 % respectively. This improvement is most probably due to the limited number of volume concentrations of MFT tested.

In the next section, low coarse concentration data are considered to investigate the accuracy and predictive capacity of the Lim et al. [23] model if limitations is placed on coarse sand concentration.

4.8.2 Lim et al. Correlation Performance - Low Coarse Concentrations

This section provides analysis of the model predictive performance considering low coarse concentrations. A set of fitting parameters, a' and c were obtained for the vane yield stress measurements of kaolin–Sil-1 tests for only low coarse concentrations ($C_s \leq 0.5\ C_{max,s}$) as shown in Figure 4-15. In this figure, the blue markers denote vane yield stress measurements associated with the highest kaolin concentration,$C_f = 0.24$, while the open markers are for $C_f = 0.20$, and the grey markers are the data for kaolin concentrations lower than $C_f < 0.20$.

From this figure, the scatters in the region of $X < 0.3$ (and shown in the box) is influenced by the concentrations of both sand and kaolin. This scatter affects the accuracy of the fit, hence the obtained fitting parameters. The values of a' and c obtained from the Sil-1, in Figure 4-15, were used to predict the LM-50 and Sil-325 vane yield stress data. Figure 4-16 is the parity plot to show the accuracy of the vane yield stress predictions for kaolin-sands suspensions at low coarse concentrations.

Although some of these data fall beyond the ±25% error margin, in comparison with the results presented in Figure 4-12, the Sil-325 and LM-50 results are predicted with an overall improved accuracy using the Sil-1 best-fit parameters.

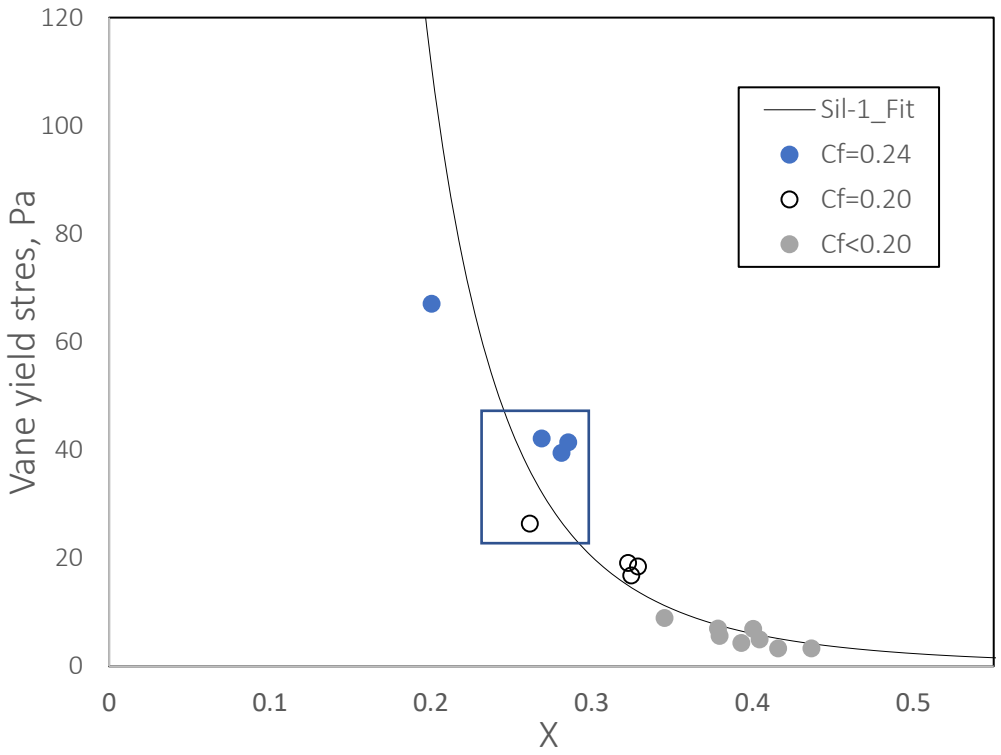

Figure 4-15: Sil-1 data fit for low coarse concentrations for kaolin suspensions. The fitting parameters $a' = 0.13$ and $c = -4.21$.

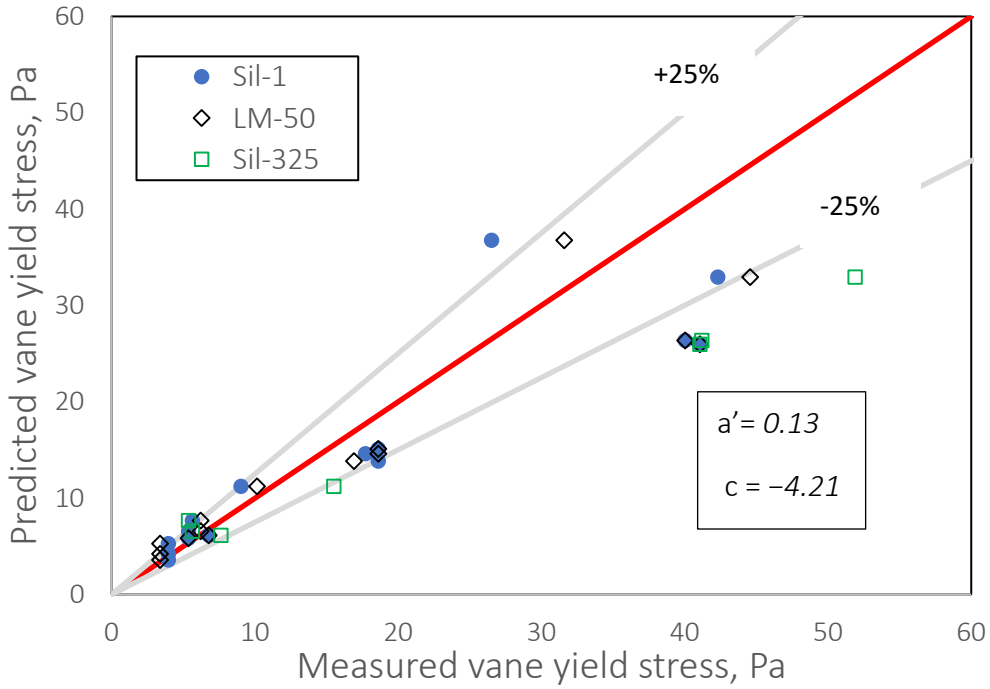

Figure 4-16: Parity plot for kaolin-sand mixtures using the fit obtained for Sil-1 ($a' = 0.13$ and $c = -4.21$) at low coarse concentration for the three sand types.

The only difference between these cases is the reduced coarse concentration limit has been used to obtain a new fitting parameter. Therefore, it can be inferred from these results that the accuracy of prediction improved at low coarse concentrations. Here, the predictions are all within about 25-30% (absolute) of the experimental measurements; for the full data set (all coarse concentrations), many predictions were wrong by 100% or more (see Figure 4-12).

In addition to investigating the accuracy of the Lim et al correlation, sensitivity analyses were conducted on the impact of the gel point and close packing fraction on the predictive capacity. These results of theses analyses show that the gel point and close packing fraction of fine did not significantly change the predictions, and these results are reported in the Appendix.

In summary, the correlation of Lim et al. [21]

- Requires, at the minimum, measurements of the gel point and close-packing fraction of the fine-particle suspension;
- Appears to require full sets of measurements to be made for all clay concentrations (and likely water chemistry and ion loading, although this was not tested) and thus cannot be considered to be a model at all;
- Provides more reasonable predictions that are independent of coarse particle size and shape if an upper limit of $0.5C_{max,s}$ is placed on the coarse solids concentration.

4.8.3 The Deltares Correlation Performance

Recall that the Deltares model requires only the water-content to carrier fluid (W_f) and linear concentration (λ), which captures the coarse particle shape and concentration. This model does not require the microstructural measurements such as, gel point and close packing fraction of the Lim et al. [23] model. First, the Deltares model was used to fit the yield stress of kaolin–LM-50 sand suspensions as shown in Figure 4-17 (which shows the semi-log graph for the vane yield stress of LM-50 plotted against water-content-to-clay ratio) to obtain the fitting parameter. The average values obtained for each of the fitting constants for different linear concentrations from Figure 4-17 were then used to predict the vane yield stress of other kaolin-sand suspensions, i.e. the Sil-1 and the Sil-325 sands.

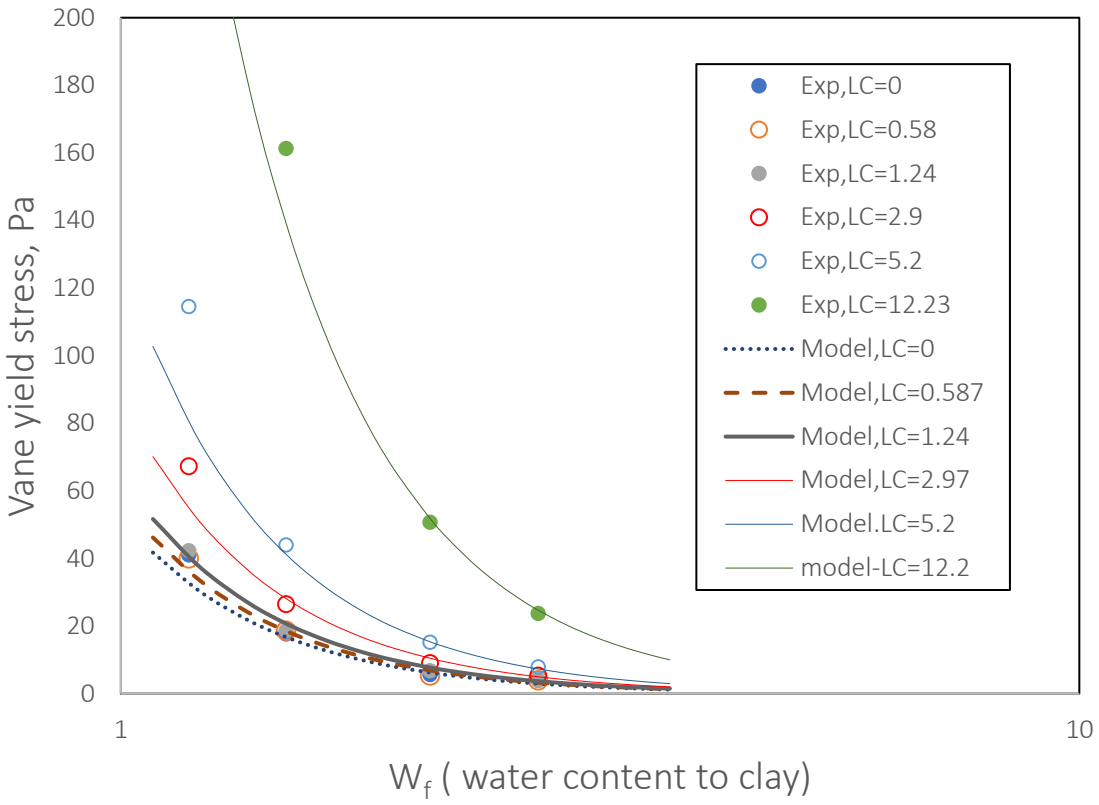

Figure 4-17: Vane yield graph for the kaolin-LM-50 data using the Deltares model, showing different values of Linear sand concentration (λ) denoted by LC. The fitting constants are A = 52, β = -2.86 and α = 0.17.

The predictions are presented in Figure 4-18. It can be seen that most of the predicted values fall within a reduced ± 15% error boundary, as compared to the ± 25% margin of the Lim et al. [23] model. The improvement is shown with the reduced maximum and average computed errors estimated for these sands which are presented in Table 4-8. This improved prediction and accuracy indicates that the Deltares model performs better than the Lim et al. [23] model for the data obtained in this study.

Furthermore, the fact that the Sil-325 data fall outside the boundaries suggests that the model may not fully capture the effect of coarse particle size on yield stress augmentation or at least the effect of fine-coarse particles. Therefore, there is a need to adapt the model to account for this parameter. It should be noted that the set of data presented in Figure 4-18, is for the full data $\left(0 \leq C_s \leq 0.8\, C_{max,s}\right)$ which has been truncated to magnify the details of the plot, and there was no need to consider low coarse concentration because the full data set predicted well.

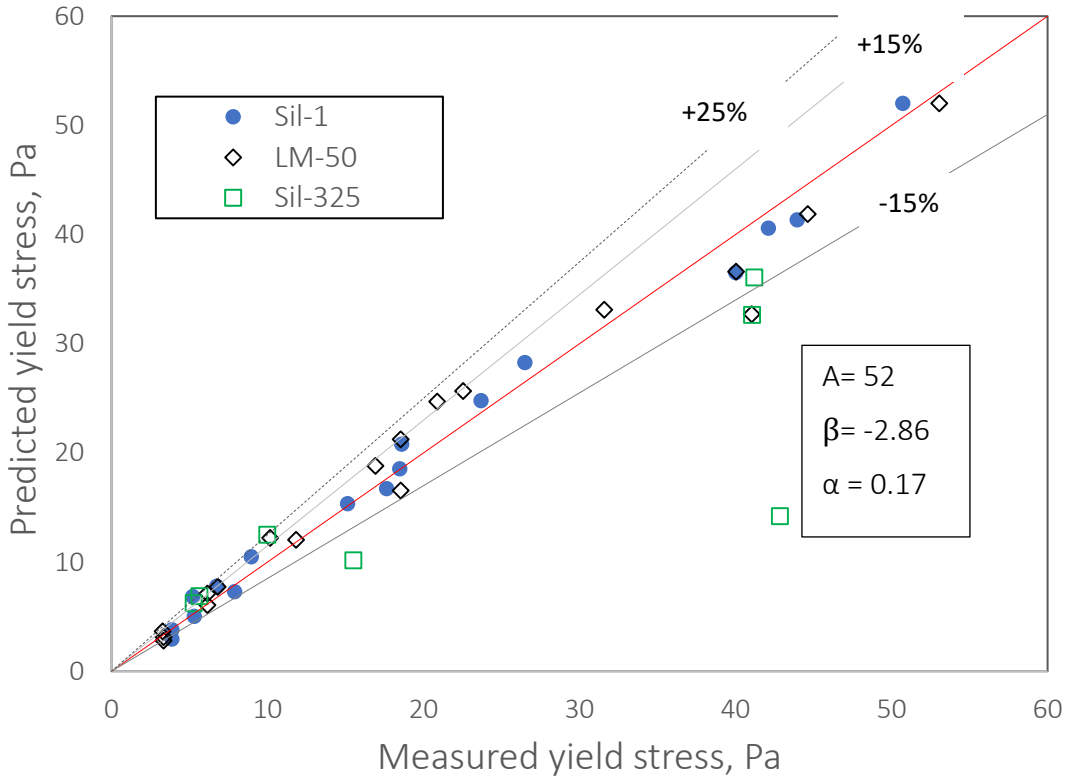

Figure 4-18: Plot to compare the accuracy and effect of coarse particle shape using the Deltares model for Sil-1, LM-50 and Sil-325 sands. The fitting constants $A = 52$, $\beta = -2.86$ and $\alpha = 0.17$ have been used for the Deltares model prediction.

Table 4-8: Absolute errors for the Deltares correlation predictions for the kaolin-sands suspensions

Error	Sil-325	Sil-1	LM-50
$\%E_{max}$	201	31.9	25.5
$\%E_{avg}$	49.9	8.89	10.9

In addition to the idealized bimodal suspension, the Deltares model was also tested on the MFT–sand suspensions. As in the case of kaolin-sand suspension above, the set of fitting constants obtained with the MFT–LM-50 sand was used to predict the vane yield stress of the MFT–Sil-1 sands as shown in Figure 4-19, which is the parity plot for the MFT–sand suspensions. It should be noted that the fitting constants obtained for the MFT–sand suspensions are different than those

obtained for the kaolin–LM-50 case. The difference can be associated with several possible reasons, such as chemistry of carrier fluid, coarse particle concentration and /or material, and the composition of the MFT. Figure 4-19 also shows that similar error margin is seen for the industrial MFT and kaolin cases using the Deltares model. The maximum error for these LM-50 and Sil-1 are 24.2 and 32.3% and the absolute average errors are 14.9 and 16.1% respectively. These error values are very close to those obtained in Figure 4-18.

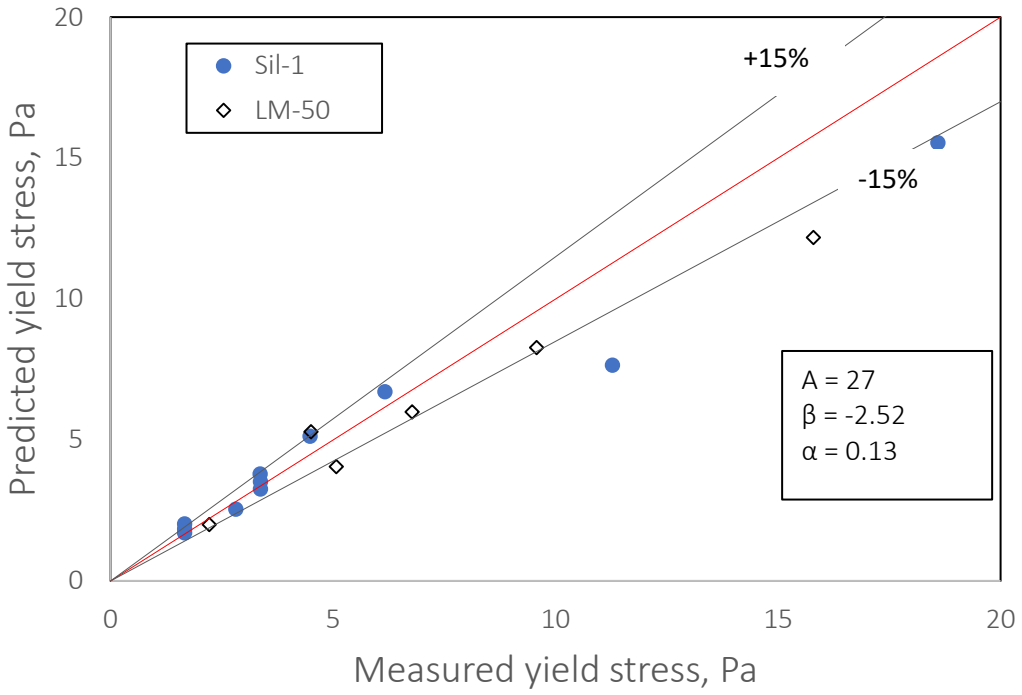

Figure 4-19: Plot to compare accuracy and effect of coarse particle shape using the Deltares correlation for Sil-1, LM-50 and Sil-325 sands In MFT suspensions; $A = 27$, $\beta = -2.52$, $\alpha = 0.13$

Therefore, according to the limited results for the industrial MFT tests, it can be deduced that the Deltares model provided a reasonable prediction, since the model captures the effect due to the shape and concentration of coarse particles through the linear concentration parameter (λ).

Furthermore, in order to investigate the general application of the Delatres model, the vane yield stress data for the kaolin-LM-50 sand suspension in this work was predicted with the estimated fitting parameter obtained from Van de Ree [26] for their “unremoulded” kaolin-sand data. According to Van de Ree [26], “unremoulded” is referred to as unsheared condition. Likewise, the vane yield stress data for the unremoulded mixture was predicted using the set of fitting

parameters obtained in the current study. The parity plots for these cases are presented in Figure 4-20.

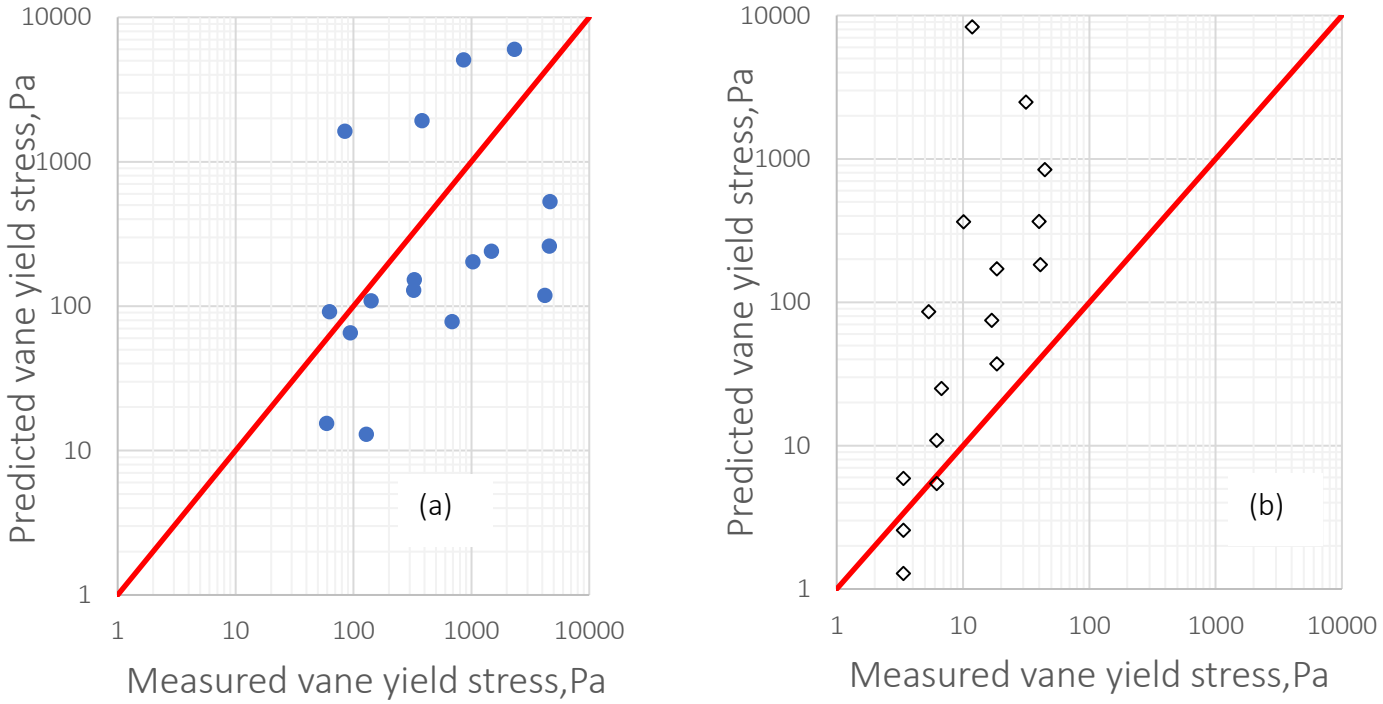

Figure 4-20: A log-log parity plot for: (a) the "unremoulded" kaolin-sand mixtures data of Van de Ree [20], using the fitting constants; $A = 52$, $\beta =$ -2.86, $\alpha = 0.17$ obtained in this study, and (b) the kaolin-LM-50 sands using the estimated fitting constants; $A = 337.8$, $\beta =$ -2.689, $\alpha = 0.121$.

As shown in this graph, there is significant deviation of the predictions from the measured values. This indicates that a poor prediction is obtained with the Deltares model using a "default" set of fitting parameters, suggesting that the model is not generally applicable.

The Deltares model does appear to provide reasonably good predictions if the model constants are tuned based in experimental measurements on the system under consideration.

4.8.4 The Thomas Correlation Performance

The Thomas [25] model was also tested on the industrial and idealized bimodal suspensions, but the vane yield stress results presented here are for the idealized case. The best fitting value of A was found to be 2 with the kaolin–Sil-1 data, and this value was used to predict the vane yield stress data of the kaolin-LM-50 sands suspensions. As shown in the parity plot, Figure 4-21, the

predicted LM-50 data followed the same trend as those of Sil-1 and did not veer away as observed with the Lim et al. [23] in Figure 4-12. This shows that the Thomas model provides more accurate predictions than the Lim et al. [23] model as seen with the reduced error boundary and absolute error values shown in Table 4-9. For the MFT–sand suspension, best fit was found with $A = 2.4$ using the kaolin–Sil-1 data, but only the idealized case is discussed in this section.

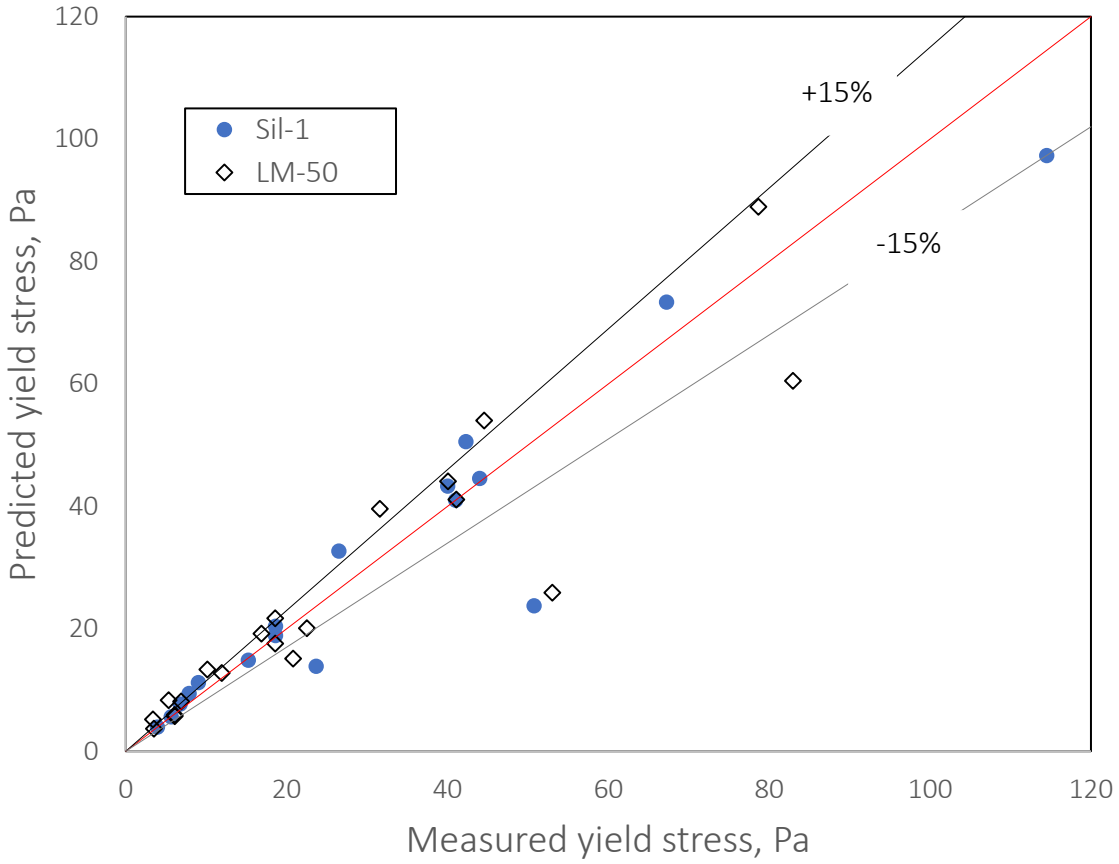

Figure 4-21: Parity plot to evaluate the predictive capacity of the Thomas correlation.

The relative accuracy of the Deltares and Thomas models was also investigated by comparing the two correlations using the kaolin–Sil-1 data as shown in the parity plot of Figure 4-22. It can be seen that the Deltares model is better than the Thomas model on the same data set.

Table 4-9: Absolute errors for the Thomas correlation predictions for the kaolin-sand suspensions

Error	Sil-1	LM-50
$\%E_{max}$	113.5	105
$\%E_{avg}$	20.1	21.7

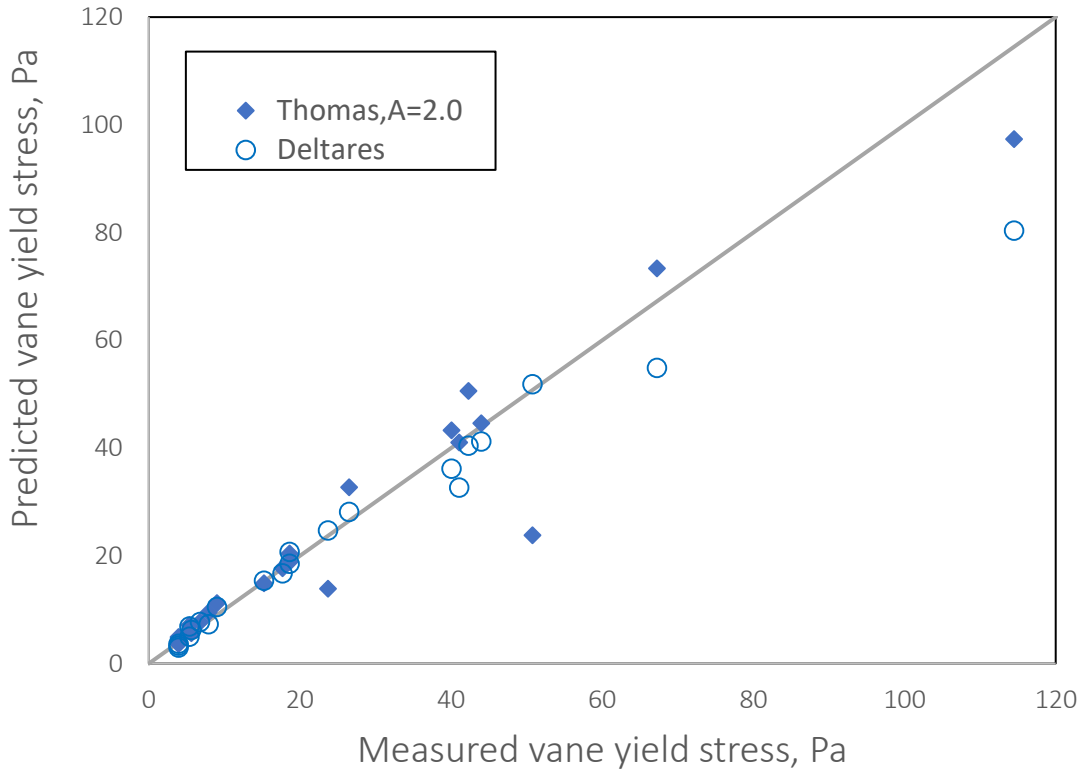

Figure 4-22: Parity plot to compare the predictive capacity of the Thomas and Deltares models using the kaolin-Sil-1 suspension.

4.8.5 Summary of Correlations: The Importance of Coarse Particle Shape Effect

The normalized concentration ratio, $C_s/C_{max,s}$, captures the effect of coarse particle shape as well as breadth of particle size distribution (PSD) and concentration in the Deltares and Thomas models. In order to compare the accuracy of these models at a glance and observe the effect of the normalized concentration, $C_s/C_{max,s}$, the parity plot for the kaolin–Sil-1 suspensions showing the predicted and measured vane yield stress using the three models is presented in Figure 4-23.

In addition to the kaolin–Sil-1 result, LM-50 is shown to compare the accuracy of the models as a function of coarse particle shape. The Deltares predictions (the blue markers) are very close to the experimental data when compared with the Lim et al and Thomas' predictions which are shown with the red and green markers respectively.

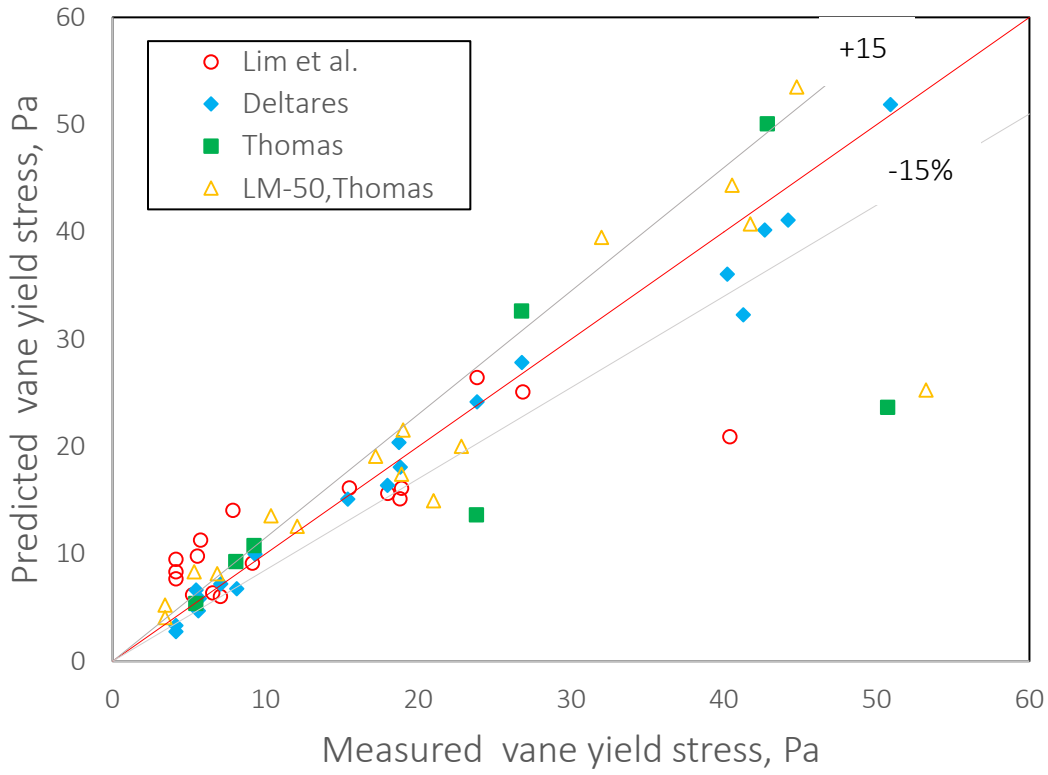

Figure 4-23: Parity plot for the kaolin-Sil-1 sand suspension to compare models' accuracy.

In this graph, predictions made using the Deltares and Thomas correlations are more accurate than those made using the Lim et al. [23] correlation as shown with the errors in Table 4-10. The reduced scatter and errors indicate the importance of the $C_s/C_{max,s}$ included in these models.

Table 4-10: Comparison of absolute errors for the kaolin-Sil-1 suspension

	Sil-1		
Error	Deltares	Lim et al.	Thomas
$\%E_{max}$	31.9	128	114
$\%E_{avg}$	8.89	36.9	20.1

To further investigate the effect of coarse particle shape in yield stress augmentation in addition to coarse particle concentration, the vane yield stress measurements for the Sil-1 and LM-50 sands are compared as shown in Figure 4-24. This figure presents a plot that compares the vane yield stress of kaolin–Sil-1 and kaolin–LM-50 sand suspensions at low coarse concentration ($0 \leq C_s \leq 0.5\ C_{max,s}$). Figure 4-24 is a variant of Figure 4-13, and as shown in these figures, the increases in yield stress between these two sands are different. In both cases, a greater increase in yield stress of fine suspensions is seen with the angular LM-50 sand when compared to the rounded Sil-1 sand.

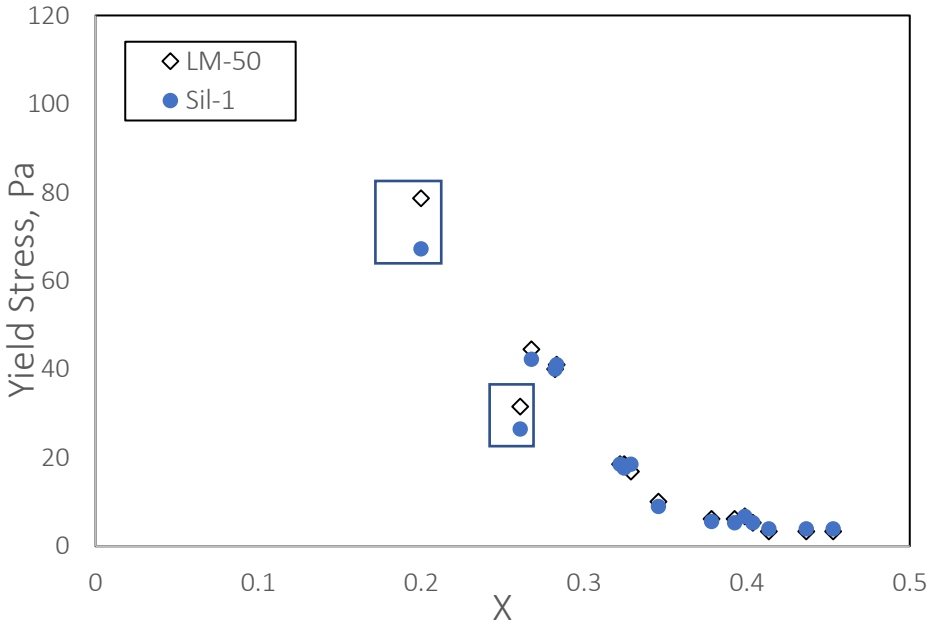

Figure 4-24: Vane yield stress measurements for kaolin-sands mixtures containing sands of comparable sizes, but of different shapes (Sil-1: d_{50}= 310μm, $C_{max,s} = 0.593$ and LM-50: d_{50}= 300μm, $C_{max,s} = 0.49$).

This result shows that the angular sand further augments the yield stress of the bimodal suspension when compared to the rounded sand and this provides additional support to previous findings and conclusions about the impact of coarse particle shape in yield stress augmentation.

Since these sands (LM-50 and Sil-1) have comparable sizes, it appears that the mechanism of interaction given by Sumner at al. [13] provides the only explanation at present. Their explanation asserts that the shape effect causes a change to the augmented yield stress, because the effective solid volume fraction of coarse particles increases in a sheared field.

In the next section, the effect of coarse particles size in augmenting the yield stress of fine suspension will be discussed in detail

4.9 Effect of Coarse Particle Size on The Yield Stress of Bimodal Suspension

In this section, the effect of coarse particle size is discussed based on the comparison between the results collected in this work, and also by comparing results in this work with those from a recent study (Spelay et al. [12]). The analysis is limited to the idealized tailings measurements (kaolin-sand) due to limited experimental data for the industrial MFT case. To investigate the contribution to yield stress augmentation related to coarse particle size, the vane yield stress measurements of kaolin-sand suspensions containing sands of similar shape, but of different sizes are compared. These measurements are expressed using the power law form of the Lim et al. correlation. This expression classifies the measured data into clear trends for each sand type, irrespective of the kaolin concentration.

First, the vane yield stress results for the Sil-1 and the Sil-4 sands were compared as shown in Figure 4-25 where the vane yield stress is plotted against X. These sands were compared because their mass median sizes are different and very distinct from kaolin, but they have a similar rounded shape. According to Figure 4-25, the Sil-1 and Sil-4 results are comparable, and no clear difference is observed in the augmented yield stress based on their size difference. Since a noticeable difference is not observed with these sands, the indication is that the interaction mechanisms of these sands in the fine suspension system are similar at these sizes.

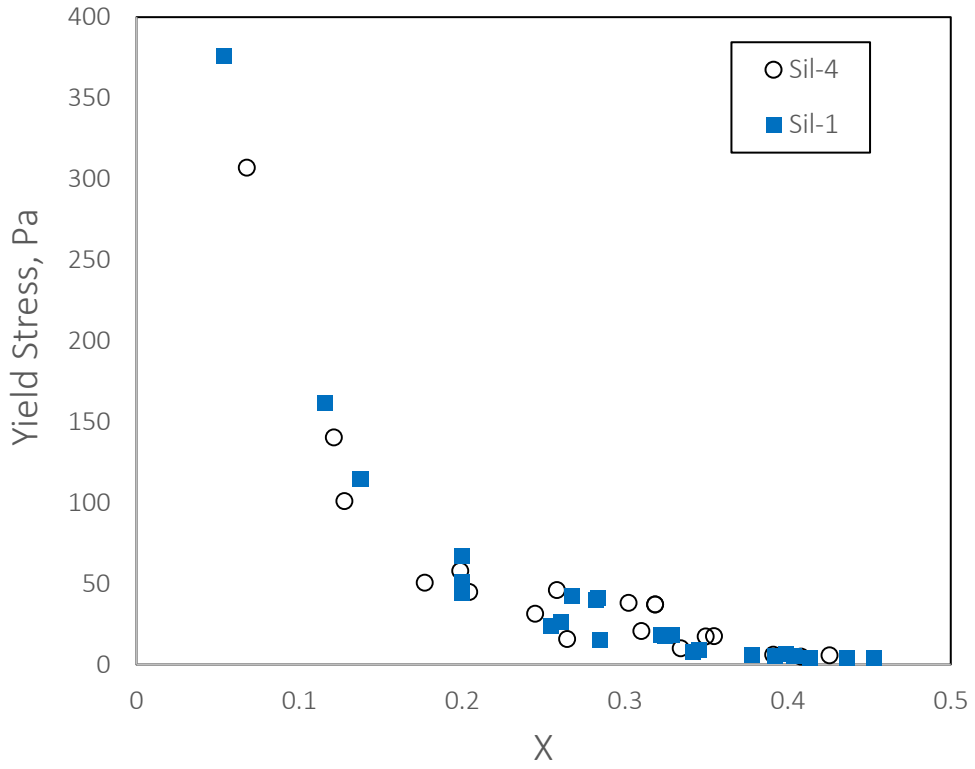

Figure 4-25: Vane yield stress data of bimodal suspensions for the Sil-1 and Sil-4 sands

Based on this limited comparison, it may be concluded that the size of the coarse particle does not play a significant role in augmenting the yield stress of an initial fine suspension. This results follows the conclusion made by Rahman [14]. However, to improve upon this conclusion about the effect of coarse particle size, extensive analysis with an array of sands that are comparable in shape, but of very distinct sizes is required.

The vane yield stress data for kaolin–Sil-1 and kaolin–Sil-325 suspensions are compared as shown below in Figure 4-26. In contrast to Figure 4-25, a clear difference in yield stress is seen with the Sil-325 and Sil-1 sands, which strongly suggests that the effect of coarse particle size is important, particularly at the size of Sil-325 (d_{50}= 28 μm).

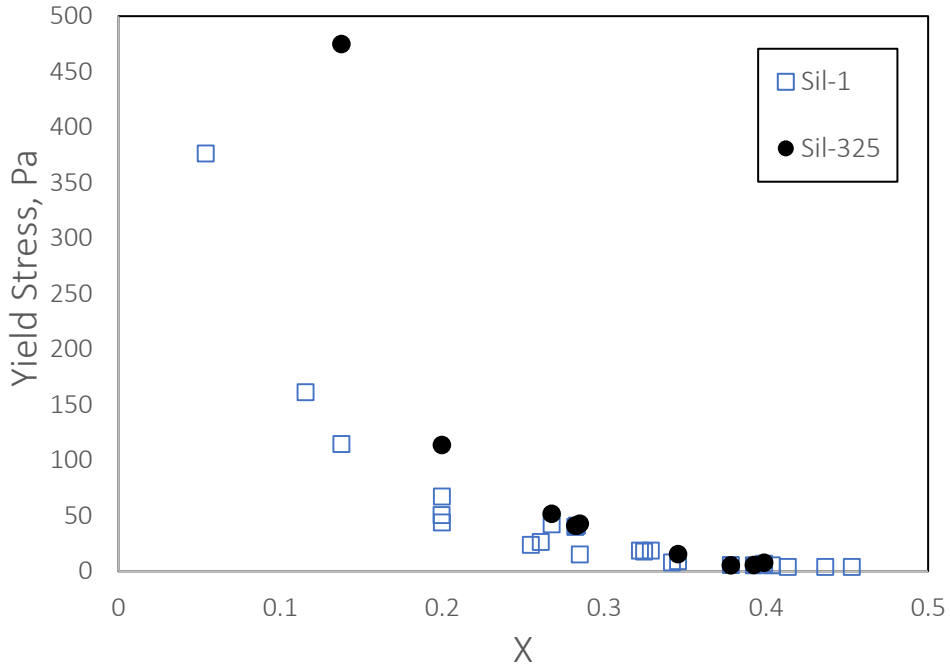

Figure 4-26: Vane yield stress data of bimodal slurries for Sil-1 and Sil-325 sands

Since the Sil-325 sand is the finest coarse sand tested in this work, it is not clear if a coarser sand–size exists ("effective size") where the effect of coarse particle size becomes significant. Therefore, the present results are further compared with those obtained from Spelay et al. [12] to investigate this condition, which is further discussed in the following section. This information is important for model adaptation.

To explain the mechanism of interaction for the Sil-1 and Sil-4 sands, it is assumed that the interaction of these sands with the aggregates of the fine suspension system is 'inert' (i.e. it only reduces the distance between aggregates, since the sands only take up space). This in turn causes the van der Waals force of attraction to have a greater effect between the surface-active aggregates, which explains the similarity in the augmented yield stress observed with the Sil-1 and Sil-4. However, with the Sil-325 results, it is possible that the fine-coarse particles become a part of the fine aggregate structure to increase the "effective solid volume fraction" of fine aggregates. This increase in solid volume fraction simultaneously reduces the space between adjacent aggregates to enhance the van der Waals force of attraction between aggregates. This "double effect" may to be responsible for the greater increase in yield stress of this bimodal suspension when compared with bimodal suspensions containing coarser particles.

This limited comparison strongly suggests that coarse particle size, in addition to coarse particle concentration and shape, significantly contributes to the yield stress increase in a bimodal suspension system.

4.9.1 Investigating Minimum Size of "Inert" Coarse Particles

To further investigate the importance of coarse particle size in yield stress augmentation, and to determine if one or more effective size(s) exist (i.e. the size in which a significant change in rheology is observed), the vane yield stress results obtained for different coarse particles grouped in Table 4-1 are compared.

First, the rounded sands were compared to investigate if any significant difference in the yield stress of kaolin suspension exist at these sizes. In Figure 4-27 the vane yield stress ratio has been plotted against linear concentration for the rounded sands, and only for kaolin concentration of 0.15 (v/v) so that the trend can be clearly observed.

According to this figure, it appears that the results do not depend on particle size for all sands except for the Sil-325.

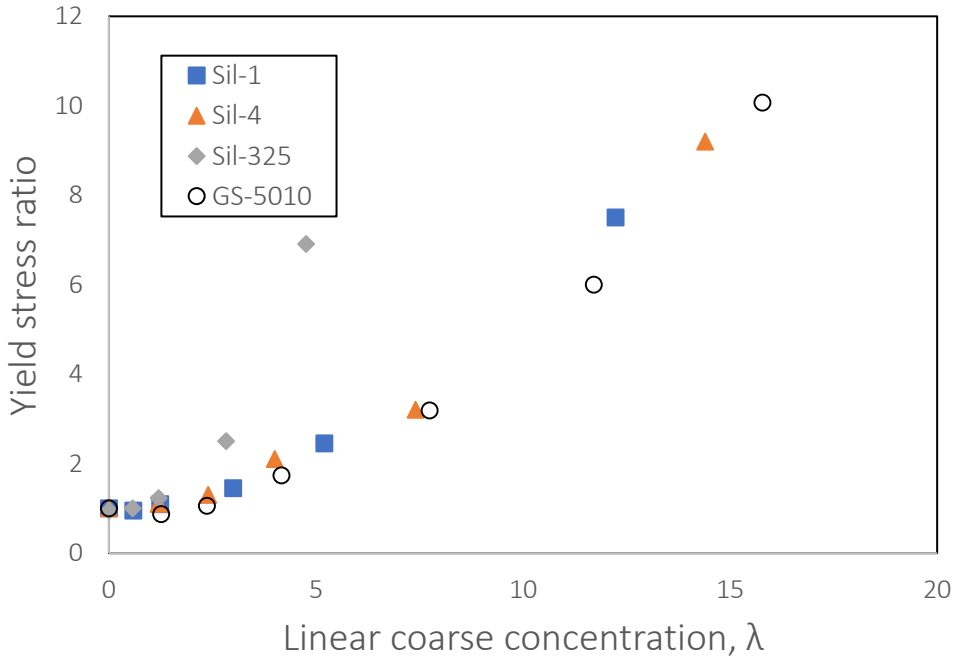

Figure 4-27: Yield stress augmentation comparisons for bimodal suspensions of kaolin at $C_s = 0.15$ (v/v) and rounded sands of different sizes.

Similarly, the vane yield stress ratio for the angular sands were compared as shown in Figure 4-28. In this figure, in addition to the angular sands, the Granusil-5010 sand was added for additional analysis. It should be noted that the Granusil-5010 sand is rounded but of similar size to the LM-70. From this plot, it can be seen that the augmented yield stress with the LM-125 sand is higher when compared to other angular sands (including the Granusil-5010).

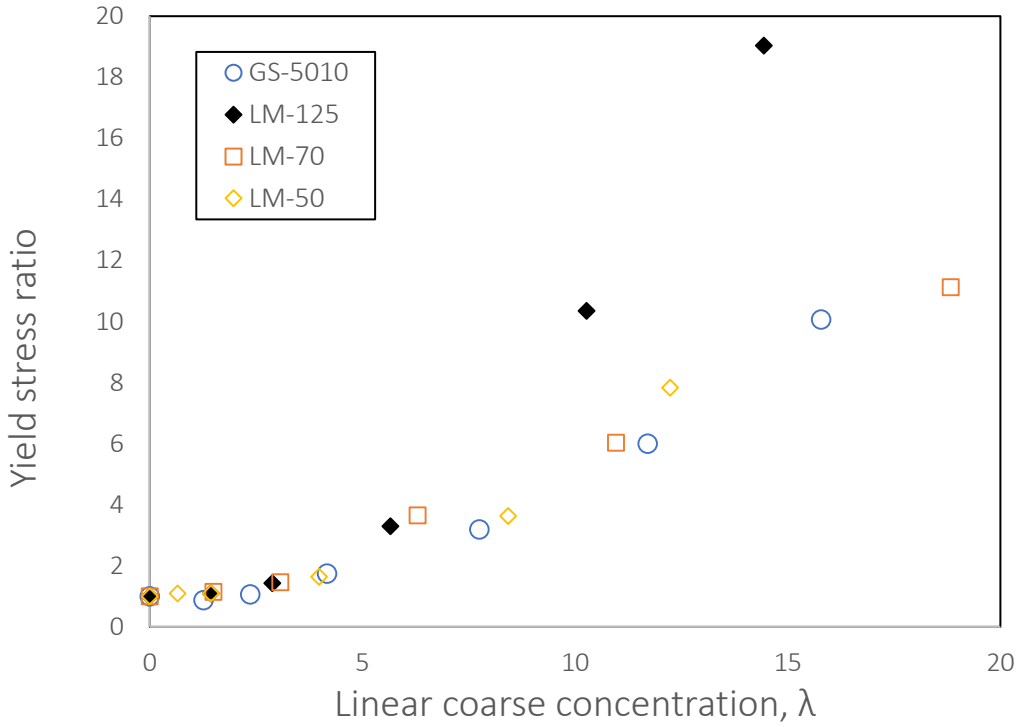

Figure 4-28: Effect of sand size on yield stress increase for bimodal suspensions of kaolin and angular sands of different for a kaolin concentration of 0.15 (v/v).

For this comparative analysis, it seems the effect of size becomes significant at the size of LM-125 sand ($d_{50} \sim 100\ \mu m$). Therefore, it can be inferred from this result that coarse particle size in yield stress augmentation becomes significant at a certain size and is most likely independent of the shape of coarse particle. To clarify the possibility of the "effective" size being a function of coarse particle shape, a comparative data analysis of the LM-125 sand and rounded sand (Ottawa sand) of similar size would be necessary. This suggests that the effect of coarse particle size in yield stress augmentation of fine-particle suspension becomes significant between a mass median diameter of $d_{50} \sim 100\ \mu m$ of the LM-125 sand and a $d_{50} \sim 160\ \mu m$ of the LM-70 sand. At $d_{50} \geq 160\ \mu m$ the effect due to size difference seems to be absent.

Lastly, this figure shows that the effect of coarse particle shape in augmenting yield stress is not evident because the Granusil sand (rounded) falls within the same yield stress ratio region when compared with the LM-70 and other angular sands. This strongly suggests that effect of angular shape is accounted for by considering the linear concentration, λ which is a function of concentration ratio, $C_s/C_{max,s}$. In addition, it also suggests that the effect of coarse particle size (effective size) is not accounted for by these functions (i.e. linear concentration and concentration ratio).

Chapter 5 CONCLUSION AND RECOMMENDATIONS

The hydraulic transport of treated (thickened) tailings is a crucial component of a sustainable, reliable, and safe mining operations that meet the economic and environmental challenges associated with tailings placement. The effective transport of thickened tailings containing coarse and fine particles through a pipeline depends on the ability to determine the mixture's Bingham yield stress, which is a critical parameter needed for pipeline design and tailings placement and storage.

Therefore, this study aimed to accurately measure the yield stress of both fines-only suspensions and fine–coarse (bimodal) suspensions using the vane viscometer. Using a vane viscometer is justified because, the vane yield stress ratio has been found to agree with the Bingham yield stress ratio obtained from concentric cylinder viscometer, but the measurements are more reliable and more easily made. The vane measurements have been carefully taken in this study, and these measurements were used to test the performance of three semi-empirical correlations. Other factors such as coarse particle size and shape that might influence the rheology of bimodal suspensions were investigated, since understanding these contributing factors is necessary to improve the prediction and accuracy of the models and correlations.

Therefore, the following are the major conclusions that have been drawn from the results of present study:

- Coarse particles did not cause a significant change to the fine suspension water chemistry and the water content. Therefore, the rheology augmentation is not caused by the adsorption of water onto the coarse particles surfaces.
- The vane viscometer provides a more accurate and reliable data set when compared with the Bingham yield stress data (collected with concentric viscometer) from previous investigations.
- The vane viscometer provides a simple, faster and a more general and comparable data, since the magnitude in data obtained from different sources are very comparable and also very repeatable.

- The semi-empirical correlation presented by Lim et al. [23] predicts the yield stress of the bimodal suspensions (model and industrial tailings) less effectively when compared to other correlations tested in this work.
- Investigation shows that the shape and size of the coarse particles affect the augmentation magnitude, as well as the interaction mechanism of the coarse particles in a fine suspension system. Therefore, these quantities, especially the coarse particle size, are required to be captured to improve prediction accuracy and generality.
- It appears that the effect of coarse particle size becomes significant for particles less than about d_{50} ~ 100 μm for the suspensions tested here.
- The linear concentration ratio normalizes the effect of shape on yield stress for narrowly sand sizes larger than d_{50} ~ 100 μm.
- The Deltares [26] correlation provided the least error with the set of fitting parameters estimated from experimental data, but still does not provide any predictive capability without experimental measurements, based on the limited comparative analysis made in this study.
- The Thomas [25] correlation predicts better than the Lim et al. approach and seems more general to predict the vane yield stress of bimodal suspension with the fitting parameter used in this work.

Based on the conclusions, experiments and analyses completed in this work, the following are recommended for future work towards achieving the goal of being able to accurately predict the yield stress of bimodal suspensions typical to the mining and mineral processing industry:

- The mechanisms by which coarse particles augment rheology need to be better understood so that the increasing effect with smaller sized coarse particles can be appropriately modelled and predicted.
- Rounded particles of similar size to the LM-125 (e.g. Ottawa sand [14]) should be tested to investigate if the suggested effective size is shape dependent.
- More experiments should be conducted using the MFT to obtain more vane yield stress data. This will improve the confidence of the fitting parameters obtained in this study because limited concentration was tested.

- More experiments should be conducted to test bimodal suspensions with broader coarse particle size distributions. Also, experiments should be conducted to test polymodal suspensions containing fine-particle suspension and two or more coarse particle types. This is necessary to investigate the impact of broader particle size distribution on rheology augmentation, and to closely represent typical tailings particle distributions.
- To date, the sieving experiments have been limited to coarser sand particles (with d_{50} > 100 μm). For instance, in this study and the investigation completed by Rahman [14], the Sil-1 and Granusil sands were used respectively for the sieving experiment and both of these sands have mass mean sizes bigger 100 μm. Since surface area per unit volume increases as particle size reduces, it is essential to investigate if coarse particle size does not affect the adsorption of water by testing smaller sand type (e.g. LM-125 sand).
- The effect of coarse particle surface area on rheology augmentation mechanism should be investigated.
- To further confirm the interaction of coarse particles in the fine suspension system, more experiments should be conducted to investigate if :
    - ✓ Sands truly become part of the fine aggregates, and if
    - ✓ Attraction exist between coarse (sands) and fine (kaolin) particles.

The conclusions drawn from this investigation show the importance of accurate measurements as well as contribution to the augmented yield stress due to coarse particle properties. The future works listed will further enhance the knowledge of this topic and aid in achieving the goal to accurately predict yield stress of poly-dispersed systems. The ability to accurately predict the yield stress of fine-coarse particle suspensions without conducting a lot of experiments is desirable, since it will reduce the cost, time, and difficulty experienced in determining the yield stress need for efficient pipeline transport and storage of thickened tailings.

REFERENCES

[1] H. Jones and D. V. Boger, "Sustainability and Waste Management in the Resource Industries," *Ind. Eng. Chem. Res.*, vol. 51, no. 30, pp. 10057–10065, Aug. 2012.

[2] C. Wang, D. Harbottle, Q. Liu, and Z. Xu, "Current state of fine mineral tailings treatment: A critical review on theory and practice," *Minerals Engineering*. 2014.

[3] R. G. Gillies, R. Sun, R. S. Sanders, and J. Schaan, "Lowered expectations: The impact of yield stress on sand transport in laminar, non-Newtonian slurry flows," *J. South. African Inst. Min. Metall.*, vol. 107, no. 6, pp. 351–357, 2007.

[4] D. J. Hallbom, "Pipe flow of homogeneous slurry," Ph.D Thesis Univeristy of British Columbia, 2008.

[5] BGC Engineering Inc., "Oil Sands Tailings Technology Review," *Oil Sands Res. Inf. Netw.*, no. July, p. 136., 2010.

[6] M. D. MacKinnon, J. G. Matthews, W. H. Shaw, and R. G. Cuddy, "Water Quality Issues Associated With Composite Tailings (CT) Technology for Managing Oil Sands Tailings," *Int. J. Surf. Mining, Reclam. Environ.*, vol. 15, no. 4, pp. 235–256, 2001.

[7] Alberta Energy Regulator, "Alberta's Tailings Management Framework," *Aer*, 2015. [Online]. Available: https://www.aer.ca/about-aer/spotlight-on/alberta-tailings-managment-framework. [Accessed: 02-Nov-2017].

[8] Suncor Energy, "Report on Sustainability," 2017. [Online]. Available: https://sustainability.suncor.com/2017/en/environment/tailings-management.aspx. [Accessed: 20-Aug-2018].

[9] Suncor Energy, "Tailings Reduction Operations," 2010. [Online]. Available: https://sustainability.suncor.com/2017/en/environment/tailings-management.aspx. [Accessed: 20-Aug-2018].

[10] J. Matthews, W. Shaw, and R. Cuddy, "Development of Composite Tailings Technology at Syncrude," *Int. J. Surf. Mining, Reclam. Environ. Swets Zeitlinger*, vol. 16, no. 1, pp. 24–39, 2002.

[11] E. Paulsen, "Investigating the effect of coarse particle addition on the measured rheological parameters of fine clay slurries," MSc Thesis, University of Stellenbosch, 2007.

[12] R. B. Spelay, S. A. Hashemi, M. H. Rahman, A. E. Olayode, and R. S. Sanders, "Effect of coarse solids concentration on the yield stress of non-Newtonian kaolin clay slurries," in *20th International Conference on Hydrotransport*, 2017.

[13] R. J. Sumner, J. J. Munkler, S. M. Carriere, and C. A. Shook, "Rheology of kaolin slurries containing large silica particles," *J. Hydrol. Hydromechanics/Vodohospodarsky Cas.*, vol. 48, no. 2, pp. 110–124, 2000.

[14] M. H. Rahman, “Yield Stresses of Mixtures with Bimodal Size Distributions.,” MSc Thesis, University of Alberta, 2011.

[15] A. Reaîtrme, J.-P. Malet, O. Maquaire, C. Ancey, and J. Locat, “Flow behaviour and runout modelling of a complex debris flow in a clay-shale basin,” *Earth Surf. Process. Landforms*, vol. 30, no. 4, pp. 479–488, Apr. 2005.

[16] “Beach Slope Prediction Methods.” [Online]. Available: http://www.tailings.info/technical/beach-slope.htm. [Accessed: 19-Aug-2018].

[17] S. Mizani, “Rheology of thickened gold tailings for surface deposition,” MSc, Carleton University, 2010.

[18] A. P. Poloski *et al.*, “Deposition Velocities of Non-Newtonian Slurries in Pipelines: Complex Simulant Testing,” no. July, 2009.

[19] K. C. Wilson and A. D. Thomas, “A new analysis of the turbulent flow of non-newtonian fluids,” *Can. J. Chem. Eng.*, vol. 63, no. 4, pp. 539–546, Aug. 1985.

[20] N. Quoc Dzuy and D. V Boger, “Yield Stress Measurement for Concentrated Suspensions Yield Stress Measurement for Concentrated Suspensions,” *J. Rheol. (N. Y. N. Y).*, vol. 271, no. 10, pp. 321–581, 1983.

[21] P. C. Kapur, P. J. Scales, D. V. Boger, and T. W. Healy, “Yield stress of suspensions loaded with size distributed particles,” *AIChE J.*, vol. 43, no. 5, pp. 1171–1179, May 1997.

[22] J. Gustafsson. M. Toivakka. K. K. Koskinen, “Rheology of strongly sedimenting magnetite suspensions,” *Nord. Rheol. Soc.*, vol. 13, 2005.

[23] S. Lim K. H. Ahn, S. J. Lee, A Kumar, N Duan, X. Sun, S.P. usher, P. J. Scales., “Yield and flow measurement of fine and coarse binary particulate mineral slurries,” *Int. J. Miner. Process.*, vol. 119, pp. 6–15, 2013.

[24] C. Ancey and H. Jorrot, “Yield stress for particle suspensions within a clay dispersion,” *J. Rheol. (N. Y. N. Y).*, vol. 45, no. 2, pp. 297–319, 2001.

[25] A. Thomas, “The influence of coarse particles on the rheology of fine particle slurries,” *Rheol. Miner. Ind. II*, pp. 113–123, 1999.

[26] T. H. B. Van De Ree, “Deposition of high density tailings on beaches,” Msc Delft University of Technology, 2015.

[27] E. Bird, R.B., Stewart, W.E and Lightfoot, *Transport Phenonena*, 2nd ed. Newyork: John Wiley & Sons,Inc., 1924.

[28] P. V. Liddell and D. V. Boger, “Yield stress measurements with the vane,” *J. Nonnewton. Fluid Mech.*, vol. 63, no. 2–3, pp. 235–261, 1996.

[29] M. Rhodes, *Introduction to Particle Technology – Second Edition*, 2nd ed. New York: John Wiley & Sons,Inc., 2008.

[30] E. Koehler and D. Fowler, “Development of a portable rheometer for fresh portland cement concrete,” 2004.

[31] R. B. Spelay, “Solids transport in laminar, open channel flow of non-Newtonian slurries.”

[32] D. M. Liu, “Particle packing and rheological property of highly-concentrated ceramic suspensions: ϕmdetermination and viscosity prediction,” *J. Mater. Sci.*, vol. 35, no. 21, pp. 5503–5507, 2000.

[33] H. A. Barnes and Q. D. Nguyen, “Rotating vane rheometry — a review,” *J. Nonnewton. Fluid Mech.*, vol. 98, no. 1, pp. 1–14, 2001.

[34] P. H. Morris and D. J. Williams, “Effective stress vane shear strength correction factor correlations,” *Can. Geotech. J*, vol. 31, pp. 335–342, 1994.

[35] J. Osterman, “Studies on the properties and formation of quick clays,” *Clays Clay Miner.*, vol. 12, pp. 87–108, 1963.

[36] N. Matsui, T. and Abe, “Shear mechanisms of vane test in soft clays,” *Soils Found.*, pp. 69–80, 1981.

[37] J. D. Mihiretu, Y and Chalaturnyk, R.J and Scott, “Tailings segregation fundamentals from flow behaviour perspective,” in *First international Oil Sands Tailings Conference. Edmonton, AB*, 2008.

[38] C. Ancey, “Role of lubricated contacts in concentrated polydisperse suspensions,” *J. Rheol. (N. Y.).*, vol. 45, no. 6, pp. 1421–1439, 2001.

[39] J. Masliyah, Z. Xu, and J. Czarnecki, *Handbook on theory and practice of bitumen recovery from Athabasca Oil Sands: Theoretical Basis*. 2011.

[40] M. Chan, “A novel flocculant for enhanced dewatering of oil sands tailings,” University of Alberta, 2011.

[41] A. S. Michaels and J. C. Bolger, “Settling Rates and Sediment Volumes of Flocculated Kaolin Suspensions,” *Ind. Eng. Chem. Fundam.*, vol. 1, no. 1, pp. 24–33, Feb. 1962.

[42] R. G. De Kretser, D. V Boger, and P. J. Scales, “Compressive rheology: an overview,” *Rheol. Rev.*, pp. 125–165, 2003.

[43] D. G. Thomas, “Laminar-Flow Properties of Flocculated Suspensions,” *A.I.C.H.E*, vol. 7, no. 3, pp. 431–437, 1961.

[44] Z. Zhou, M. J. Solomon, P. J. Scales, and D. V Boger, “The yield stress of concentrated flocculated suspensions of size distributed particles,” vol. 651, no. May 2016, 2015.

[45] M. S. Zbik, R. S. C. Smart, and G. E. Morris, “Kaolinite flocculation structure,” *J. Colloid Interface Sci.*, vol. 328, pp. 73–80, 2008.

[46] P. Coussot and J. Piau, “The effects of an addition of force-free particles on the rheological properties of fine suspensions,” *Can. Geotech. J.*, vol. 32, no. 2, pp. 263–270, 1995.

[47] E. Paulsen, R. J. Sumner, and R. S. Sanders, “The effect of coarse particle addition on the rheology of fine clay slurries,” in *18th International conference on Hydrotransport*, 2010, pp. 22–24.

[48] D. G. Thomas, “Suspensions to Rheological Parameters,” *A.I.C.H.E*, vol. 9, no. 3, pp. 310–316, 1963.

[49] D. G Thomas, “Transport characteristics of suspension: VII. A note on the viscosity of Newtonian suspensions of uniform spherical particles,” *colloid Sci.*, vol. 9, no. 3, pp. 267–277, 1965.

[50] R. F. Landel, B. G. Moser, and A. J. Bauman, “Rheology of concentrated suspensions - effect of a surfactant,” *Proc. 4th Int. Congr. Rheol. II*, pp. 663–692, 1963.

[51] J. S. Chong, E. B. Christiansen, and A. D. Baer, “Rheology of concentrated suspensions,” *J. Appl. Polym. Sci.*, vol. 15, no. 8, pp. 2007–2021, Aug. 1971.

[52] J. Schaan, R. J. Sumner, R. G. Gillies, and C. A. Shook, “The effect of particle shape on pipeline friction for newtonian slurries of fine particles,” *Can. J. Chem. Eng.*, vol. 78, no. 4, pp. 717–725, Aug. 2000.

[53] M. Z. Sengun and R. F. Probstein, “Bimodal model of slurry viscosity with application to coal-slurries. Part 1. Theory and experiment,” *Rheol. Acta*, vol. 28, no. 5, pp. 382–393, 1989.

[54] M. Schatzmann, P. Fischer, and G. R. Bezzola, “Rheological Behavior of Fine and Large Particle Suspensions,” *J. Hydraul. Eng.*, vol. 129, no. 10, pp. 796–803, Oct. 2003.

[55] Y. B. He and J. S. Laskowski, “Rheological Properties of Magnetite Suspensions,” *Miner. Process. Extr. Metall. Rev.*, vol. 20, no. 1, pp. 167–182, Jan. 2000.

[56] B. T. Zengeni, “Bingham Yield Stress and Bingham Plastic Viscosity Of Homogeneous Non-Newtonian Slurries,” MSc thesis, Cape Peninsula University of Technology, 2016.

[57] J. L. J. Hanssen, “Towards improving predictions of non-Newtonian settling slurries with Delft3D theoretical development and validation in 1DV,” MSc Thesis, Delft University of Technology, 2016.

[58] W. Jacobs, “Sand-mud erosion from a soil mechanical perspective,” PhD thesis, Delft University of Technology, 2011.

[59] S. P. Usher, R. Spehar, and P. J. Scales, “Theoretical analysis of aggregate densification: Impact on thickener performance,” *Chem. Eng. J.*, vol. 151, no. 1–3, pp. 202–208, 2009.

[60] R. B. Spelay, “Solids transport in laminar, open channel flow of non-Newtonian slurries,” PhD Thesis,University of Saskatchewan, 2007.

[61] J. Schaan, R. J. Sumner, R. G. Gillies, and C. A. Shook, “The Effect of Particle Shape on Pipeline Friction for Newtonian Slurries of Fine Particles,” *Can. J. Chem. Eng.*, vol. 78, 2000.

[62] D. P. Gillies, “Particle Contributions to Kinematic Friction in Slurry Pipeline Flow,” MSc Thesis, University of Alberta, 2013.

[63] N. R. Sarker, “A Preliminary Study of Slurry Pipeline Erosion Using a Toroid Wear Tester, MSc Disertation,” University of Alberta, 2016.

[64] H. Van Olphen, “An introduction to clay colloid chemistry,” in *Wiley Interscience*, New York, 1977.

[65] Q. D. Nguyen and D. V. Boger, “Application of rheology to solving tailings disposal problems,” *Int. J. Miner. Process.*, vol. 54, no. 3–4, pp. 217–233, Aug. 1998.

[66] P. J. Scales, S. B. Johnson, T. W. Healy, and P. C. Kapur, “Shear yield stress of partially flocculated colloidal suspensions,” *AIChE J.*, vol. 44, no. 3, 1998.

[67] M. D. Green and D. V. Boger, “Yielding of Suspensions in Compression,” *Ind. Eng. Chem. Res.*, vol. 36, no. 11, pp. 4984–4992, Nov. 1997.

[68] Shane P. Usher, “Suspension dewatering: characterization and optimization,” PhD Thesis, The University of Melbourne, 2002.

[69] T. J. Akroyd and Q. D. Nguyen, “Continuous rheometry for industrial slurries,” *Exp. Therm. Fluid Sci.*, vol. 27, no. 5, pp. 507–514, May 2003.

[70] M. D. Green, “Characterisation of suspensions in settling and compression,” PhD Thesis, University of Melbourne, 1997.

[71] C. P. Chu, S. P. Ju, D. J. Lee, and K. K. Mohanty, “Batch gravitational sedimentation of slurries.,” *J. Colloid Interface Sci.*, vol. 245, no. 1, pp. 178–86, 2002.

[72] G. D. Scott and D. M. Kilgour, “The density of random close packing of spheres,” *J. Phys. D. Appl. Phys.*, vol. 2, no. 6, p. 311, Jun. 1969.

[73] R. J. Flatt and P. Bowen, “Yodel: A yield stress model for suspensions,” *J. Am. Ceram. Soc.*, vol. 89, pp. 1244–1256, 2006.

[74] J. L. Smith, “Measurement of Carrier Fluid Viscosities for Oil Sand Extraction and Tailings Slurries,” MSc thesis, University of Alberta, 2013.

[75] J. Du and M. Lakes, “Control of Aggregate Structure , Settling and Dewatering in Mineral Tailings Processing,” PhD Thesis, University of South Australia, Mawson Lakes, South Australia, 2010.

[76] C. Shook, R. Gillies, and R. Sanders, “Pipeline hydrotransport: With applications in the oil sand industry,” *SRC Pipe Flow Technol. Cent.*, 2002.

Appendix A Preliminary Experimental Data

A.1 Result for the shear conditioning of the industrial MFT

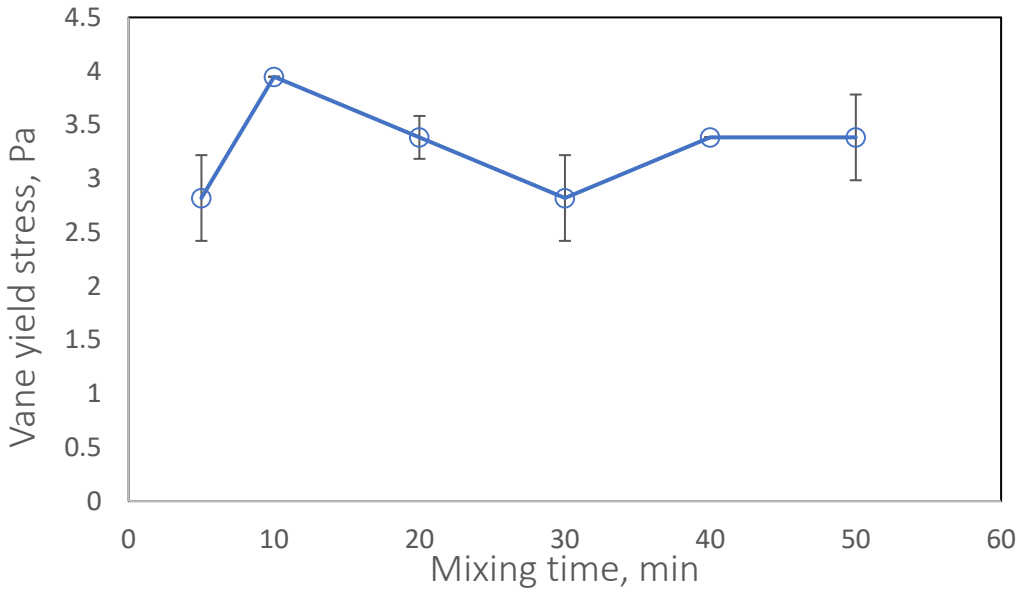

Figure A-1: Shear sensitivity plot for MFT, C_s = 0.14 (v/v), using the overhead mixer at $N = 280$ RPM

A.2 Additional test to compare vane yield stress measurement from different sources

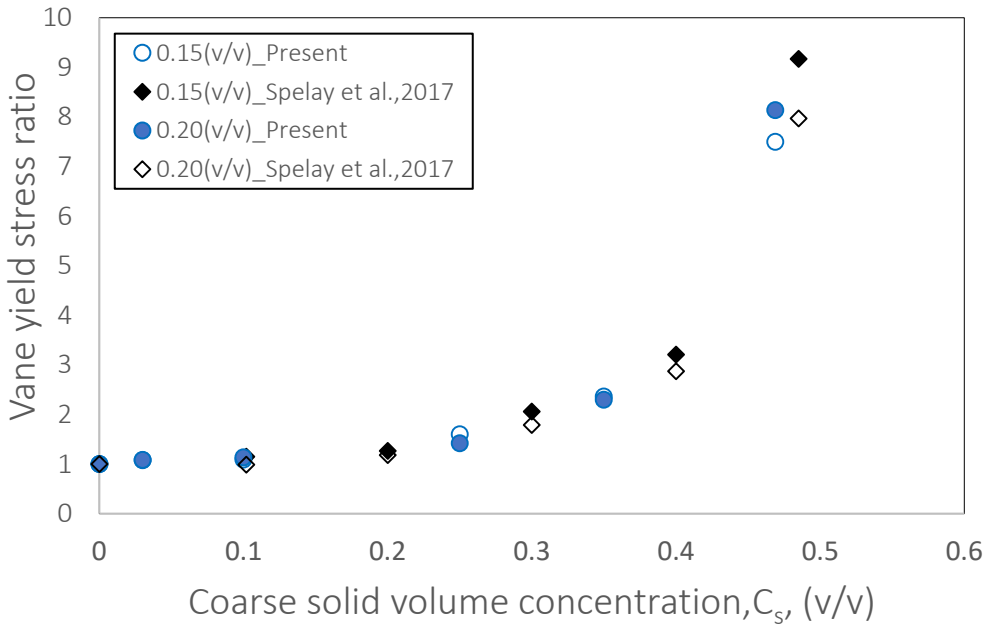

Figure A-2: Comparison of the vane yield stress measurements for similar fine and coarse concentration from different sources using the Sil-1 from current study and Sil-4 sands [8].

Table A-1: Comparison between the vane yield stress measurements obtained from the batches of kaolin used in this study

Solid volume fraction, C_f (v/v)	Vane Yield Stress (Pa)	Vane Yield Stress (Pa)	% difference
	#1	#2	
0.12	2.82	2.82	0
0.15	6.20	6.20	0
0.17	-	9.59	n/a
0.20	18.6	17.5	-6.07
0.24	40.6	43.9	8.32

where the sign (#) connotes kaolin batch.

A.3 Determination of Initial solid volume fraction

Several estimations were made using different initial solid volume fractions. The results obtained from these settling tests are presented in Table A.2- A.5

Table A-2: Data for an initial solid volume fraction of 0.08 (v/v).

Initial suspension height, h_o(cm)	final suspension height, h_f(cm)	Average solid volume fraction, C_{avg}	P_{base}
2.60	1.80	0.120	33.6
8.36	4.81	0.140	108
5.23	3.35	0.120	67.7
12.75	6.98	0.150	165
13.91	7.52	0.160	180
22.6	11.5	0.160	292

Table A-3: Data for an initial solid volume fraction of 0.05 (v/v).

Initial suspension height, h_o(cm)	final suspension height, h_f(cm)	Average solid volume fraction, C_{avg}	P_{base}
2.60	1.30	0.100	21.0
5.00	2.40	0.100	40.4
11.0	4.60	0.120	88.9
13.9	5.50	0.130	113
19.0	7.00	0.140	154
22.6	8.00	0.140	183

Table A-4: Data for an initial solid volume fraction of 0.035 (v/v).

Initial suspension height, h_o(cm)	final suspension height, h_f(cm)	Average solid volume fraction, C_{avg}	P_{base}
2.61	1.00	0.09	14.7
8.30	2.40	0.12	46.9
5.00	1.50	0.12	28.3
13.9	3.50	0.14	78.7
22.6	5.00	0.15	128

Table A-5: Data for an initial solid volume fraction of 0.02 (v/v)

Initial suspension height, h_o(cm)	final suspension height, h_f(cm)	Average solid volume fraction, C_{avg}	P_{base}
2.60	0.60	0.087	8.41
5.00	1.00	0.100	16.1
8.30	1.60	0.103	26.8
11.0	1.90	0.115	35.7
13.9	2.30	0.120	44.9
19.0	2.90	0.130	61.5
22.6	3.50	0.129	73.1

A plot of these data shows that below an initial solid volume fraction of 0.05, the extrapolated gel point values tend to converge, and the 0.02 was used since it provided the base pressure closest to zero.

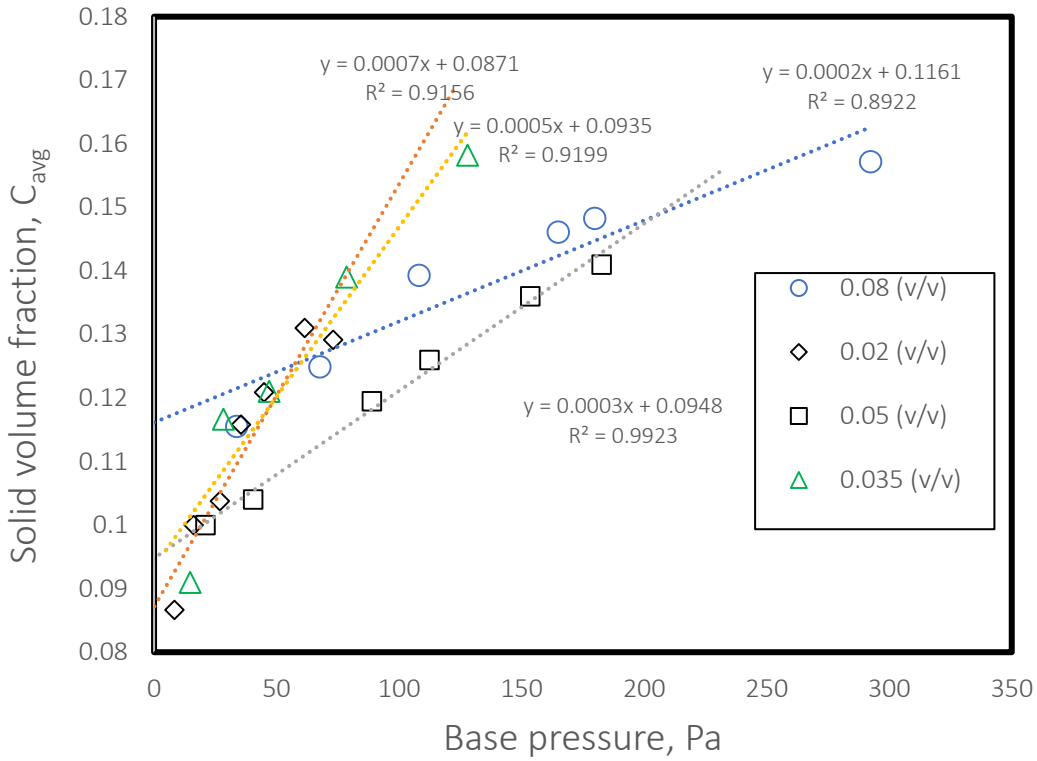

Figure A-3: Estimated gel point of kaolin at different initial solid volume fraction

For these preliminary settling tests, even though the dimensions of settling columns used were the same, the shape of the base of these columns were different (flat and bulged). This condition affects the results obtained as shown with the summary Table A.6 for the kaolin.

Table A-6: Data for the gel point of kaolin at an initial solid volume fraction of 0.02 with settling columns of different base shape.

Base-type	Flat	Bulged	Combined
Gel point	0.061	0.079	0.087
R^2	0.98	0.927	0.916

Therefore, for the actual experiment, only flat bottom columns were used, and the results was communicated in Chapter 4 and in Table B-4 in Appendix B.

A.4 Sensitivity analysis of the Lim et al. correlation: Impact of the gel point and close packing fraction of fines (kaolin)

The sensitivity analyses were conducted using the Koalin-Sil-1 sands suspension. The gel point of kaolin was varied between 0.04 to 0.08 while the close packing fraction and fitting parameters were kept constant. The coefficient of correlation (R^2) and absolute average errors are reported in Table A-7. Since the R^2 values and the absolute average error remain approximately the same, it indicates that the sensitivity of the correlation is not significantly altered by the gel point of fine.

Table A-7: Sensitivity analysis of the Lim et al. correlation on kaolin-Sil-1 sand data (full data set) at $C_{cp,f} = 0.52$

Gel point	R^2	a'	c	$\%E_{avg}$
0.04	0.86	1.76	-2.04	57.1
0.05	0.86	1.76	-2.04	57.8
0.06	0.86	1.76	-2.04	56.8
0.07	0.87	1.76	-2.04	56.4
0.08	0.87	1.76	-2.04	56.1

The close packing fraction of kaolin was also varied between 0.50 to 0.55 and the results are presented in Table A-8. The close packing fraction is more sensitive compared to the gel point, but only marginally alters the predictive capacity of the Lim et al. correlation.

Table A-8: Sensitivity analysis of the Lim et al. correlation on kaolin-Sil-1 sand data (full data set) at $C_{g,f} = 0.06$

Gel point	R^2	a'	c	$\%E_{avg}$
0.50	0.85	1.76	-2.04	71.3
0.52	0.86	1.76	-2.04	56.8
0.53	0.87	1.76	-2.04	53.8
0.54	0.87	1.76	-2.04	51.8
0.55	0.87	1.76	-2.04	51.1

Appendix B Actual Experimental Data

The experimental results for the kaolin-only, the kaolin-sand, and the MFT-sand suspensions are provided in this section. Also, in this section, the results for the gel point and close packing fractions of kaolin are detailed.

B.1 Gel point and close packing fraction of kaolin

Table B-1: Experimental results for the batch settling test to estimate the gel point of kaolin

P_{base}(Pa)	Average solid volume fraction, C_{avg} (v/v)
3.24	0.067
16.5	0.085
18.1	0.093
25.2	0.104

B.2 Close packing fraction of kaolin

Table B-2: Experimental results for the vane yield stress of kaolin only suspensions to estimate the close packing fraction of kaolin

C_f (v/v)	Vane yield stress (Pa)
0.08	0.52
0.11	1.74
0.13	4.33
0.15	5.67
0.17	13.0
0.19	18.6
0.22	35.8

B.3 Repeatability Test Results

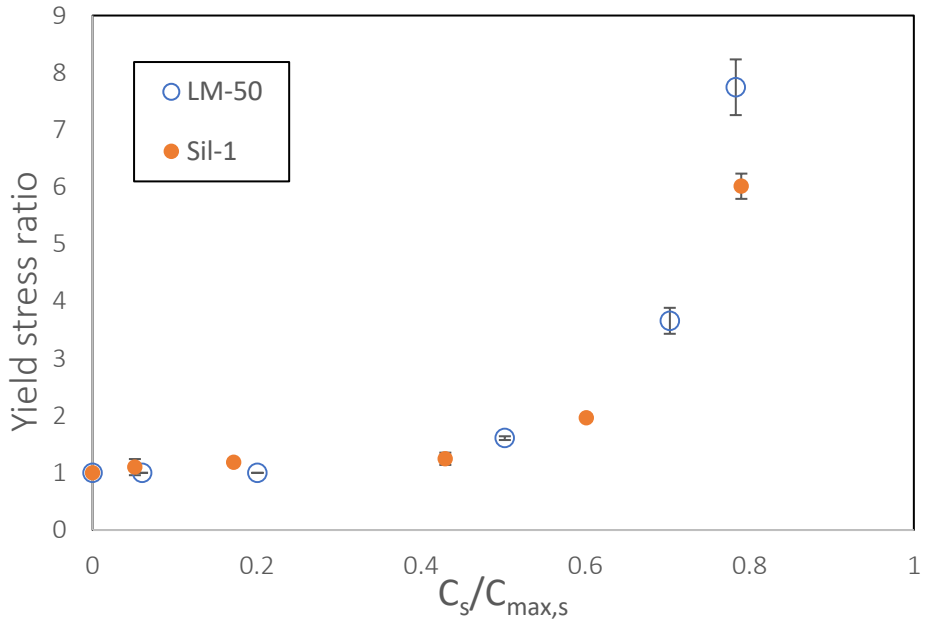

Figure B-1: Vane yield stress ratio measurements for a 0.12 (v/v) kaolin concentration and sands at different concentrations, showing the initial and repeated data

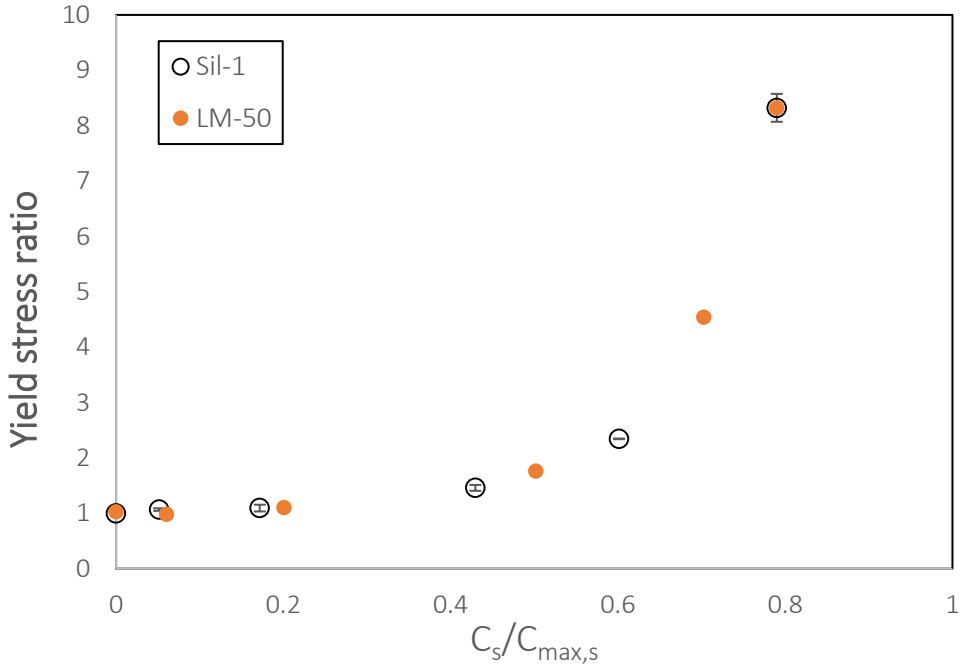

Figure B-2: Vane yield stress ratio measurements for a 0.20 (v/v) kaolin concentration and sands at different concentrations, showing the initial and repeated data

B.4 Bingham yield stress and viscosity of kaolin-only suspensions

Table B-3: Bingham yield stress and vane yield stress of kaolin-only suspensions

Concentration(v/v)	Bingham yield stress (Pa)	Viscosity (mPa.s)
0.05	0.45	3.60
0.08	1.36	4.10
0.10	3.85	6.30
0.13	7.09	8.30
0.15	10.1	8.80
0.17	22.8	11.8
0.19	38.7	17.7
0.22	60.5	23.6

B.5 Kaolin–Sand Suspensions:

- Kaolin–Sil-1 Suspensions

Table B-4: Experimental results for kaolin and kaolin–Sil-1 suspensions

C_f	C_s	$\tau_{y,f}$	$\tau_{y,m}$	τ_r	ρ_f	ρ_m	
Kaolin concentration (v/v)	Sand concentration (v/v)	Vane yield stress of kaolin only (Pa)	Vane yield stress of mixture (Pa)	Vane yield stress ratio (Pa)	Density of carrier fluid (Kg/m^3)	mixture density (Kg/m^3)	pH
0.12	0.00	3.95	3.95	1.00	1209	-	3.35
0.12	0.03	3.38	3.95	1.17	1209	1242	3.48
0.12	0.10	3.95	3.95	1.00	1209	1401	4.02
0.12	0.25	3.95	5.35	1.36	1209	1631	4.37
0.12	0.35	3.95	7.90	2.00	1209	1784	4.62
0.12	0.47	3.95	23.7	6.00	1209	1880	4.74
0.15	0.00	5.64	5.64	1.00	1240	1240	3.31
0.15	0.03	5.64	5.36	0.95	1240	1276	3.52
0.15	0.10	6.20	6.77	1.09	1240	1413	3.82
0.15	0.25	6.20	9.02	1.45	1240	1671	4.28
0.15	0.35	6.20	15.3	2.45	1240	1783	4.47
0.15	0.47	6.20	50.8	8.18	1209	1918	4.62

C_f	C_s	$\tau_{y,f}$	$\tau_{y,m}$	τ_r	ρ_f	ρ_m	
Kaolin concentration (v/v)	Sand concentration (v/v)	Vane yield stress of kaolin only (Pa)	Vane yield stress of mixture (Pa)	Vane yield stress ratio (Pa)	Density of carrier fluid (Kg/m^3)	mixture density (Kg/m^3)	pH
0.20	0.00	17.7	17.7	1.00	1360		3.67
0.20	0.03	17.7	18.6	1.05	1360	1364	3.89
0.20	0.10	16.4	18.6	1.13	1360	1511	4.2
0.20	0.25	18.1	26.5	1.46	1360	1680	4.44
0.20	0.35	18.6	43.9	2.37	1360	1760	4.61
0.20	0.47	18.6	161	8.67	1360	1952	4.88
0.24	0.00	41.1	41.1	1.00	1401		3.63
0.24	0.01	41.1	40.0	0.99	1401	1423	3.74
0.24	0.10	41.1	42.3	1.04	1401	1568	4.00
0.24	0.25	41.1	67.3	1.66	1401	1711	4.36
0.24	0.35	41.1	114	2.82	1401	1852	4.49
0.24	0.47	41.7	376	9.01	1401	1988	4.67

- Kaolin–LM-50 Suspensions

Table B-5: Experimental results for kaolin and kaolin–LM-50 suspensions

C_f	C_s	$\tau_{y,f}$	$\tau_{y,m}$	τ_r	ρ_f	ρ_m	
kaolin concentration (v/v)	sand concentration (v/v)	Vane yield stress of kaolin only (Pa)	Vane yield stress of mixture (Pa)	Vane yield stress ratio (Pa)	Density of carrier fluid (Kg/m^3)	mixture density (Kg/m^3)	pH
0.12	0.00	2.82	2.82	1.00	1220		3.70
0.12	0.03	3.38	3.38	1.00	1220	1286	3.84
0.12	0.10	3.38	3.38	1.00	1220	1379	3.9
0.12	0.25	3.38	5.36	1.58	1220	1623	4.06
0.12	0.35	3.38	11.8	3.50	1220	1726	4.21
0.12	0.38	2.82	20.9	7.40	1220	1790	4.33

C_f	C_s	$\tau_{y,f}$	$\tau_{y,m}$	τ_r	ρ_f	ρ_m	
kaolin concentration (v/v)	sand concentration (v/v)	Vane yield stress of kaolin only (Pa)	Vane yield stress of mixture (Pa)	Vane yield stress ratio (Pa)	Density of carrier fluid (Kg/m^3)	mixture density (Kg/m^3)	pH
0.15	0.00	6.20	6.20	1.00	1270		3.70
0.15	0.03	5.64	6.20	1.10	1270	1352	3.78
0.15	0.10	6.20	6.77	1.09	1270	1430	3.88
0.15	0.25	6.20	10.2	1.64	1270	1672	4.11
0.15	0.35	6.20	22.6	3.64	1270	1740	4.54
0.15	0.38	6.20	53.0	8.55	1270	1798	4.66
0.20	0.00	17.7	18.6	1.05	1360		3.67
0.20	0.03	17.7	16.9	0.96	1360	1380	3.69
0.20	0.10	16.4	18.6	1.13	1360		3.74
0.20	0.25	18.6	31.6	1.70	1360	1729	3.87
0.20	0.35	18.6	82.9	4.46	1360	1790	4.12
0.20	0.38	18.6	157	8.44	1360	1854	4.32
0.24	0.00	41.1	41.1	1.00	1413		3.80
0.24	0.03	40.0	40.6	1.01	1413	1486	3.87
0.24	0.10	40.0	44.6	1.11	1413	1564	3.97
0.24	0.25	43.7	78.7	1.80	1413	1715	3.98
0.24	0.35	43.9	187	4.25	1413	1842	4.01
0.24	0.38	43.7	421	9.65	1413	1980	4.23

- Kaolin–Sil-325 Suspensions

Table B-6: Experimental results for kaolin and kaolin–Sil-325 suspensions using the batch-1 kaolin.

C_f	C_s	$\tau_{y,f}$	$\tau_{y,m}$	τ_r	ρ_f	ρ_m	
kaolin concentration (v/v)	sand concentration (v/v)	Vane yield stress of kaolin only (Pa)	Vane yield stress of mixture (Pa)	Vane yield stress ratio (Pa)	Density of carrier fluid (Kg/m^3)	mixture density (Kg/m^3)	pH
0.15	0.00	5.64	5.36	1.00	1256		3.7
0.15	0.03	5.64	5.64	1.00	1256	1290	3.78
0.15	0.10	6.20	7.61	1.23	1256	1412	3.88
0.15	0.25	6.77	15.5	2.29	1256	1637	4.11
0.15	0.35	6.20	42.9	6.91	1256	1769	4.54

C_f	C_s	$\tau_{y,f}$	$\tau_{y,m}$	τ_r	ρ_f	ρ_m	
kaolin concentration (v/v)	sand concentration (v/v)	Vane yield stress of kaolin only (Pa)	Vane yield stress of mixture (Pa)	Vane yield stress ratio (Pa)	Density of carrier fluid (Kg/m^3)	mixture density (Kg/m^3)	pH
0.24	0.00	41.1	41.1	1.00	1410		3.80
0.24	0.03	40.6	41.2	1.01	1410	1467	4.07
0.24	0.10	40.6	51.9	1.28	1410	1564	4.19
0.24	0.25	40.6	113	2.80	1410	1760	4.24
0.24	0.35	41.7	474	11.4	1410	1867	4.54

B.6 MFT–Sand Suspensions:

- Investigation of sand inertness on MFT suspension:

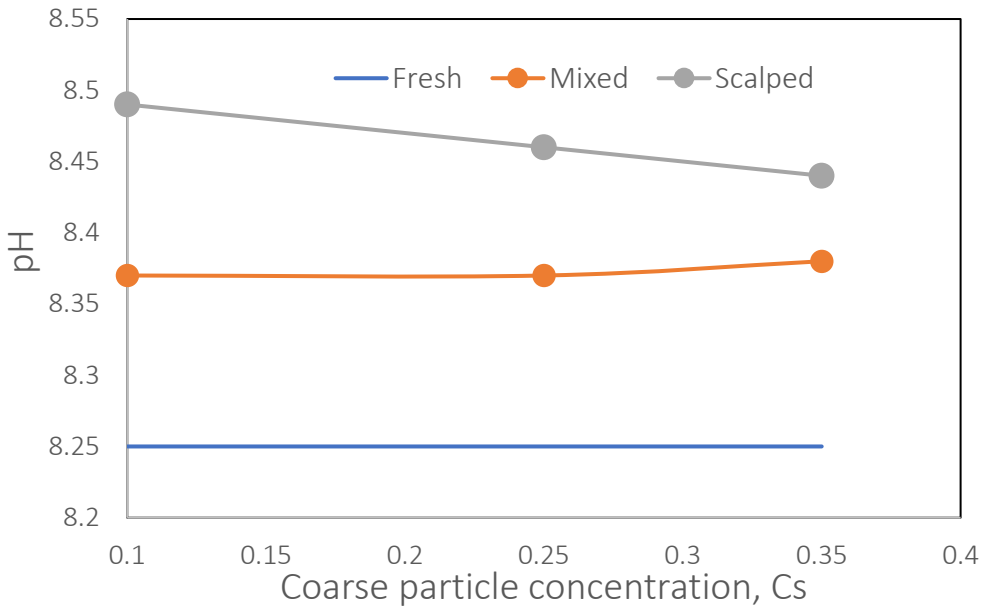

Figure B-3: Comparing pH measurements between Fresh, binary and scalped suspensions of the 26.9%(w/w) MFT, using Sil-1 sand at different concentrations. Fresh-Kaolin only; Mixed-Kaolin-Sil-1 suspension and Scalped-sieved.

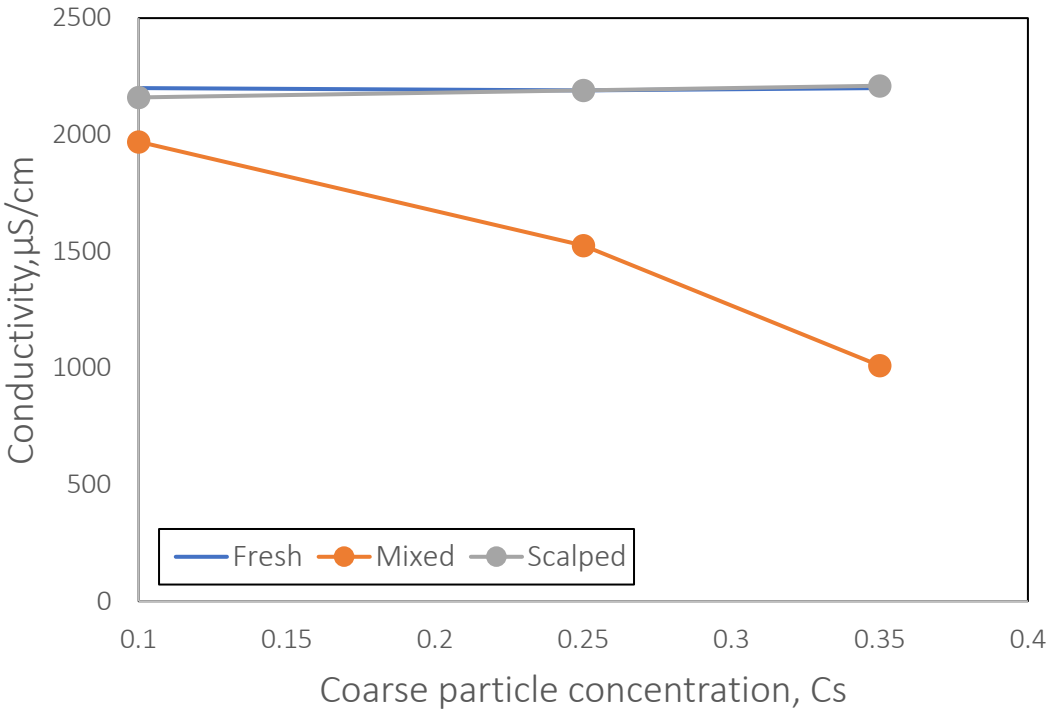

Figure B-4: Comparing conductivity measurements between Fresh, binary and scalped suspension for the sieved 26.9%(w/w) MFT, using the Sil-1 sand at different concentrations. Fresh-Kaolin only; Mixed-Kaolin-Sil-1 slurry, Scalped-sieved

- MFT-Sil-1 Suspensions

Table B-7: Experimental results for MFT and MFT–Sil-1 suspensions

C_f	C_s	$\tau_{y,f}$	$\tau_{y,m}$	τ_r	ρ_f	ρ_m	
kaolin concentration (v/v)	sand concentration (v/v)	Vane yield stress of kaolin only (Pa)	Vane yield stress of mixture (Pa)	Vane yield stress ratio (Pa)	Density of carrier fluid (Kg/m^3)	mixture density (Kg/m^3)	pH
0.11	0.00	1.69	1.69	1.00	1190		8.27
0.11	0.03	1.69	1.69	1.00	1190	1234	8.47
0.11	0.10	1.69	1.69	1.00	1190	1300	8.37
0.11	0.25	1.69	2.8	1.67	1190	1620	8.37
0.11	0.35	1.69	3.4	2.00	1190	1710	8.37
0.11	0.47	1.69	11.3	6.67	1190	1880	8.31

C_f	C_s	$\tau_{y,f}$	$\tau_{y,m}$	τ_r	ρ_f	ρ_m	
kaolin concentration (v/v)	sand concentration (v/v)	Vane yield stress of kaolin only (Pa)	Vane yield stress of mixture (Pa)	Vane yield stress ratio (Pa)	Density of carrier fluid (Kg/m^3)	mixture density (Kg/m^3)	pH
0.14	0.00	3.38	3.41	1.00	1234		8.17
0.14	0.03	3.38	3.41	1.00	1234	1276	8.17
0.14	0.10	3.38	3.41	1.00	1234	1383	8.28
0.14	0.25	3.38	4.53	1.33	1234	1600	8.33
0.14	0.35	3.38	6.24	1.83	1234	1773	8.43
0.14	0.47	2.82	18.6	6.60	1234	1895	8.56

- MFT-LM-50 Suspensions

Table B-8: Experimental results for MFT and MFT–LM-50 suspensions

C_f	C_s	$\tau_{y,f}$	$\tau_{y,m}$	τ_r	ρ_f	ρ_m	
kaolin concentration (v/v)	sand concentration (v/v)	Vane yield stress of kaolin only (Pa)	Vane yield stress of mixture (Pa)	Vane yield stress ratio (Pa)	Density of carrier fluid (Kg/m^3)	mixture density (Kg/m^3)	pH
0.11	0.00	1.69	1.69	1.00	1190		8.27
0.11	0.03	1.69	1.69	1.00	1190	1234	8.47
0.11	0.10	1.69	2.31	1.33	1190	1300	8.37
0.11	0.25	1.69	2.84	1.67	1190	1620	8.42
0.11	0.35	1.69	5.07	3.00	1190	1710	8.39
0.11	0.47	1.69	6.78	4.01	1190	1880	8.44
0.14	0.00	3.38	3.38	1.00	1234		8.17
0.14	0.03	3.38	3.38	1.00	1234	1276	8.17
0.14	0.10	3.38	3.38	1.00	1234	1383	8.39
0.14	0.25	3.38	4.51	1.33	1234	1600	8.35
0.14	0.35	3.38	9.63	2.83	1234	1773	8.43
0.14	0.47	3.38	15.8	4.67	1234	1895	8.47

The gel point of kaolin was used for the MFT-sand suspension when testing the model by Lim et al. [23]

Appendix C Details of Experimental Set-ups

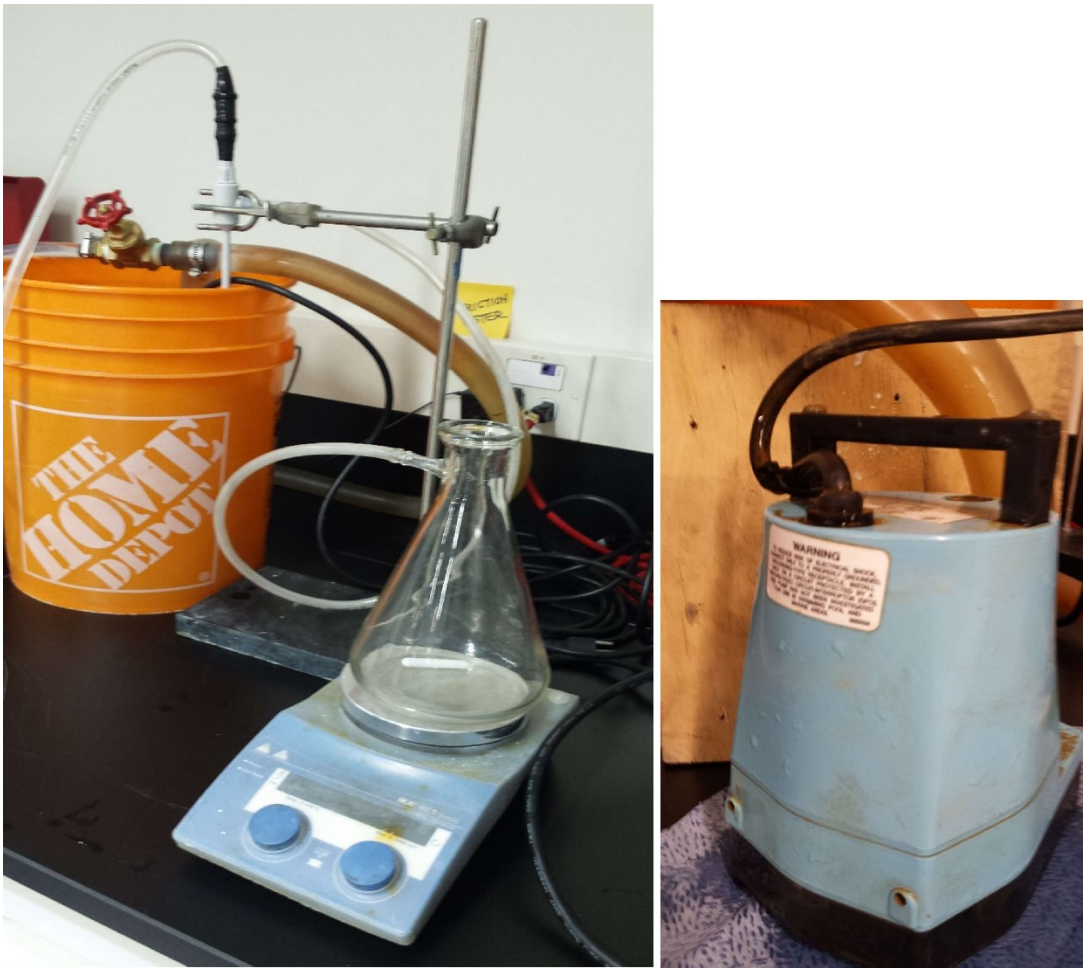

(A) (B)

Figure C-1: (a) Vacuum operations set-up, (b) Submersible pump

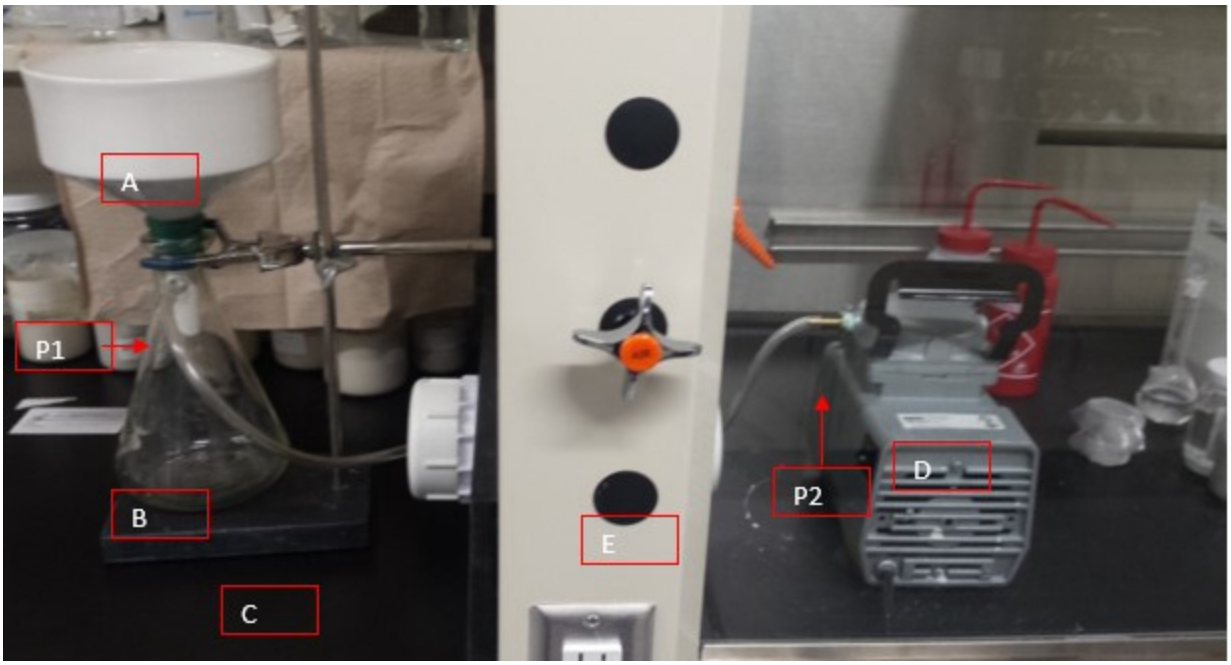

Figure C-2: Vacuum filtration set-up

A – Buckner funnel

B – Vacuum Flask

C – Retort Stand

D – Vacuum Pump (Gast)

E – Fume Hood

P1 – Connection between flask and tube

P2 – Connection between tube and vacuum pump

Appendix D Bingham yield stress estimation from concentric viscometer

The concentric cylinder viscometer, which is also called a cup-and-rotor or Couette flow viscometer, is a system with two cylinders of different diameters to create an annulus to shear fluids. The type of flow within an annulus is referred to as Couette flow. Shear flow of the suspension in the annulus is induced when one of the two cylinders rotates while the other remains fixed [27]. In this work, the inner cylinder rotates while the outer cylinder is stationary, as shown in Figure D.1.

6. When the inner cylinder is immersed in a fluid, the torque, T, required to spin the rotor of radius R_1 and length L at a set angular velocity, ω, is measured [76]. The spinning action creates a shear stress profile across the annulus gap between the moving rotor and static cup surfaces. This action shears the suspension, and the rheological data can be obtained using appropriate equations.

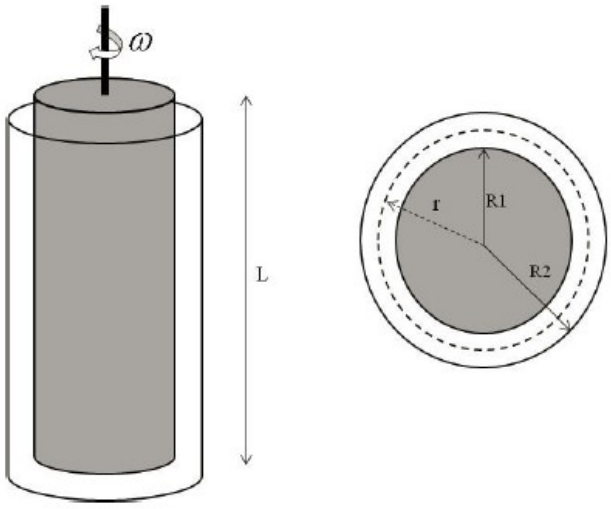

Figure D-1: Concentric cylinder geometry of rotational viscometer [38]

The relationship between measured torque (T) and shear stress at any given distance between the surface of the cup and rotor is given by:

$$\boldsymbol{T = 2\pi r^2 L \tau_{r\theta}} \quad \text{(D.1)}$$

where $\tau_{r\theta}$ is the local shear stress at a distance, and r, is the distance from the center of the rotor to a point within the annulus gap in the fluid.

For a non-Newtonian, viscoplastic fluid that can be described by the Bingham model, the integrated relationship between angular rotor speed, ω, and torque, T, under laminar flow conditions is mathematically expressed by [76]:

$$\boldsymbol{\omega = \frac{T}{4\pi L \mu_p}\left[\frac{1}{R_1^2} - \frac{1}{R_2^2}\right] - \frac{\tau_{y,B}}{\mu_p} ln\left(\frac{R_2}{R_1}\right)} \tag{D.2}$$

The dynamic yield stress is obtained indirectly as a fitting parameter from torque and angular velocity data. From the geometry of the concentric cylinders and a linear regression of the data using Equation (A.2), the yield stress and plastic viscosity can be calculated [76]. The yield stress estimated with this procedure, called the Bingham yield stress, is higher than the true yield stress, which would be obtained directly from a vane viscometer.

The accuracy of the estimated quantities, μ and τ, however, requires that the data are obtained in conditions where Equation (A.2) applies. Specifically, the conditions must lie between a critical angular velocity, ω_{crit}, at the upper boundary, and the critical minimum torque, T_{crit}, at the lower boundary. Above the critical angular velocity, secondary flow develops [27]. This value for ω_{crit} is defined by the critical Reynolds number or Taylor number. At the lower boundary, T_{crit}, must be greater than the yield stress to ensure that the fluid within the annulus gap is uniformly and fully sheared. The two criteria can be expressed as:

$$\boldsymbol{\omega_{crit} = Re_{crit} = 45\sqrt{\frac{R_{avg}}{R_1 - R_2}}} \tag{D.3}$$

and

$$\boldsymbol{\tau_{r\theta} = \left(\frac{T_{min}}{2\pi R_2^2 L}\right) > \tau_{y,B}} \tag{D.4}$$

$$\boldsymbol{R_{avg} = \left(\frac{R_1 + R_2}{2}\right)} \tag{D.5}$$

Since the Bingham yield stress is estimated from the flow curve, low shear rate values are more desirable for accurate results.